

UDC 66.021.1:532.5,661.15,661.15 66.021.1:532.5

No of state registration 0120U100476

Inv. No

Ministry of Education and Science of Ukraine

Sumy State University

40007, Sumy, R.-Korsakova str., 2;

phone. (0542) 33-41-08/33-40-49

APPROVED

Vise-rector for scientific work

D.Sc. (physics and mathematics),  
professor

\_\_\_\_\_ A.M. Chornous

REPORT

ON RESEARCH WORK

TECHNOLOGICAL BASES OF MULTISTAGE CONVECTIVE DRYING IN SMALL-SIZED  
DEVICES WITH UTILIZATION AND HEAT RECOVERY UNITS

(final)

Manager of research work

Ph.D. (technical sciences),

N.O. Artyukhova

2022

The manuscript was complete on November 18, 2022.

The results of this work were considered by the Scientific Council, Minutes from 2022.11.24 No. \_

## LIST OF AUTHORS

Manager of research work  
Ph.D. (technical sciences)

N.O. Artyukhova

## **ABSTRACT**

Report on research work: 147 p., 59 figures, 7 tables, 9 references.

### **DIRECTIONAL MOTION OF THE FLUIDIZED BED, DRYING, MULTISTAGE DRYER, PERFORATED SHELF, HYDRODYNAMICS, KINETICS**

The following new *scientific results* were obtained during the research:

1. The model of calculation of hydrodynamic indicators of movement of streams in the multistage shelf dryer is created.
2. A model for calculating the kinetics of changes in temperature and humidity parameters of the dispersed phase and the drying agent at the stage of the dryer is created.
3. Theoretical data and data of experimental researches concerning the description of processes of heat and mass transfer during drying are received.
4. The main hydrodynamic modes of operation of shelf dryers are determined.
5. Data on the mechanisms of motion control of the dispersed phase in the dryer in different hydrodynamic modes are obtained.
6. The fields of gas flow velocity in the working space of the gravity shelf dryer are obtained. The limits of existence of each of the hydrodynamic modes of operation of the device are shown experimentally.
7. Temperature-humidity characteristics of interacting flows and values of efficiency of stages of the dryer depending on the design of shelves and the organization of movement of the drying agent are received. It is shown that the most significant influence on the change of temperature and humidity characteristics has the time of the material on the step, which is due to the angle of the shelves and their length.
8. Under different conditions of the experiment, the range of efficiencies of individual stages of the dryer in the range of 0.12-0.47 was determined. The amount of moisture removed from the material may be from 4 to 8% of the mass. The initial value of the moisture content of the dispersed material of 13% of the mass.

9. It is shown that by changing the design of the shelf and the organization of the drying agent (in particular, in the case of its bypass), it is possible to control the drying time of the material and the efficiency of the steps of the dryer. The angle of the shelf can have a minimum value that corresponds to the angle of the natural slope of the material.

*The practical significance of the obtained results.* Based on the received data, the technique of engineering calculation of shelf dryers with vertical sectioning of working space, and also a technique of an estimation of energy efficiency of convective dryers is created. An improved design of a multistage shelf dryer is proposed, which allows controlling the residence time of the dispersed phase in the volume of the apparatus, ensures uniform contact of the drying agent and dispersed material in the suspended layer mode, avoids unwanted changes in the properties of dispersed material (overheating, abrasion, cracking reduces the probability of removal of the commodity fraction of the dispersed material from the boundaries of the inclined perforated contact shelf. Experimental samples of porous ammonium nitrate were obtained, which passed the final drying stage in a gravity shelf dryer and are characterized by a developed porous surface. The obtained scientific results are prepared for implementation in the implementation of economic agreements. A project proposal for participation in the competition of joint Ukrainian-Czech research projects for implementation in 2021 - 2022. Together with representatives of Alexander Dubcek University of Trencin (Slovakia), as well as the University of Pardubice and J.E. Purkyne University in Usti nad Labem (Czech Republic) based on the obtained theoretical and experimental data is the development of a software package for calculating the technological parameters of the gravity shelf dryer and its design dimensions.

## TABLE OF CONTENTS

Introduction.....	6
1 Modeling of the aerodisperse systems hydrodynamics in apparatuses with directional motion of the fluidized bed.....	11
2 Investigation of the convection drying process in a multistage apparatus with a differential thermal regime.....	22
3 Morphological features of the nanoporous structure in the ammonium nitrate granules at the final drying stage in multistage devices.....	27
4 Multistage shelf devices with fluidized bed for heat-mass transfer processes: experimental studies and practical implementation.....	39
5 Experimental-industrial implementation of the technology for producing nanoporous layers on ammonium nitrate: the final drying stage in multistage devices.....	71
6 Drying machines with combined hydrodynamic regimes.....	88
7 Fluidized bed in gravitational shelf dryers: optimization calculation...	98
8 Analysis of parameters and operating modes of dryers in terms of minimizing the environmental impact.....	108
9 Modeling of erosion of construction materials in the working space of multistage convective dryers.....	126
Conclusions.....	141
References.....	145

## **INTRODUCTION**

*Report section "Introduction" is prepared in according to data [1,2] and references in this work.*

Among various dispersed flows, fluidized bed plays the most significant role in modern technology. The fluidization technique has become widely used due to high intensity of processes.

Disadvantages of the fluidized bed device can include: different residence time of a particle in the device, a need for thorough cleaning of the exhaust air and material entrainment (in particular it is applicable to small particles of the system). In addition, a significant drawback is the return of fine particles back in the fluidized bed zone. The analysis of various fluidized bed granulation equipment in chemical, food and pharmaceuticals industries showed the urgent need to organize the mutual flow motion, which will enhance the quality of the final product.

It is rational to use the same device for multiple processes in low-tonnage and multi-assortment production in order to reduce the range of the equipment. Implementation of the new forms to organize mutual flows motion (while keeping the same principles of the fluidized phases contact), which would intensify processing of the dispersed materials without considerable increase in the energy costs, is a promising direction for the development of heat and mass exchange processes in the heterogeneous systems.

Among the major techniques of controlling the polydisperse particles residence time in the device, one should notice the following:

1. To develop a direct movement of particles using accelerating elements (gas distributors of vortex type).
2. To design the device with a variable cross-sectional area applied to the granulation, cooling and dedusting process.
3. The promising direction to reduce financial and energy costs on the heat and mass transfer processes in the fluidized bed is the application of sectioning (vertical

and horizontal) to create different conditions for the particle heightwise (lengthwise) motion in the device.

There are various possibilities to apply suspended layer (fluidized bed, weighted layer). There are many successful cases regarding the introduction of this method in industrial practice, while in others it is at the stage of laboratory research. The processes taking place in heterogeneous systems using the suspended layer method have a great industrial application. It can be used to stove sulphide, arsenic and antimony ores to facilitate the extraction of gold or silver, for pyrite and pyrrhotine roasting to obtain SO<sub>2</sub> in the production of sulfuric acid.

The suspended layer is in great demand in metallurgy for stoving of copper, cobalt and zinc sulfide ores to obtain valuable metals.

Fluidized bed devices for drying solid materials (coal, cement, limestone, etc.) are known in the whole world. Economic considerations make the use of these devices particularly interesting when large-tonnage materials are to be processed. A suspended layer dryer can also be used as a classifier since the drying and classification processes take places simultaneously in the device.

The world practice of recent years in the small power engineering has shown that the fluidized bed technology is effective for the utilization of different biomass types, industrial waste and effluents.

The development and implementation of fluidized bed devices are held back in many industries by the lack of reliable methods for calculating them. One of the main reasons is the lack of knowledge of complex and varied processes in the fluidized bed.

When constructing a mathematical model, one should take into account that there is a huge amount of particles in the operating device. These particles are of different sizes and they move at a different rate in all directions.

Mathematical modeling lets to establish and to optimize mode and technological parameters of the investigated process, as well as to minimize the use of additional automation tools.

The flows motion hydrodynamics modeling is carried out by the finite-volume method (a numerical method of the differential equations system integration in the differential derivatives). An important benefit of the finite-volume method is that the conservation law of integral values (of the flow rate, of motion quantity) is implemented on every chamber of the computational grid, but not only within it, due to the strong thickening of the computational grid. A closed area of the fluid or gas flow is selected in the calculation. The macroscopic values fields (in this paper – velocity), describing the environment in time and satisfying the definite laws, formed mathematically, are searched for it. The conservation laws in Eulerian variables are mostly used. This model is the most common and the most complicated among multi-phase flow models. The substance of every phase is a solid phase, and the substance motion of every phase is modeled with Navier-Stokes (Reynolds) equations system, equation of continuity and energy. According to this model, the motion equations for every phase, are solved together.

Modern manufacturing requires development of the new energy- and resource-saving technologies for the disperse materials drying in order to obtain high quality products, to increase the specific production capacity, to reduce the size of equipment, and to intensify the process. Therefore, the scientists should deal with the topical task, that is the improvement of the drying methods and the design of efficient dryers.

Various energy-consuming methods are applied for the disperse material drying.

Even though energy-consumption in convection drying is not the lowest, the convection dryers are often used for the disperse materials due to numerous advantages. An active hydrodynamic regime used in such dryers contributes to the intensification of the process without reducing its cost efficiency, and it has the following advantages:

- the hydrodynamic sustainability of the process;
- an increase in the relative velocity of the interacting phases motion;
- a developed surface of the contacting phases interaction;

- the approximation of a hydrodynamic model of flows in the apparatus to an ideal displacement model;
- the reduced energy-consumption of the process and a lower specific amount of metal in apparatuses.

The choice of such a dryer is justified by its productive capacity, energy and construction costs, work safety, the reliability, the possibility to control technological parameters, the maintainability and the availability of the appropriate transporting equipment.

Convection drying requires transporting of the large volumes of the drying agent. It implies big financial and ecological problems – significant losses of heat energy with the waste drying agent, particularly during the drying of materials with a high moisture content. As a result, these losses make 70 % out of total losses during the drying. It involves a need for utilization and re-use of heat of the waste drying agent.

The drum dryers and apparatuses with a boiling layer are of large sizes and highly energy-consuming. The pneumatic tube dryers do not ensure the necessary contact time of the damp material with the drying agent, and they are characterized by a high altitude. A perspective direction in the improvement of the drying equipment is a design of the combined apparatuses with an active hydrodynamic regime, which ensures the intensified heat exchange and minimal energy expenditures for the fluidized bed. An effective method of the process intensification is the organization of local, counterflow and/or combined regimes of the interaction of the drying agent flow with the product, and a selection of an optimal method of the drying agent inlet to the workspace of the apparatus and its re-use.

The literature analysis of the author presents the following measures on how to reduce the energy costs for the disperse materials drying:

- to re-use heat of the waste drying agent;
- to improve the construction of the dryers;

- to improve the dryer layout and the efficiency of their use (for the multistage dryers – the drying efficiency on each stage);
- an introduction of the improved technology of a recycle dryer;
- a differential thermal regime;
- to reverse and to recirculate the drying agent, including the waste one.

There has been little research reported on the patterns for the dehydration of the materials upon their multistage contact with the drying agent, which changes its properties. The intensity of dehydration differs on each stage of the shelf dryer, and the drying kinetics on each stage must be additionally examined.

Due to repeated contacts of the disperse material with the drying agent in the gravitational shelf dryers, a reduction in energy consumption per unit of the extracted moisture is achieved. It is of special interest to study the moisture removal efficiency on each stage of the dryer under different organizations of the drying agent motion.

# 1 MODELING OF THE AERODISPERSE SYSTEMS HYDRODYNAMICS IN APPARATUSES WITH DIRECTIONAL MOTION OF THE FLUIDIZED BED

*This section is prepared in accordance to data [1] and references in this work. Description of the simulation methodology and research and industrial installation - in accordance with [10]*

In order to carry out modeling, it is convenient to solve the above equations by the numerical methods (DEM - Discrete Element Method), identifying a discrete set of values in the proper place (mesh, node of grid), space (during the stationary regimes of the flows motion) instead of the continuous solution. In order to achieve the maximum accuracy of solutions, that method to demonstrate discrete values is chosen, which due to the discretization complies with algebraic equations analogues. As a result, the mathematical problem to solve the differential or integral equations system can be reduced to the algebraic equations system.

There is also a method to describe the axisymmetric motion of the swirling gas flow, based on a system of Navier-Stokes equations (1) and the continuity equation (2):

$$\frac{\partial}{\partial t}(\rho_g V_i) + \frac{\partial}{\partial q_j}(\rho_g V_i V_j) = -\frac{\partial p}{\partial q_i} + \frac{\partial}{\partial q_j} \left[ \varepsilon \left( \frac{\partial V_i}{\partial q_j} + \frac{\partial V_j}{\partial q_i} \right) \right] + f_i, \quad (1)$$

$$\frac{\partial \rho_g}{\partial t} + \frac{\partial}{\partial q_j}(\rho V_j) = 0, \quad (2)$$

where  $\varepsilon$  is a coefficient of turbulent viscosity;  $t$  – time;  $V_i$  – instantaneous component of the velocity on the given axis;  $\rho_g$  – gas density;  $p$  – pressure;  $f_i$  – component, characterizing the action of the bulk forces;  $q_j$  – axes of coordinates.

Analysis of the previous works in the two-phase flows modeling sector, which consists of gas as a disperse phase and disperse particles, showed that one of the most

perspective methods to calculate the motion of the particles is a trajectory method. Authors concluded that in case of the compressed motion modeling of particles with large diameter (0.5-5 mm), the Lagrangian model regarding the force analysis of the particle motion by the differential equations of motion forms the base for it. The trajectory method with highly accurate results can be used only if there is any software which enables to export theoretical model of the single-particle motion and to consider the flow constraint degree.

The motion of particles in the workspace was simulated on the basis of the differential equations system of the particle motion:

$$\left. \begin{aligned} m \frac{d^2 q_1}{dt^2} &= -g + \psi \cdot \frac{\pi \cdot \mu_g \cdot d}{8 \cdot m} (V_1 - W_1), \\ m \frac{d^2 q_2}{dt^2} &= \frac{W_3^2}{r} + \psi \cdot \frac{\pi \cdot \mu_g \cdot d}{8 \cdot m} (V_2 - W_2), \\ m \frac{d^2 q_3}{dt^2} &= -\frac{W_2 W_3}{r} + \psi \cdot \frac{\pi \cdot \mu_g \cdot d}{8 \cdot m} (V_3 - W_3) \end{aligned} \right\}, \quad (3)$$

where  $m$  – particle's mass;  $r$  – a current radius of the workspace in a unit;  $w_1, w_2, w_3$  – radial, circumferential and flow rate components of the particle's velocity correspondingly;  $g$  – gravitational acceleration;  $\psi$  – a linear coefficient of particle resistance to the gas flow;  $\mu_g$  – gas flow viscosity;  $d$  – a particle's diameter.

Criteria to choose the two-phase system flow model are the following.

1. Ratio  $\beta$  of the disperse phase substance mass ( $d$ ) to the mass of the carrier phase substance ( $c$ ):

$$\beta = \gamma \frac{F_d}{F_c}, \quad (4)$$

where  $F_d$  and  $F_c$  – volume fractions,  $\gamma$  – the ratio of the disperse phase density to the carrier phase density,  $\gamma = \rho_d / \rho_c$ .

If  $\beta$  has high values, the dispersed particles have a great impact on the carrier phase flow, so it is necessary to use only the multi-phase Eulerian model for the proper flow modeling.

2. Stokes number  $St$ :

$$St = \frac{t_d}{t_c}, \quad (5)$$

where  $t_d$  – time, which describes the particles motion,  $t_d = (\rho_d d_d^2) / (18 \mu_c)$ ,  $d_d$  – diameter of the particle,  $\mu_c$  – viscosity of the carrier phase substance,  $t_c = L_c / U_c$  – time, which describes the carrier phase,

$L_c$  – characteristic length,  $U_c$  – characteristic velocity.

The authors suggest taking into account the constrained mode of motion when we calculate the particle residence time in the workspace of the device

$$\tau_{cm} = \tau f_{er}(\psi), \quad (6)$$

where  $\tau_{cm}$  - velocity of the constrained motion of particles in the disperse phase;  $\tau$  - a velocity of a single particle motion;  $f_{er}(\psi)$  - an empirical influence function of the constraint conditions on the residence time of a particle in the workspace.

The function  $f_{er}(\psi)$  is:

$$f_{er}(\psi) = (1 - \psi)^{-m}, \quad (7)$$

where  $m$  – an empirical measure of the stage (a constraint coefficient for the time calculations).

Ansys CFX and Ansys Fluent (<https://www.ansys.com>) software is based on a finite-volume method of solving hydrodynamic equations and using a rectangular adaptive mesh with local grinding. In order to approximate curvilinear geometry with

higher accuracy, the technology of geometry grid density is used. This technology enables to import geometry from CAD systems and to share information with finite element analysis systems. This technology has solved the problem of automatic mesh generation – in order to generate a mesh, it is enough to set only a few parameters, after which the mesh is automatically generated for a computational area that has the geometry of any complexity degree.

The calculation starts with some initial approximation set as the initial data. At each global iteration, the velocity and pressure fields, obtained after the time specified as the integration step, are calculated. The stationary solution of the problem is achieved after a sufficiently large number of global iterations corresponding to a long period of time.

When performing the calculation, the program automatically breaks the calculation area into separate subareas, subdomains, the size of which is proportional to the velocity of the appropriate processor. The calculation algorithm works in such a way that each processor calculates the flow only in its own subdomain, and after each global iteration, the resulting solution is “adhesion”. The parallelization algorithms used in modern software products let to achieve acceleration with an efficiency close to 100%. In other words, the calculation time is inversely proportional to the total computing power.

As a rule, the adhesion condition is set as boundary conditions on all solid walls (the velocity is zero), the distribution of all velocity components in the inlet section, and the first derivatives (in the direction of flow) of the velocity components in the outlet section are equal to zero. In practice, if the flow rate at the inlet is approximately uniform in the intersection, the user sets only the average velocity (or flow rate) at the inlet, and sets nothing at the output - it is assumed that the user chose the output section far enough from the areas of intensive restructuring of the flow.

In the upper section of the device the inclined shelves (angle of lean  $30^\circ$ ) with ratio  $l/B$  (where  $l$  is the distance from the end of the shelf to the wall of the device;  $B$  – width

of the device) in the amount of  $l/B=1$  (free channel) to  $l/B=0.3$  were installed. The results of the previous investigations, show that the efficiency to extract the small fraction (with the size less than 1 mm) into the ablation has the maximum value with the ratio  $l/B=0.5$ .

Thus, at the first stage of theoretical studies, it was necessary to find the optimal value of the free area in the shelf for the ablation efficiency of the fraction less than 1mm.

The results of the computer modeling show that the efficiency to extract the small fraction into the ablation is achieved with the reduction of the perforation degree of the shelf. While installing the solid shelf in the separation zone of the device, the whole gas flow guaranteed passes through the outloading space. It defines the extraction of the small fraction of the material precisely in this zone. 5 % of perforation in the shelf causes the redistribution of the gas flow, directing its share through the hole in the shelf. Therefore, the gas flow intensively is interconnected with the material and not only in the outloading space zone but also on the shelf surface. It causes the increase of the fraction ablation efficiency, which is less than 1 mm.

The further increase of the free area of the inclined contact shelf is followed by the reduction of the small fraction extraction efficiency into the ablation. It is explained by the increased effect of the gas flow redistribution. The gas flow velocity in the outloading space decreases so much that the small fraction extraction process of the material in this zone is not very intensive. The total area of holes does not provide sufficient phase contact.

There are three perforated shelves in the drying (granulation) zone of the device. Moreover, while changing the distance between the end of the shelf and the wall of the device, it is possible to create different velocities of the gas flow

Regime I. Transition regime (figs 1a,b). The upward gas flow force in this regime causes the gradual change of its motion trajectory from the translational to the pulse-forward ones in direction of the outloading gap. Therefore the dispersed material starts

to move into the weighted state, and the inertial force is compensated by the upward flow force of the drying agent.

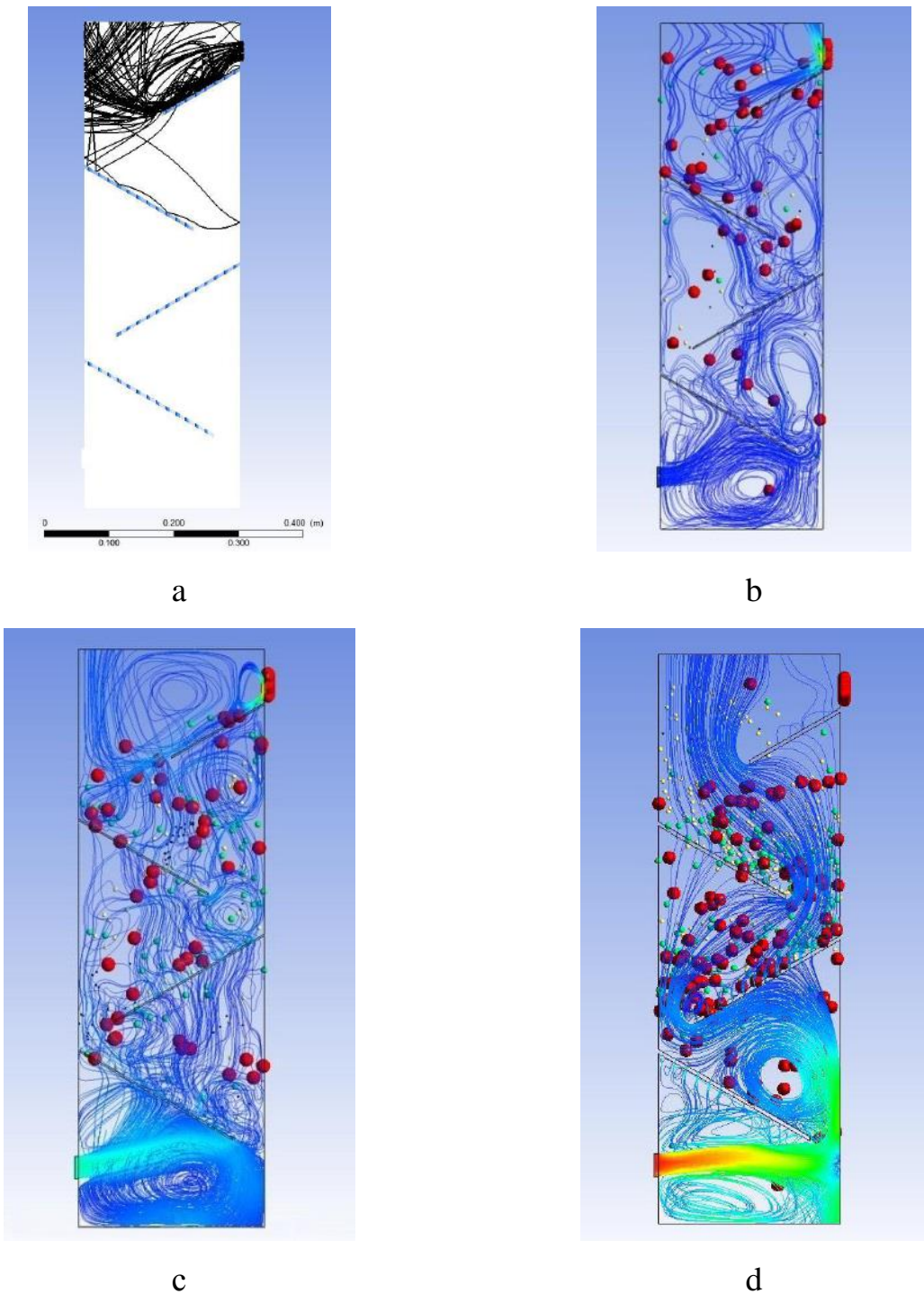


Fig. 1. Typical operation regimes of the shelf multistage device: a – separation of the small fraction in the shelf dryer; b – transition operation regime of the dryer; c – weighted layer regime of the dispersed material motion; d – developed weighted layer regime of the dispersed material motion

Regime II. The weighted layer regime (fig. 1c). The effect, made by the upward flow of the heat transfer agent in such regime leads to the creation of the stable weighted layer thanks to the compensation of the inertial force and the rolling-down force on the sloping surface. The gas flow velocity reaches the first critical value, and then it increases and is within the range of the working velocity. Regime III. The regime of the developed weighted layer (fig. 1d). This regime is described by a dominant effect of the upward gas flow force on the dispersed material and by the increase of its displacement vertical component. Therefore, at first, the share of the dispersed material is taken out from the surface of the shelf and then it moves to the outloading gap. The above results for the modeling of the operating regimes in devices let to select the following optimal parameters to implement the target process:

- configuration of the workspace in the device and the way to create the directed motion of the dispersed phase flow;
- duration of the dispersed phase in the workspace of the device;
- technological features of the related processes (separation, classification, heat exchange)
- properties of the raw material and commodity product – temperature and humidity features, fractional composition, hardness index, special properties (porosity, selectivity etc.).
- energy indicators of the process implementation.

In general, the algorithm to calculate the device with the directed fluidized bed can be represented by means of blocks (fig. 2), which are logically interconnected between each other. The peculiarity of the algorithm includes its universality and ability of “flexible” implementation of separate blocks.

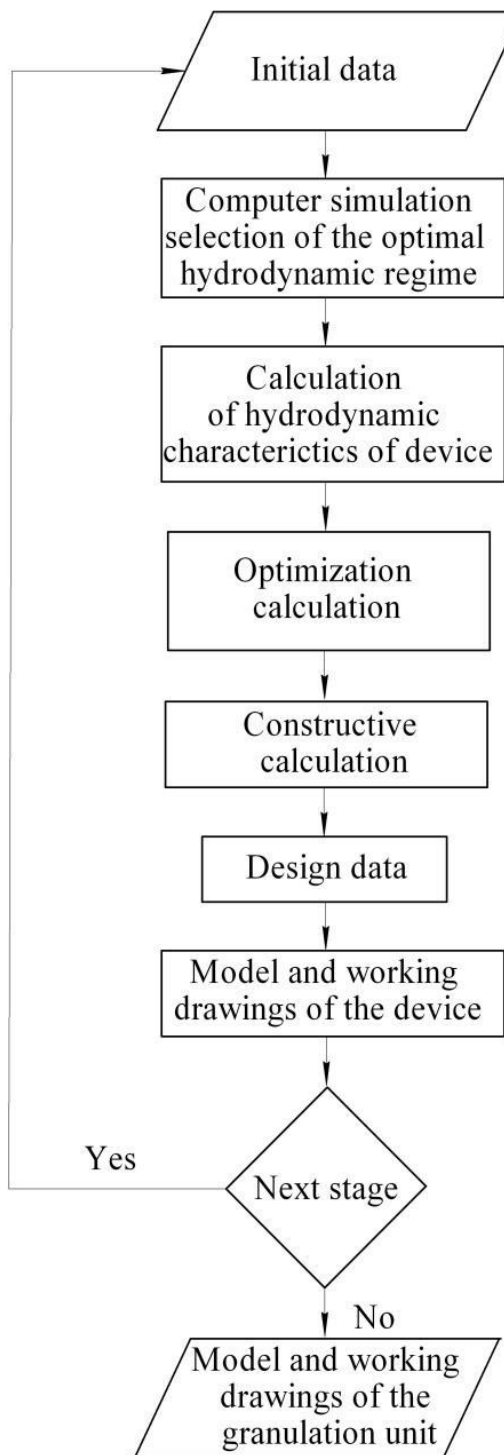


Fig. 2 Block-scheme of the granulation unit calculation

The modeling and calculation results with the use of authors' software, description of which is represented in the work, are exported to the cluster Granulation Unit<sup>©</sup> in the form of separate structural blocks (fig. 3).



Fig. 3. Cluster Granulation Unit<sup>©</sup>

Fig. 5 demonstrates the technological scheme of the porous ammonium nitrate production. In this scheme the devices, operating regime modeling of which is shown above, are used as the main technological equipment.

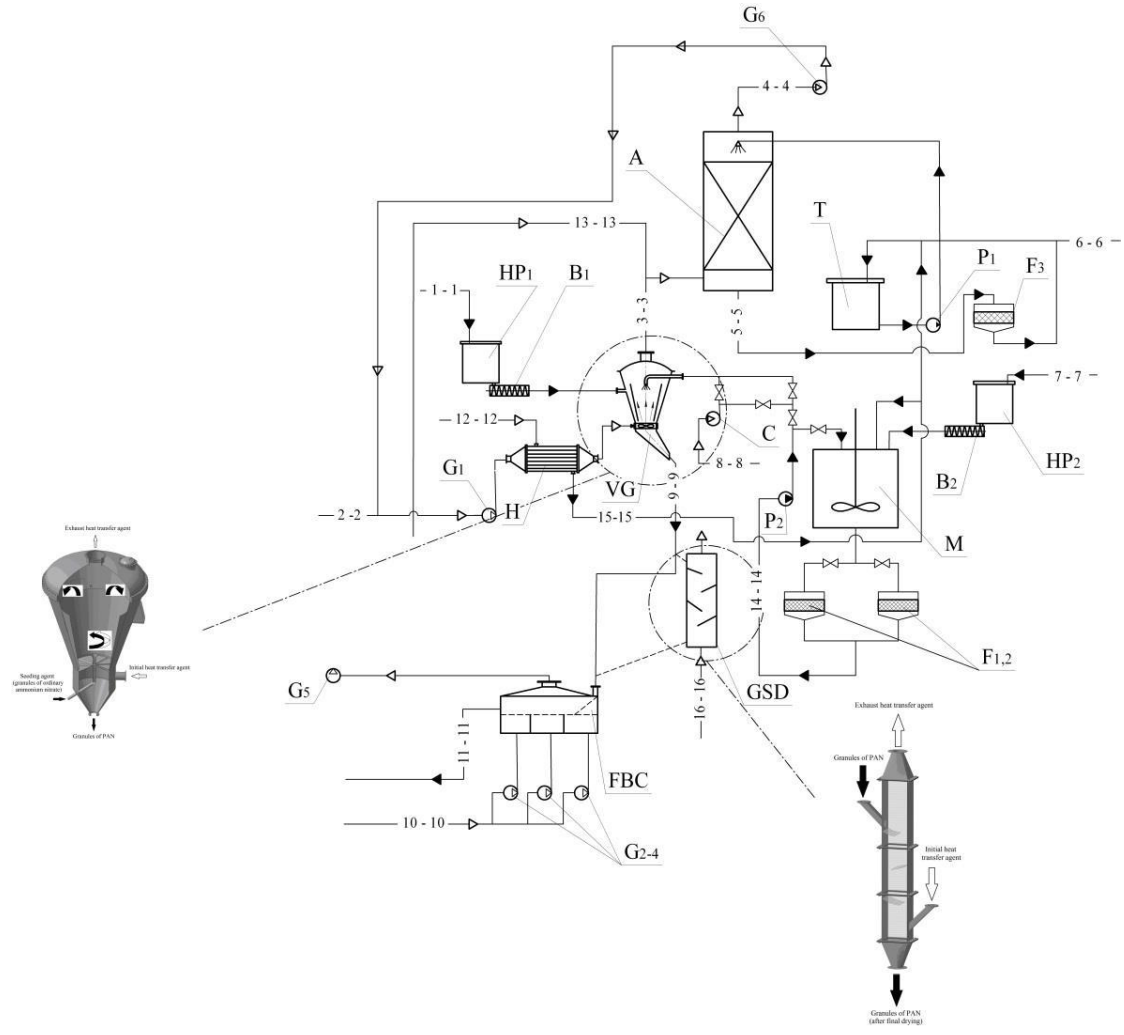


Fig. 5. A unit for the production of PAN granules by using a vortex granulator (multistage shelf granulator) and a gravitational shelf dryer

Elements of the unit:

VG – a vortex granulator; H – a heater; GSD – a gravitational shelf dryer; FBC – a fluidized bed cooler; A – an absorber; F – a filter; M – a mixer; B – a batcher; HP – a hopper; G – a gas blower; P – a pump; T – a tank; C – a compressor.

The main flows:

1-1 – a seeding agent; 2-2 – manufacturing air; 3-3 – polluted air; 4-4 – purified air; 5-5 – polluted water; 6-6 – water; 7-7 – substandard granules; 8-8 – air for the spraying of the liquid materials (solution, melt); 9-9 – the product; 10-10 – air for cooling of granules; 11-11 – granules for packaging; 12-12 – steam; 13-13 – dusty gas; 14-14 – liquid materials (solution, melt); 15-15 – water condensate; 16-16 – a drying agent.

The operation principle of the gravitational shelf dryer is the following.

The drying agent, which at first is evenly distributed over the intersection of the body and then rises upwards, is brought to the lower section of the device. Therefore, it passes some (calculated, in this case – three) perforated inclined inserts (shelves), then it is output from the upper section of the device. Together with the motion of the drying agent, the dispersed material, which is necessary to dry, is fed to the upper shelf of the body. During the counteraction with the drying agent flow, the dispersed material is heated and the small fraction is removed with a purpose to balance the weighted layer porosity on the upper inclined contact shelf. The length of the inclined contact shelf provides the residence time of the dispersed material, which promotes the complete heating of the material, separation of the small dispersed particles and removal of the unbound humidity from the surface layer of the dispersed material during the constant drying velocity. The dispersed material is gradually moving along the upper shelf, is output through its free end and comes to the middle shelf, during drying by the drying agent flow. As the dispersed material moves through the middle shelf, unbound humidity is further removed from the surface layer of the dispersed material during the constant drying velocity as a result of the counteraction with the drying agent flow. The dispersed material is gradually output through the free end of the shelf and reaches the lower shelf. As the dispersed material moved through the lower shelf, the bound humidity is removed from the depth of the material during the drying velocity decrease. The dispersed material is output from the device after the drying process.

This device may be used to dry granular materials, for granulation, encapsulation of the mineral fertilizers granules. In order to obtain the final product with a low level of the small dispersed (fine) particles, the process should be carried out with the initial separation, which is implemented on the upper shelf of the device. There are hydrodynamic conditions under which the small fraction of particles (with the size less than 1 mm) is removed from the basic material.

## 2 INVESTIGATION OF THE CONVECTION DRYING PROCESS IN A MULTISTAGE APPARATUS WITH A DIFFERENTIAL THERMAL REGIME

*This section is prepared in accordance to data [2] and references in this work.*

Consider the drying efficiency on the i-stage of the dryer as a ratio of moisture differences of the disperse material before drying to after drying  $x_{i-1}-x_i$  and the maximum possible (theoretic) moisture differences of the flows on the stage  $x_{i-1}-b_i$ ,

$$E_i = \frac{\Delta x_m}{\Delta x_{\max}} = \frac{x_{i-1} - x_i}{x_{i-1} - b_i}, \quad (8)$$

where x – moisture of the disperse material; b – moisture of the drying agent

To determine the maximum efficiency of the process on each stage of the gravitation shelf dryer, the test installation ensured the conditions under which the drying was performed until no change in the moisture content of the disperse material has occurred.

To determine the maximum value of  $\Delta x_m$  the shelf in the test installation was fixed horizontally without the uploading gap, and the intake of the disperse material charge was complemented by the determination of its moisture. The determination of the maximum value of  $\Delta x_m$  was completed when the value of  $\Delta x_m$  did not change between the two measurements of the moisture content.

The calculation results of the maximum difference in the moisture contents of the material, corresponding to the maximum efficiency on each stage, are presented in Tab. 1.

Tab. 1 The maximum difference in the moisture contents of the material (polypropylene), corresponding to the maximum efficiency on the stage

A stage number (according to the path of the material)	Maximum difference in the moisture contents $\Delta x$ , mass fraction
1	0.083
2	0.076
3	0.069

While studying the drying kinetics in the gravitational shelf dryer by computer modeling, we investigated the counterflow motions of the drying agent and the disperse material with the recirculation of the drying agent.

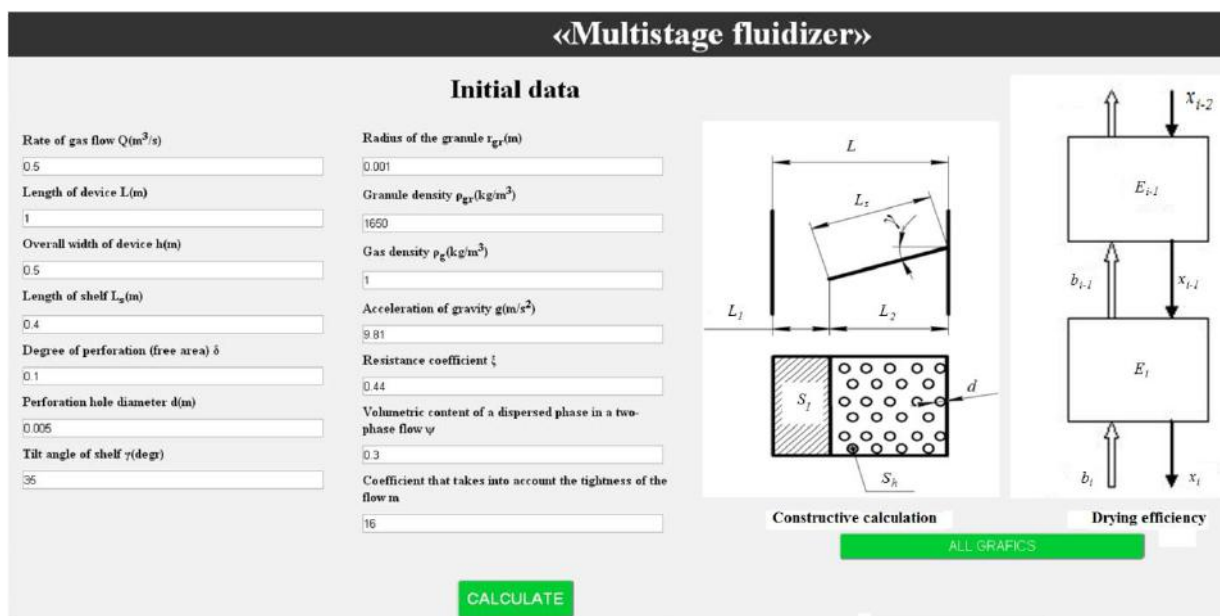


Fig. 6. The main page of the Multistage fluidizer® software

The program Multistage fluidizer® used Hyper markup language HTML, cascading style sheet (CSS) and programming language JavaScript (including the library JQuery). HTML is presented as a tagging of web based app, CSS pages formatting. JavaScript is used to calculate and to transfer data, to create animation and data validation effect. In the validation block of JavaScript data accuracy is checked. In the block input info basic data fields indices are accepted and they are written to the object of input

information.

Index.html (fig. 6) is the main page of web based app. It is responsible for reflection of the main menu, for main calculation of gas flow and for jumping the other pages, where main dependences between key features to calculate gas flow and resistance time of the material on the shelf are calculated and dependences diagrams are formed.

The organization of the drying agent motion may have a considerable influence on the quality indicators of the dried material and the properties of the drying agent. That has evolved several studies, the results of which are presented in figs. 7 – 11. Their analysis allows us to select the method of the organization of the drying agent motion, which consumes the least energy, and ensures the necessary complete removal of moisture from the disperse material.

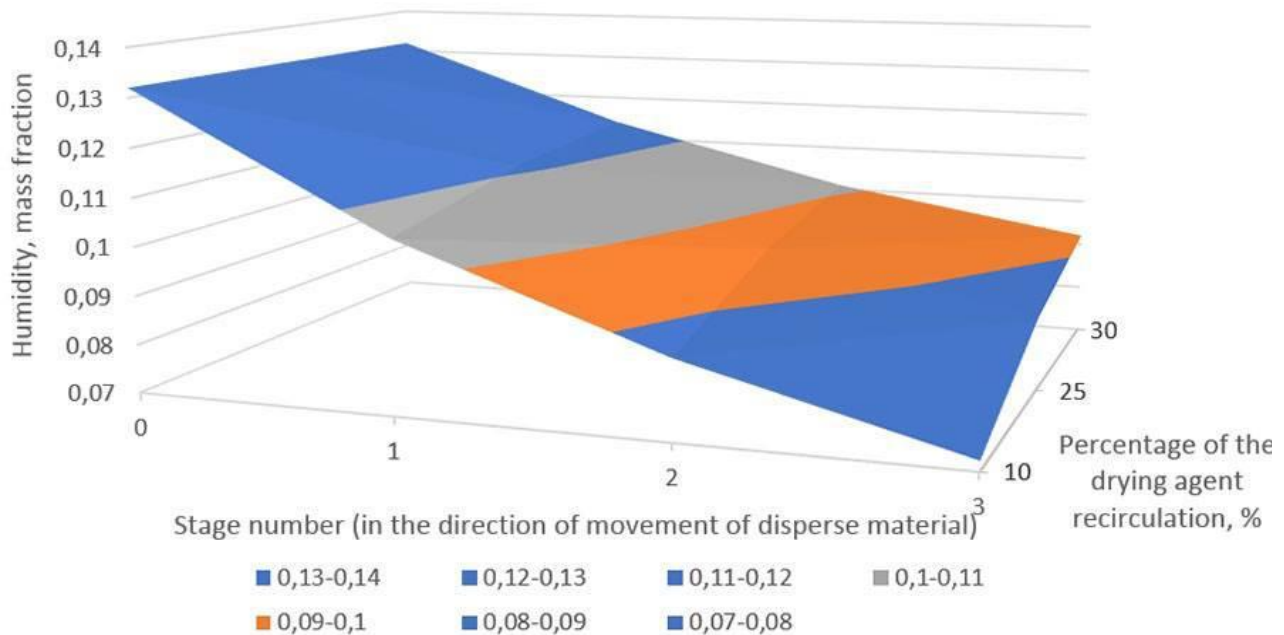


Fig. 7. An influence of the drying agent recirculation method on the change of the moisture content in the disperse material

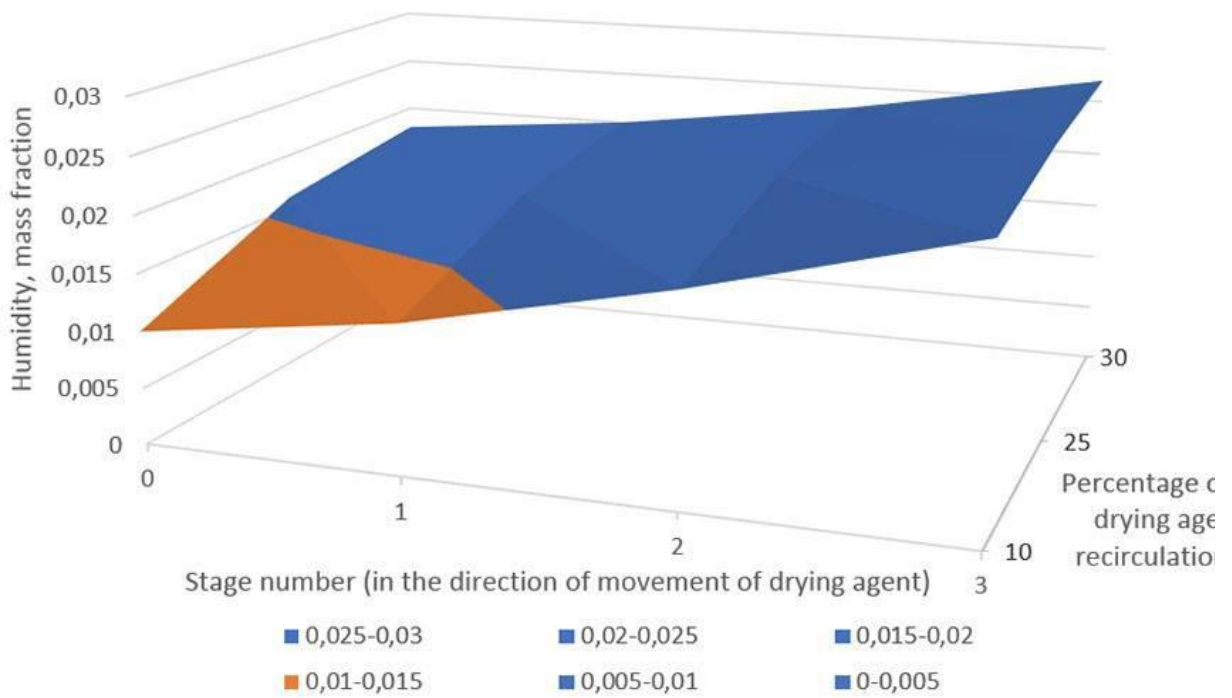


Fig. 8. An influence of the drying agent recirculation method on the change of the moisture content in the drying agent

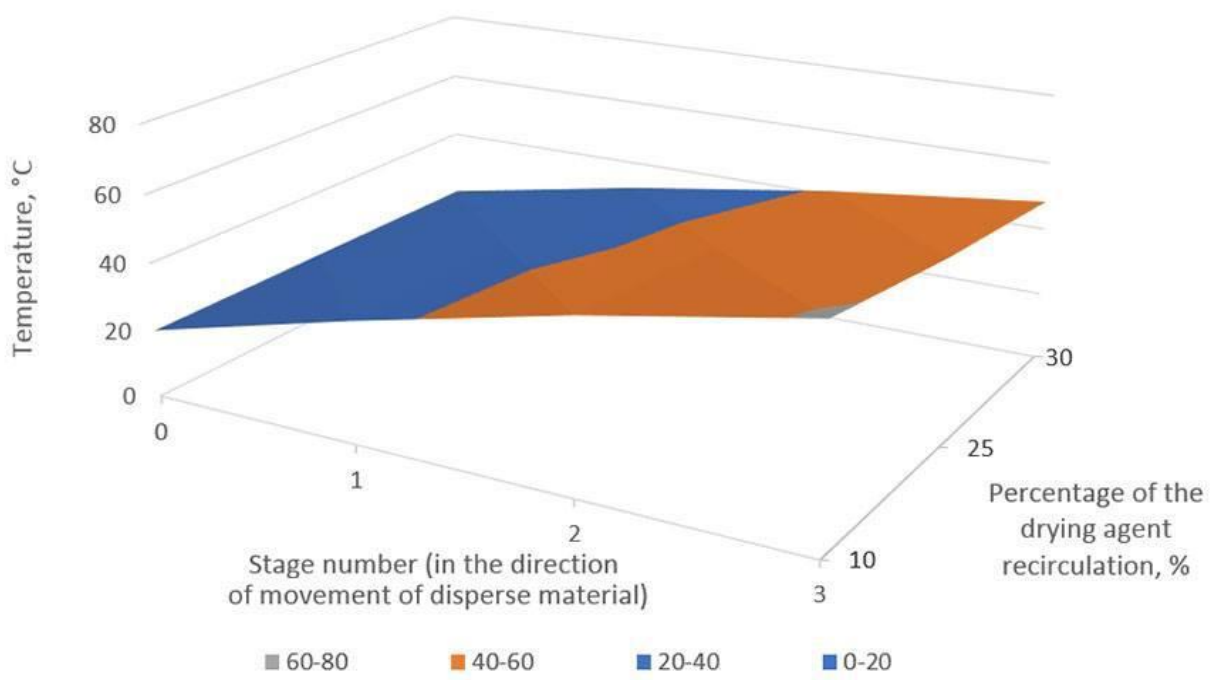


Fig. 9. An influence of the drying agent recirculation method on the temperature change of the disperse material

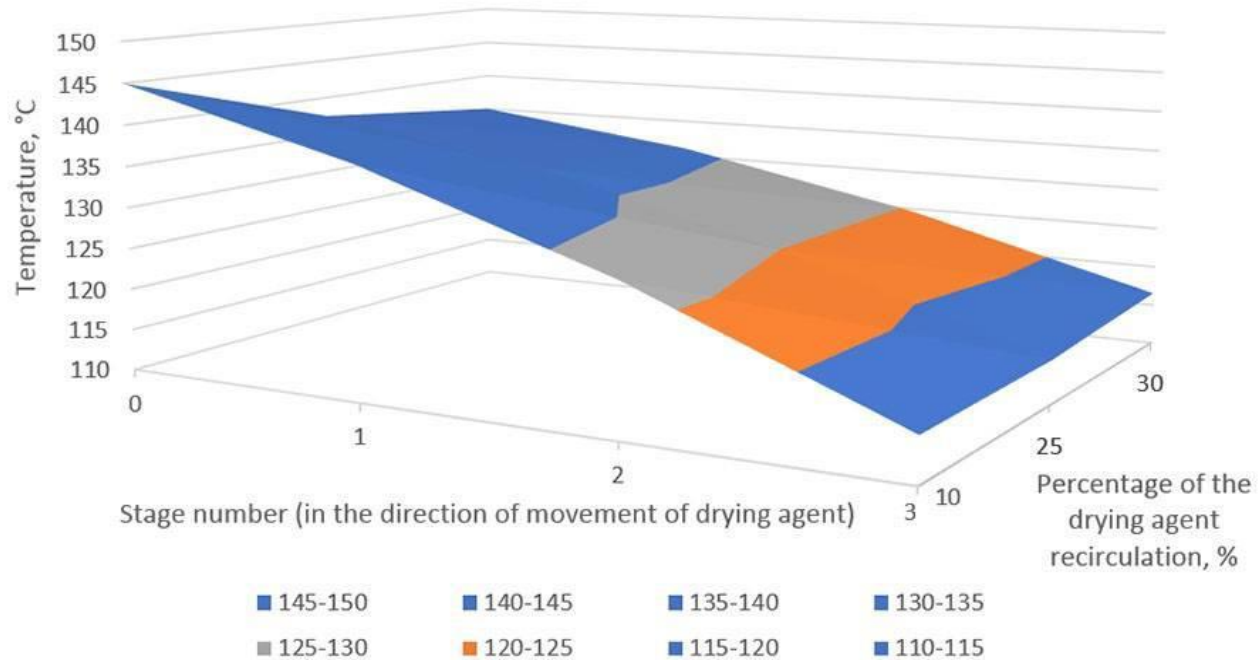


Fig. 10. An influence of the drying agent recirculation method on the temperature change of the drying agent

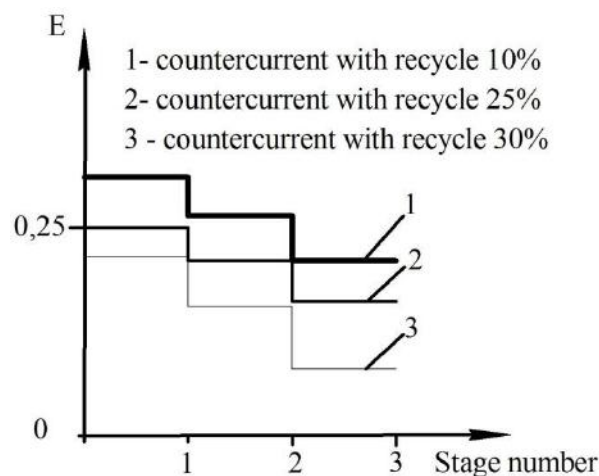


Fig. 11. An influence of the drying agent recirculation method on the drying efficiency (stage number - in the direction of movement of disperse material)

### **3 MORPHOLOGICAL FEATURES OF THE NANOPOROUS STRUCTURE IN THE AMMONIUM NITRATE GRANULES AT THE FINAL DRYING STAGE IN MULTISTAGE DEVICES**

*This section is prepared in accordance to data [3] and references in this work.*

The most cost-effective way is to use ammonium nitrate granules as a component of industrial explosives. An ordinary ammonium nitrate (mineral fertilizer) and ammonium nitrate with increased porosity (porous ammonium nitrate - PAN)] can be used to prepare a mixture of ammonium nitrate with diesel distillate (ANFO).

The ordinary ammonium nitrate can be prepared to be used as a component of an industrial explosive using the following operations:

- the crushing of granules;
- removal of the shell (powder from various inert substances), which reduces the caking of the granules.

All these operations are aimed at increasing the volume of gaps and cracks after mechanical destruction of the original granules. In this case, despite the high absorptivity, the retentivity does not fit the minimum standard indicator. Therefore, ANFO based on the ordinary ammonium nitrate, should be prepared directly at the blasting places and stored for a short time (due to the intensive draining of diesel distillate).

It is more successfully to use PAN in the technology for obtaining ANFO. Granules with a developed porous structure can reliably hold diesel distillate during transportation to the place of blasting and storing the industrial explosives.

Researchers face the task to investigate new methods for producing PAN with a developed nanoporous structure, which will provide the necessary standard indicators of granules for their successful use as ANFO components.

Table 2. PAN production methods

No	A method to obtain granules	The structure of granules
1	Prilling of “dry” melt and cooling of granules in a monotonic mode	Spherical bodies with a smooth surface and a shrink shell in a dense crystalline array
2	Prilling of “dry” melt, foaming of droplets with poroform and cooling in a monotonic mode	Spherical bodies with a smooth surface and closed gas inclusions in a dense crystalline array
3	Prilling of “wet” melt and cooling with drying in a staged mode	Rounded bodies with a rough surface and cavity in a loose crystalline array
4	The formation of granules by spraying melt on the seeding agent (granulation)	Rounded bodies with a rough surface and homogeneous granular structure in the array
5	The formation of granules with additives of iron salts, followed by surface-active reagents in a drum	Rounded bodies with such formations as flakes on the surface and a granular structure of the body
6	Heat treatment - “porization” of finished granules according to paragraphs 1,2,5 with phase transitions	It fits the original ammonium nitrate, but is saturated with cracks on the surface and inside the granule
7	Humidification followed by heat treatment (drying) with phase transitions	The core of the granule fits the initial ammonium nitrate, the surface and nearsurface layers of the granule form a combination of nanopores of various sizes, depths and configurations

Porous ammonium nitrate can be obtained directly during the formation of granules (product manufacturing) or by physical and thermal effects on the already formed

ammonium nitrate granules to change its structure and create the so-called “mechanical” pores. The first group of methods requires various additives to intensify the pore formation process. The necessity to introduce these additives is the reason to increase the cost of the finished product. The second group of methods lets to obtain a developed porous structure without the pore-forming additives. A brief description of the PAN obtaining methods within the presented classification is shown in Table 1.

Method 6 from table 2 was used as a basic variant. However, the research part shows that as a result of heat treatment, only “mechanical” pores are formed in the micrometer range that do not reliably retain diesel distillate during transportation and long-term storage. Therefore, the authors propose to produce PAN industrial explosives directly at the blasting place, which is not always advisable.

An improved scheme for producing PAN (method 7 in table 2) enables to obtain pores in the nanometer range, which positively affects the retentivity of the granules. However, this method provides destruction of the ordinary ammonium nitrate granules due to the high value of the final humidity.

Table 2. Modification of the ammonium nitrate

Modification	Temperature variation range for various modifications, ° C	Type of symmetry	Change in volume, %
I	169,6-125,2	Cubic	-2,13
II	125,2-84,2	Tetragonal	-1,33
III	84,2-32,3	Rhombic monoclinic	+0.8
IV	32,3-(-17)	Rhombic bipyramidal	-3,3
V	(-17)-(-50)	Tetragonal	+1,65

PAN granules with excess final humidity are characterized by the following

properties:

- insufficiently developed nanoporous structure;
- many "mechanical" pores that have a straight configuration;
- weak core of the granule (as a result of a significant number of "mechanical" pores);
- many rectilinear macropores in the nanoporous structure of the granule.

It is explained by the high intensity of moisture removal when the drying velocity increases (heating of the material and the first drying period in accordance with accepted terminology).

Here one should consider the regarding the ammonium nitrate modifications (table 3). Solid ammonium nitrate in the temperature range from -17 to 169.6 ° C has five crystalline modifications, each of which has a strictly defined temperature range.

In terms of the production and storage conditions, the polymorphic transformations of ammonium nitrate can adversely affect its physical and mechanical properties. The transition from one modification to another (polymorphic transition) is accompanied by a change in the crystal structure and volume of the crystal grid. The transition processes of one modification of ammonium nitrate to another are reversible. Transitions from one modification to another are reversible and proceed with breakage of the structure, which negatively affects the strength of the granule with an increase in the transitions' number. The preservation of the initial flowability of ammonium nitrate granules under long-term storage conditions significantly depends on the frequency of III↔IV conversion, proceeding at 32.3 ° C with a decrease in the specific volume by 3.7%. The strongest granules will be produced if the modification transformations of ammonium nitrate proceed with minimal volume and structural changes, i.e. without significant deformation of its crystals. This condition will be observed when the sequentially flowing chain of transformations II → III → IV is replaced with the transformation II → IV. The transformation II → IV is stabilized with a decrease in the residual moisture content in PAN.

The balanced temperatures of the modification transformations of ammonium nitrate

can be changed by increasing the amount of moisture in the granule, which will affect the polymorphic transitions kinetics. According to [9], so far as the water content increases from 0.5 to 3.4%, the transition temperature IV → III decreases from 48 to 37 ° C, with an increase in water content from 0.03 to 0.5%, the transition temperature I → III decreases from 125 to 120 ° C. This fact justifies the need to carry out not only the heat treatment process of the granules, but also its preliminary humidification. However, moisture does not change the nature of the modification transitions.

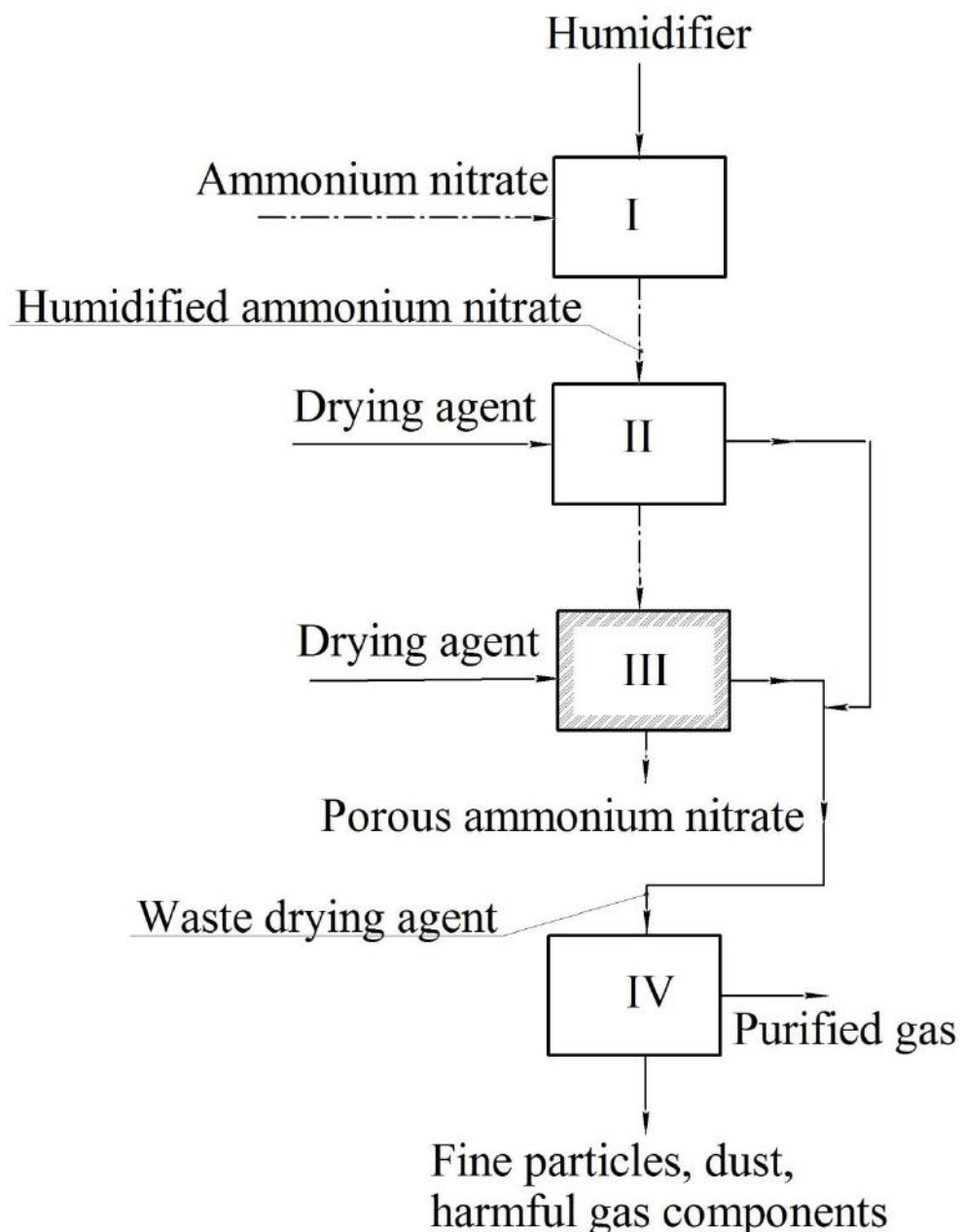


Fig. 12. Scheme of PAN production: 1 – humidification of ordinary ammonium nitrate

granules; 2 - granulation-drying; 3 - final drying; 4 - purification of exhaust gases.

The final value of the absorptivity can be increased due to more intensive drying under falling velocity. It is possible to carry out this process with prolonged drying in a drying agent's vortex stream only with a decrease in the strength index of the granules.

One should also note that ammonium nitrate is highly hygroscopic, that is one of the reasons for its caking. In the open air, it quickly becomes wet, then spreads out and loses its crystalline form. Therefore, the final drying stage, in addition to the possibility to obtain a developed nanoporous structure, can increase the storage period of PAN granules keeping their normative indicators.

An additional drying stage under the falling velocity mode in the active (but less turbulized) hydrodynamic mode will let us to achieve the necessary changes in the nanoporous structure of the granules.

Thus, the finally improved scheme for PAN production with the final drying stage is in fig. 12.

The experimental unit provides three stages of final drying.

The morphology of the  $\text{NH}_4\text{NO}_3$  granules surface was studied by scanning the electron microscopy using the device FEI Nova NanoSEM 650.

Other devices and equipment:

- thermocouple TC10-C; recording potentiometer KSP-3 – to measure the temperature in the heater;
- thermal imager Fluke Ti25, pyrometer Victor 305B – to measure the temperature in the granulator's workspace;
- multimeter DT-838 – to measure humidity of granules and air.

FTIR spectra were obtained by ATR technique using Nicolet iS50 FT-IR spectrometer (fy Thermo Scientific) in range from 4000 to 400  $\text{cm}^{-1}$  with resolution of 4  $\text{cm}^{-1}$  (no. of scans: 32) (sensitivity for finding of peaks was 95 %).

Four samples are prepared for research:

- the original granules of ordinary ammonium nitrate;
- granules of ammonium nitrate after heat treatment;
- granules of ammonium nitrate after the "humidification-heat treatment" stages in a vortex granulator;
- granules of ammonium nitrate after the "humidification -heat treatment" stages in a vortex granulator and the "final drying" stage in a multistage shelf device.

A thin film of an electrically conductive substance (carbon) was sprayed onto the surface of the samples to carry out the research.

The initial granule structure of ordinary ammonium nitrate is shown in fig.13.

A complete surface without a developed network of pores is peculiar for the sample. The surface structure is characterized by "mechanical" pores in the micrometer range. These pores arose directly upon production of the granules due to temperature stresses and mechanical effect on the packed granules during their transportation from the production place. Such granules can be used as an ANFO component without prior preparation. The absorptivity of the sample is quite high due to the large "mechanical" pores. The retentivity of the sample does not meet the standard indicator. The reason is that the diesel distillate easily leaves the granule (it flows from faults on its surface influenced by the gravity).

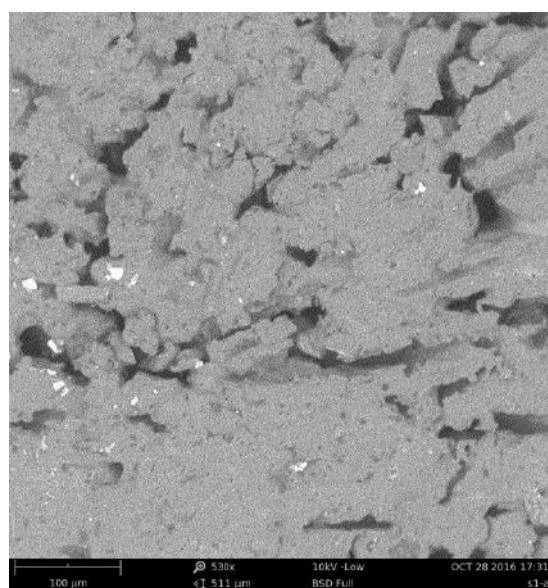


Fig. 13. The initial granule structure of ordinary ammonium nitrate

A sample of ordinary ammonium nitrate granules after heat treatment ("porization") is shown in fig. 14.

The formation of new "mechanical" pores in the micrometer range, appeared due to temperature stresses in the granule after an additional heat treatment cycle, is peculiar for the sample. Such granules have a high absorptivity. As for the retentivity in relation to the diesel distillate, it is sufficient to obtain an effective ANFO without its subsequent long-term storage and transportation.

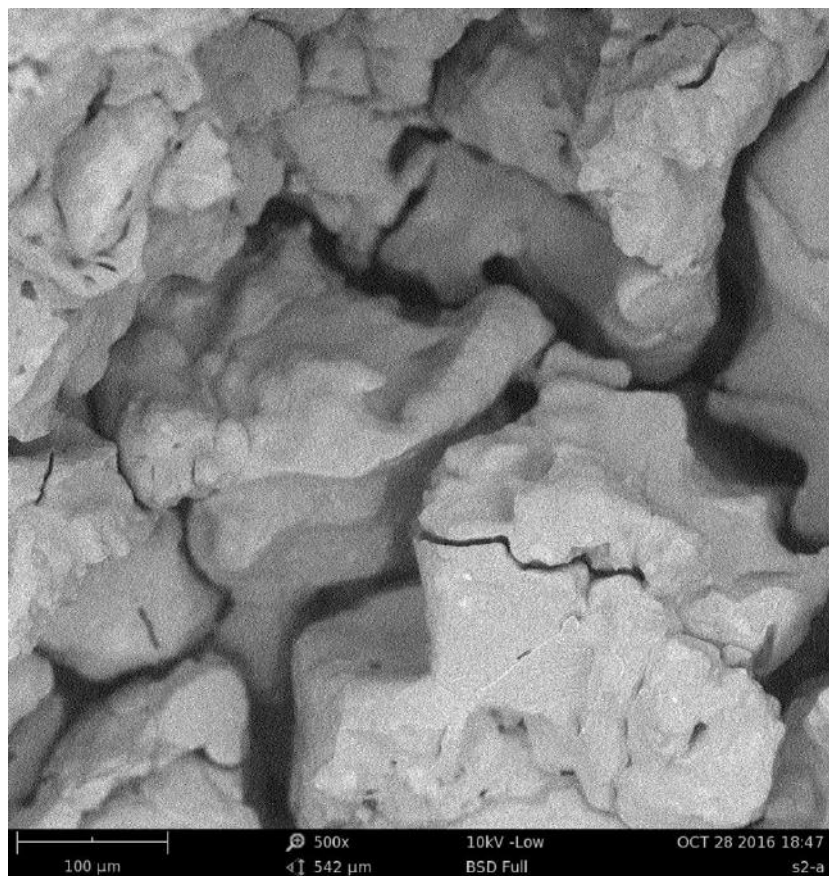


Fig. 14. The structure of the ammonium nitrate granules after heat treatment ("porization")

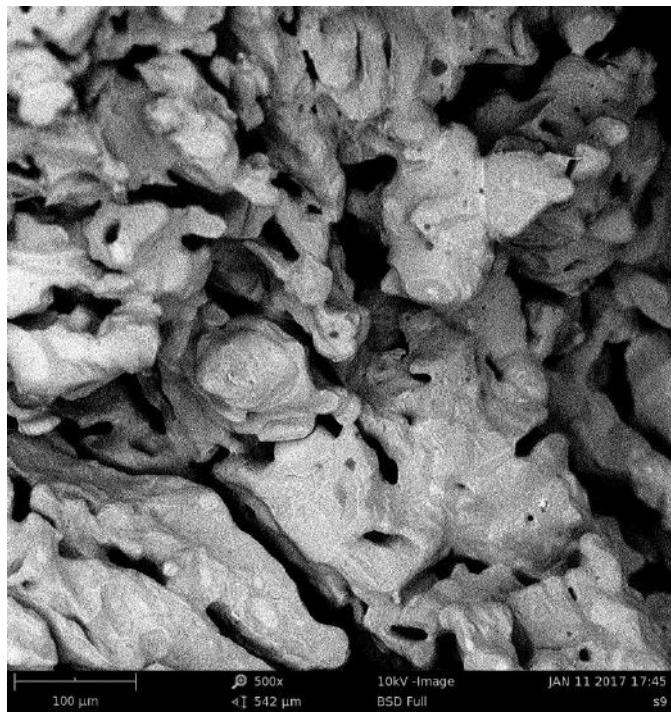


Fig. 15. PAN granule sample, obtained by humidification in a vortex granulator with subsequent heat treatment in the workspace of the same device

The PAN granule sample, obtained by the humidification method in a vortex granulator with subsequent heat treatment in the workspace of the same device, is shown in fig. 15. In addition to “mechanical” pores (their number is not greatly increased in comparison with the initial ordinary ammonium nitrate sample), “modification” pores of nanometer size are also present in the surface structure. The presence of these pores increases the retentivity of the PAN granules and provides the storage and transportation of ANFO to the blasting place. However, the presence of moisture in the granule leads to an undesirable change in the polymorphic transformations chain. A sequentially flowing chain of transformations II → III → IV replaces the transformation II → IV (the advantages of such a chain is described above). The granule becomes more porous and can be destroyed even due to a small external physical impact.

A PAN sample after the final drying stage in a multistage shelf device is shown in fig. 16.

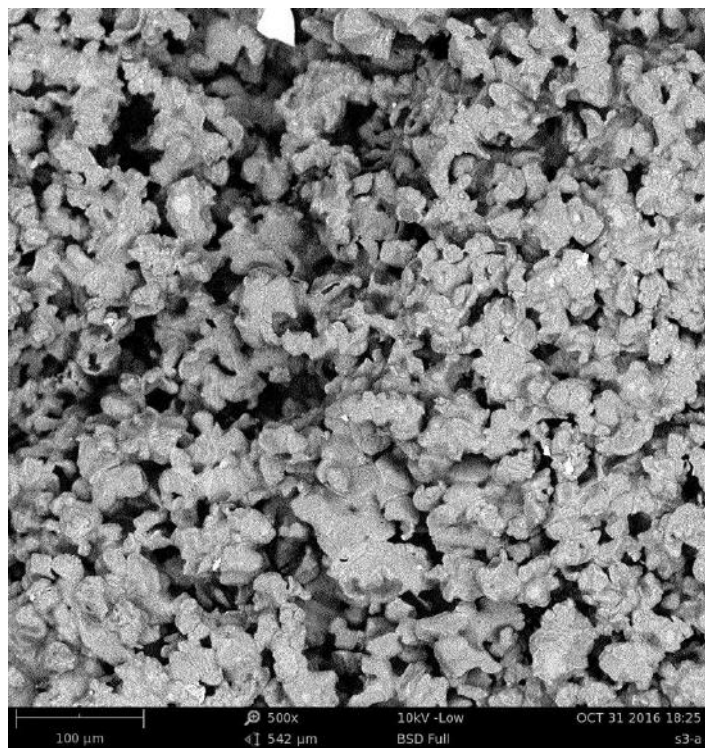


Fig. 16. PAN granules after the "humidification-heat treatment" stages in a vortex granulator and the "final drying" stage in a multistage shelf device.

The sample is characterized by an extensive network of deep curved (tortuous) mesopores of a "modification" nature and their uniform distribution over the entire surface of the granule. In this case, each pore is physically separated from the other and there are practically no united pores in the surface structure. Such a PAN sample (among other inherent advantages in the previous sample) can be successfully stored together with a diesel distillate in the pores due to a slight increase of the granules retentivity.

Sectioning of the dryer's workspace allows to carry out the final drying stage in the "soft" mode. At the same time, at each stage of the dryer's stage there are conditions, which ensure the minimum temperature stresses in the granule.

One should note that as time goes by, granules influenced by the diesel distillate, begin to loosen and soften. Therefore, it is not recommended to store PAN granules together with diesel distillate for a long time.

During the PAN obtaining process by the method of physical and thermal effects on the ordinary ammonium nitrate granule, it is important to ensure the constancy of the sample phase composition.

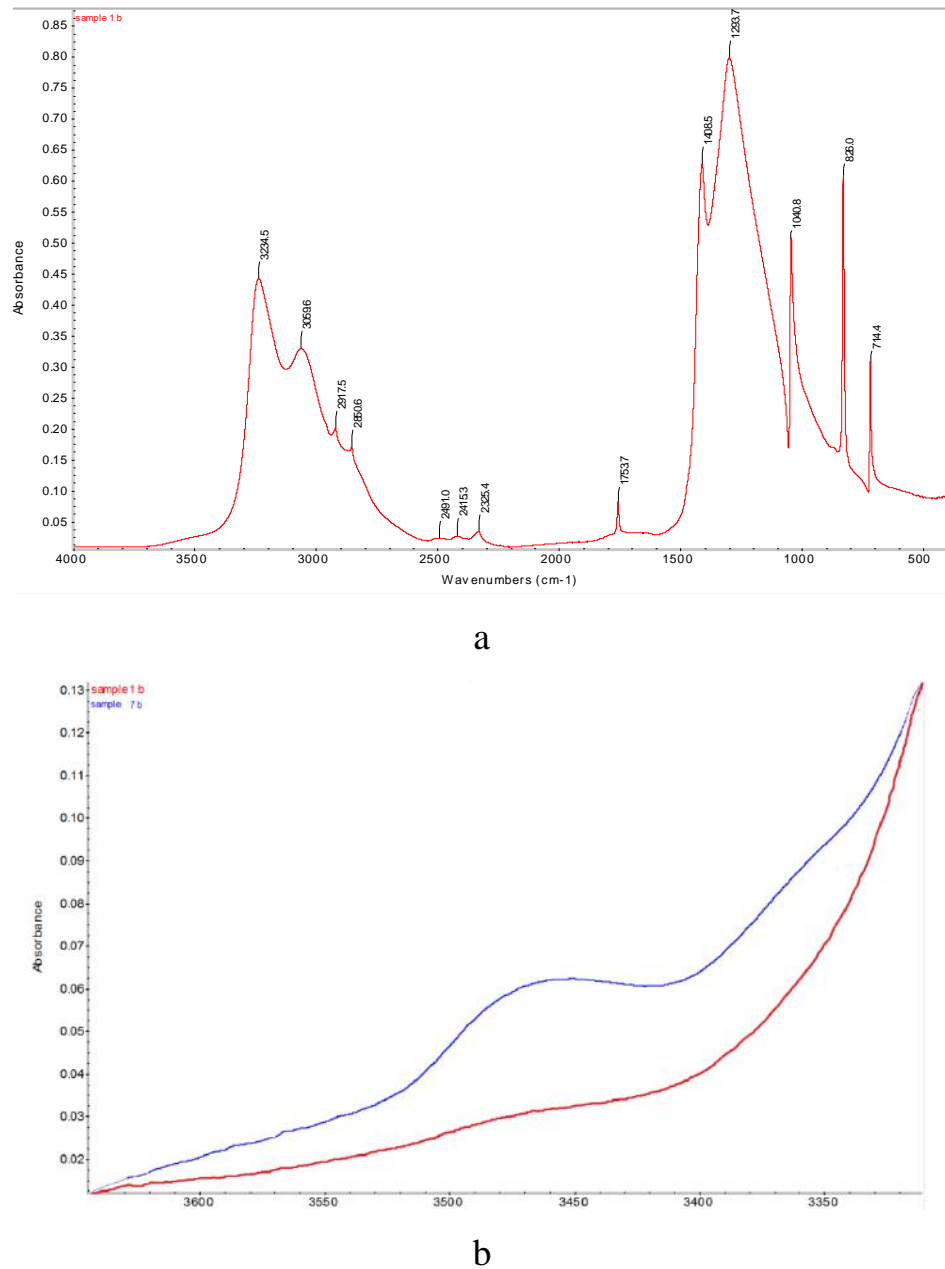


Fig. 17. FTIR spectra of PAN granule after the “humidification-heat treatment” stages in a vortex granulator and “final drying” stage in a multistage shelf device (a), an example of the comparative description of the FTIR spectra part of the initial granule (sample 1b) and PAN granules after the “humidification - heat treatment” stages in a vortex granulator and the “final drying” stage in a multistage shelf device (sample 7b,

area between wavenumbers 3390 and 3540 cm<sup>-1</sup>) (b)

The results of studies of FTIR spectra regarding the PAN granules for the last sample show that new phases are not formed during the implementation of the described method (fig 17 a). The presence of some splashes of intensity (as, for example, shown in fig 17 b) relates to the presence of moisture in the ammonium nitrate sample and to an increase in the heat treatment time due to the use of a multistage dryer.

## **4 MULTISTAGE SHELF DEVICES WITH FLUIDIZED BED FOR HEAT-MASS TRANSFER PROCESSES: EXPERIMENTAL STUDIES AND PRACTICAL IMPLEMENTATION**

*This section is prepared in accordance to data [4] and references in this work.*

Today the granular mineral fertilizers and bulk granular products are produced using several typical technological processing schemes. When developing technical plans for producing mineral fertilizers, developers and constructors face the difficulties in selecting the necessary equipment for the operating production departments, namely, for the granulation and enlargement of granules, their drying, cooling, and pneumatic separation.

The most effective units to implement the above purposes are fluidized bed devices. One should mention that despite effective processes in the fluidized bed, the heat-mass transfer ends at a low layer height, nearby the grid zone. In this case, most energy in the gas flow is taken for the hydrodynamic stabilization of the fluidized bed, the height of which reaches 0.2–0.5 m. It increases energy consumption and abrasion of particles, causing the necessity to install energy-intensive and metal-intensive dust cleaning systems.

Thus, scientific research in the field of dispersed system processes intensification should be oriented primarily to the development of energy-saving fluidized-bed devices with a new organization of gas-dispersed flows, in which minimal costs for the process and dust cleaning provide an adequate efficiency. Multistage shelf devices implement these tasks. In shelf devices, active aerodynamic regimes of solid particles weighing are implemented, and the conditions for their creation, unlike typical fluidized bed devices, can be easily changed over a wide range of gas flow velocities without fundamental changes in the construction.

Devices with various construction are used for granulation in a fluidized bed. The shape of the unit defines the hydrodynamic features of the process. In the conical-cylindrical part of the device, fluidization is uniform over the entire section in a more than

300 mm height bed that increases the energy cost for weighing a high bed. There is a local spouting zone with an additional supply of gas flow in the center of the gas distribution grid. This approach increases the heat-mass transfer process efficiency. However, it requires a separate supply of gas flow into the holes of the gas distribution grid and the nozzle in its center. In some fluidized bed granulators, a special spraying mode of the melt by the nozzle is formed, or a fluidization jet-pulsating mode is created.

The fluidized bed enables to intensify the contact of the phases between the drying agent and the surface of the particles, which are convectively dried. Moreover, both traditional drying technologies in a fluidized bed and special drying using acoustic fields, microwave heating, vibration, or special mixing methods are implemented. The microwave heating of ceramic microspheres in a fluidized bed made it possible to control the drying kinetics without significant agglomeration of the dried particles. The vibrational oscillations overlaid on a fluidized bed of solid particles are mostly applied in the fluidization method. A positive effect has been proved in the intensification of phase contact in a vibrating fluidized bed, in comparison with a stationary layer, optimal features are selected. It is indicated that gas-vibro-fluidization usually has higher circulation velocities compared to conventional gas-fluidization. The vertical oscillations overlaying the vibration layer shows that vibration can help fluidize particles, and the axial and radial distribution of holes in a layer with vibration is more uniform than without it.

Fluidized bed devices in the mineral fertilizers producing technology are mostly known as coolers for granular materials. Although heat exchange processes in a fluidized bed are efficient enough, these devices are characterized by increased specific consumption of cooling air.

The authors proposed to use a vertical device with a fluidized bed of granules on vibrating blades for cooling granules. It is indicated that synchronous oscillations of the blade and the fluidization regime affect the final temperature and humidity of the granules during the cooling process. However, the complexity and operational unreliability of the construction is confirmed by the presence of cushioning springs and vibration devices.

In fluidized bed units, during fluidization, small particles are separated with the ascending gas flow. Their number is identified either by hydrodynamic factors (gas flow velocity) and layer height or by granulometric composition and physical properties of the particles in the initial product. The positive effect of vibrational oscillations on the separation process of small particles from the fluidized bed is noted.

The constructive parameters also identify the fluidization quality. Thus, in, the motion of particles in a stable turbulence regime of a fluidized bed was studied when the air distribution blades were installed at different angles, which led to stable layer fluidization of particles of various sizes and shapes. In the work, a system for the more uniform supply of the product to a fluidized bed was studied, and the authors indicated that hydrodynamics and heat transfer can be significantly improved due to the internal circulation of solid particles using two gas distributors.

The complex hydrodynamics of the fluidized bed by a gas flow is described by disordered mixing of solid particles and the formation of gas bubbles. The effect on the fluid dynamics of a fluidized bed of various parameters was studied: gas injection time into the bed, gas flow velocity and bubbling regime, bubble dynamics during nonspherical particles fluidization, continuous injection of the central air jet into the bed, and features of the pseudo-two-dimensional two-zone gas–solid fluidized bed, from the features of solid particles and gas bubbles. Researchers also paid attention to the study of the interphase heat transfer intensity between particles and the gas flow and heat transfer to heat exchange surfaces located in the layer. One research studied the effect on the heat transfer of the gas flow uneven distribution, which led to the heat transfer intensification due to the higher packet updating frequency. Next research considered the influence of the rate of contact renewal between solid particles and a vertical heat tube placed in a fluidized bed. The influence of the bubble frequency and gas retention on heat transfer with vertical tubes dipped into a fluidized bed was studied. Since the coefficients of heat transfer between particles and heat transfer surfaces are higher in the center of the layer than at its periphery, it is proposed in to use a gas distributor with an inhomogeneous nozzle array to overcome the unevenly distributed heat transfer.

Thus, the above review of scientific articles showed that researchers direct their efforts to a detailed study of the hydrodynamic and structural features of the fluidized bed to increase the operating efficiency of the device. However, at the same time, one of the significant drawbacks of fluidized beds consists of rather high energy costs to weigh a significant amount of material on a gas distribution grid (more than 1–2 m<sup>3</sup> of gas/kg of product). The separation of small particles of less than 500 μm in size from the fluidized bed leads to the formation of large volumes of dusty exhaust gas with a low dust concentration in it. Purification of such gases from dust requires powerful gas cleaning systems.

The fluidized bed devices for organizing the motion of gas-dispersed flows are between shaft-type devices (with particles of material falling downward and moving countercurrent of gas) and pneumatic transportation devices (with direct ascending flow motion). Both types have disadvantages—insignificant contact of phases and, accordingly, low heat transfer coefficients between particles and gas flow, as well as the short residence time of particles in a flow. Therefore, such devices are not so effective and are very high-priced.

One of the solutions that allow stabilizing the operation of a fluidized bed apparatus is the swirling of flows, which has found application, for example, in the granulation devices. The data of theoretical and computer modeling of the operation of such devices as applied to the production of porous ammonium nitrate is confirmed by the successful testing of product samples.

The authors of this article have chosen another way to improve the fluid dynamics of the fluidized beds—namely, a method to weigh solid particles on a gas distribution grid. The gas distribution grid (shelf) is installed in a vertical channel at an angle of 25–45° to the horizon forming the outloading space between the end of the shelf and the channel wall. There can be several shelves throughout the height of the device. This feature enables to create various gas-dispersed flow modes in shelf units, in which not only the basic features of the flow are quantitatively changed (concentration of solid particles in the gas flow, velocities, heat-mass transfer coefficients), but there are

qualitative changes in flow structure, phase motion mechanism, and heat-mass transfer conditions under certain critical conditions. Thanks to the various hydrodynamic modes of the solid particles transfer (from the gravitationally falling to the weighted layer), the shelf contact elements provide higher efficiency of heat-mass transfer and separation processes with a lower gas flow rate and hydraulic resistance than typical fluidized bed devices do.

High efficiency, lower capital and operating costs, small dimensions and hydraulic resistance, higher specific productivity of shelf devices in comparison with typical units of a weighted layer, make the first up-and-coming devices for being used in various industries.

Experimental research was carried out in the device with a cross-section of  $50 \times 100$  mm and a height of up to 1 m with a separation space (fig. 18).

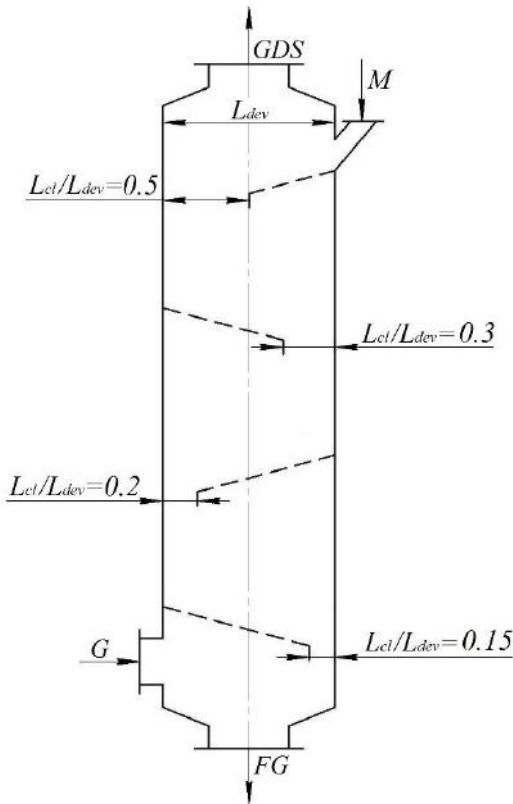


Fig. 18. Multistage shelf device circuit: M—raw material; G—gas; GDS—gas-dispersed substance; FG—finished granules.

Shelf contact elements differ from gas distribution grids of fluidized-bed devices and wedge-shaped elements plates primarily due to the presence of outloading space between the end of the shelf and the wall in the unit (fig. 19). The width of the outloading space is expressed by the ratio  $L_{cl}/L_{dev}$ , where  $L_{cl}$  is the distance between the end of the shelf and the wall of the device, and  $L_{dev}$  is the length of the side section of the device. It is possible to influence the gas flow distribution between the outloading space and the holes of the shelf, as well as on the ascending flow velocities in the separation space and the solid phase, moving along the shelf, by varying the  $L_{cl}/L_{dev}$  ratio, the perforation degree of the shelf  $\psi$ . The tilt angle of the shelf  $\gamma$  to a lesser extent affects the velocities profile of the gas flows over the outloading space and the holes of the shelf. The optimal tilt angle of the shelves is  $\gamma = 25^\circ$  to the horizontal plane (Figure 2). The material particles lay on the surface of the shelf at a smaller angle. The particles quickly roll down to the outloading space and do not form a weighted layer above the shelf at a larger angle. The distance between the end of the upper shelf and the beginning of the lower shelf  $L_s$  is determined by the ratio between this distance to the length of the lateral part of the section in the device— $L_s/L_{dev}$ . If  $L_s/L_{dev} < 0.5$ , the gas flow velocity in the outloading space increases. As a result, the free flow of material particles is impeded through the outloading space to the lower shelf. As the distance  $L_s$  increases, the gas flow velocity in the outloading space naturally decreases. When  $L_s = L_{dev}$  the flow rate is constant. Therefore, we take  $0.5 < L_s/L_{dev} \leq 1$  in the construction of the device.

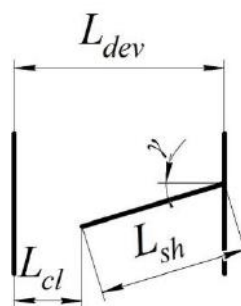


Fig. 19. The basic elements of the shelf device construction.

A polydisperse granular superphosphate mixture in the form of a 0.1–5 mm granule with a shape factor of 0.85 was used in the studies. The sieve analysis using wire sieves with aperture sizes (the size of the square hole side) 0.5, 1.0, 1.6, and 2.5 mm defined the

granulometric composition of the polydisperse mixture. The sieves were folded in a vertical block with decreasing hole sizes from top to bottom and installed on a vibrating table with a control unit. Sieve analysis was carried out for 15–20 min, corresponding to the measurement accuracy. Several samples were analyzed according to the methodology to assess the accuracy of the measurement. The deviation of the results for each sample did not exceed 1.5–2.0%. The results of the sieve analysis of the initial polydisperse mixture are as follows: +2.5 mm—10%; 2.5 + 1.6 mm—25%; 1.6 + 1 mm—25%; 1 + 0.5 mm—20%; 0.5 mm—20%. According to the reference data, the true and bulk density of superphosphate granules obtained by the nodulizing method in a drum granulator was 2250 kg/m<sup>3</sup> and 1100–1200 kg/m<sup>3</sup>.

The laboratory unit consisted of a device equipped with a loading hopper with a belt feeder and an unloading hopper, a centrifugal cyclone to capture fine fractions with an unloading hopper, a high-pressure fan for pumping air through the device, and a cyclone. The walls in the device from the front side were transparent for visual observation and filming.

The initial mixture of the granulated superphosphate with amount of 3 kg was weighed on an electronic scale with an accuracy of 0.1 g. The mixture was heated to 90–95 °C in the loading hopper with electric heating elements (it corresponds to the temperature at the outlet of the drum granulator dryer) and fed by the belt feeder into the device on the upper shelf. The moisture content of the granules was less than 1 wt% at this temperature, not affecting the heat transfer process. The specific productivity of the raw material was 6–10 kg/(m<sup>2</sup>·s). Air was sucked through the device by a high-pressure fan. The air flow was regulated and measured by a calibrated collector with a control valve. The air temperature at the inlet to the device was equal to the temperature in the laboratory: in summer conditions—22–27 °C; in winter conditions—18–22 °C. The material cooled to a temperature of 40–45 °C, was accumulated in the unloading hopper and unloaded at the end of the experiment. A small fraction of the material was trapped in the cyclone by the ascending air flow. When the device operated in a stationary mode (it was installed 15–20 s after turning on the feeder), 5–6 were selected from the unloading

hopper and after the cyclone. The unloading hoppers were doubled to eliminate air leaks during material sampling. Spring-loaded valves were installed in the lower hopper. Then, the samples were weighed on an electronic scale with an accuracy of 0.1 g. For sieve analysis, the arithmetic mean value was taken from the weights of the selected samples. Several samples taken during repeated experiments under the same conditions were analyzed to assess the accuracy of the performed measurements. The deviation of the measurement results for each fraction between the selected samples was 1.5–2.0%. There were six experiments to eliminate the influence of random factors on the reliability of the measurement results.

The research regarding the features of one- and two-phase flows motion hydrodynamics in a shelf device was carried out with gas flow velocities of 1–5 m/s. A semiconducting thermoanemometer with an accuracy of 0.001 m/s measured the gas flow velocities in the workspace of the device. The measuring sensor was installed in the unloading space and the area above the shelf every 10 mm along the horizontal line. The measuring sensors were moved in height every 40 mm. There were four horizontal measurement lines above the shelf. The position of the thermoanemometer sensor was determined by the  $X_{dev}/L_{dev}$  ratio, where  $X_{dev}$  is the current distance from the initial plane (the left wall of the device) along the section length  $L_{dev}$  of the device.

An alcohol U-shaped manometer measured the pressure difference of the device. One tube of the manometer was connected to a point of the body under the lower shelf, and the second—at the gas outlet after the upper shelf. The measurement error when setting two levels (on each tube) was  $\pm 2$  mm at an ambient temperature of  $20 \pm 5$  °C.

One used filming under stroboscopic illumination at a frequency of 32 frames per second through the transparent walls of the device for establishing the mechanism and peculiarities of the gas-dispersed flow motion.

The research on the heat transfer peculiarities between the solid phase and the gas flow was carried out by cooling the superphosphate granules with an air flow. The temperature regime in the workspace of the device was controlled by thermocouples

“Chromel-Copel” with open junctions through a self-recording potentiometer with an accuracy of 0.5 °C.

The thermocouple sensor was a protective metal case like a tube with a diameter of 1 mm and 60 mm long. There was a junction of interconnected chrome and copel thermoelectrodes 0.1 mm in diameter at the end of the tube. The heat capacity of this junction is negligible. It enables to perform measurements under conditions of continuously changing temperatures. Temperature sensors were installed at the following points: in the outside air supply pipe—to the device, in the loading hopper and unloading hoppers—after the device and the cyclone, in the separation space—at the outlet of the gas-dispersed flow from the device. The weighted layer temperature on the lower shelf was measured by placing three sensors along the entire length of the shelf at the height of up to 5–8 mm, one in the unloading space area and two at the gas flow outlet from the weighted layer.

The heat transfer coefficient was calculated from the basic equation of heat transfer, while the total surface area of the particles was estimated per unit volume of the layer. The velocities of solid particles in the layer are small compared to the gas flow rate. The ratio between the gas velocity in the free section of the device and the gas velocity between the particles in the layer varies over the section and height of the device. Therefore, it is advisable to consider the gas flow rate in the free section of the device when determining the Reynolds criterion.

As a criterion for assessing the cooling degree of the product in the cooler, a cooling coefficient was used, which is the ratio of the actually removed heat to the amount of heat that is removed when the material is completely cooled to the initial temperature of the cooling air:

$$K_{cool} = \frac{Q_{act}}{Q_{ful}} = \frac{t_{gi} - t_{gf}}{t_{gi} - t_{ai}}, \quad (9)$$

where  $t_{gi}$ ,  $t_{gf}$ ,  $t_{ai}$ —respectively, the initial, final temperature of the granules, and the initial temperature of the cooling air, °C.

The efficiency of small particles separation from the weighted layer was characterized by the small fraction extraction degree into the ablation  $\varepsilon_m$ , representing the ratio of the small fraction size in the ablation to its amount in the raw material.

The total aerodynamic resistance  $\Delta P$  is defined as a set of resistances of the degrees in the shelf device (pressure loss on the shelf)  $\Delta p_i$ :

$$\Delta P = \sum_{i=1}^n \Delta p_i \quad (10)$$

The aerodynamic resistance of each shelf contact depends on the nature of the gas flow interaction with the shelves, installed at a certain angle, the shelf perforation degree  $\psi$ , the dispersed material amount in the inter-shelf space, characterized by the layer porosity  $\varepsilon$  or the concentration of the solid particles in the workspace of the device  $\beta$ . One should note that the specified pressure drop in the holes will decrease along the shelf. Therefore, the efficiency of the perforation holes with the same diameter will also decrease approaching the outloading space.

The pressure loss for elementary jet moving along a perforated shelf can be considered as the sum of the losses along the shelf length with the current coordinate X and local loss through the perforation holes:

$$\Delta p_i = const = \lambda \cdot \frac{X}{d_e} \cdot \frac{\rho_{gas} \cdot W_{gas}^2}{2} + \xi_{hol} \cdot \frac{\rho_{gas} \cdot W_{hol}^2}{2}, \quad (11)$$

where  $\lambda \cdot \frac{X}{d_e} \cdot \frac{\rho_{gas} \cdot W_{gas}^2}{2} = \Delta p_l$  —pressure loss along the shelf length with current coordinate, Pa (where  $\lambda$ —friction coefficient);  $d_e$  is the equivalent diameter of the shelf

contact, m;  $d_e = \frac{4L_{sh}B_{dev}}{2(L_{sh} + B_{dev})}$ ;  $L_{sh}$  is the shelf length, m;  $B_{dev}$  is the width of the device, m;  $W_{gas}$  is the cross section velocity of the gas flow, m/s;  $\rho_{gas}$ —gas flow density, kg/m<sup>3</sup>;  $\xi_{hol} \cdot \frac{\rho_{gas} \cdot W_{hol}^2}{2} = \Delta p_{hol}$ —local loss in the perforation hole, Pa (where  $\xi_{hol}$  is the coefficient of the hole resistance);  $W_{hol}$ —flow velocity in the perforation holes, m/s.

Thus, the total pressure loss between the control cross-sections consists of two components:

$$\Delta p_i = \Delta p_{hol} + \Delta p_l, \quad (12)$$

where

$$\Delta p_{hol} = \Delta p_i - \Delta p_l. \quad (14)$$

Air velocity in the perforation holes:

$$W_{hol} = \varphi \cdot \sqrt{\frac{\Delta p_{hol}}{\rho_{gas}}} = \varphi \cdot \sqrt{\frac{\Delta p_i - \Delta p_l}{\rho_{gas}}} = \varphi \cdot \sqrt{\frac{\Delta p_i - zX}{\rho_{gas}}}, \quad (15)$$

where  $\varphi$  is the velocity coefficient, which is 0.97–0.98 according to the experimental data;  $z$ —specific pressure loss along the length, Pa/m.

The air flow loss through the holes of the shelf perforation is the following:

$$V_{sh} = \int_0^{L_{sh}} W_{hol} df_{sh} = \varphi \cdot B_{dev} \int_0^{L_{sh}} \psi \cdot \sqrt{\frac{\Delta p_i - zX}{\rho_{gas}}} dX, \quad (16)$$

where  $df_{sh} = dX \cdot B_{sh}$ ;  $\psi$ —degree of shelf perforation (free shelf cross-section);  $f_{sh}$ —shelf area, m<sup>2</sup>.

In the outloading space  $L_{cl}$  (fig. 19) the pressure drop  $\Delta p_{cl}$  will be minimal:

$$\Delta p_{cl} = \Delta p_i - zL_{sh}, \quad (17)$$

and the air flow loss is defined as

$$V_{cl} = \varphi \cdot L_{cl} \cdot B_{dev} \cdot \sqrt{\frac{\Delta p_i - zL_{sh}}{\rho_{gas}}}. \quad (18)$$

Total air flow rate is  $V_{sh} + V_{cl}$ . We will define the total air flow rates by integrating the ascending velocity function along the length of the perforated shelf and taking the constant perforation degree:

$$V = B_{dev} \int_0^{L_{sh}} W_{hol} dX = \varphi \cdot \psi \cdot B_{dev} \int_0^{L_{sh}} \sqrt{\frac{\Delta p_i - zX}{\rho_{gas}}} dX. \quad (19)$$

Substitution of the subintegral expression by a function  $y = \Delta p_i - zX$ , where  $dy = -z dX$  enables to obtain the integration result within  $(0, L_{sh})$ :

$$V_{sh} = \frac{-B_{dev} \cdot \varphi \cdot \psi}{z \cdot \sqrt{\rho_{gas}}} \int_0^{L_{sh}} y dy = \frac{2 \cdot B_{dev} \cdot \varphi \cdot \psi}{3 \cdot z \cdot \sqrt{\rho_{gas}}} \cdot \left( \sqrt{\Delta p_i^3} - \sqrt{(\Delta p_i - z \cdot L_{sh})^3} \right). \quad (20)$$

The share of the flow through the outloading space is added to the balance equation of air flow rate along the cross-section of the shelf unit:

$$\begin{aligned} W_{gas} \cdot L_{dev} \cdot B_{dev} &= V_{sh} + V_{cl} = \\ &= \frac{2 \cdot \varphi \cdot \psi}{3 \cdot z \cdot \sqrt{\rho_{gas}}} \cdot B_{dev} \cdot \left( \sqrt{\Delta p_i^3} - \sqrt{(\Delta p_i - z \cdot L_{sh})^3} \right) + \varphi \cdot L_{cl} \cdot B_{dev} \cdot \sqrt{\frac{\Delta p_i - z \cdot L_{sh}}{\rho_{gas}}}, \end{aligned} \quad (21)$$

where  $W_{gas} \cdot L_{dev} \cdot B_{dev}$  —total air flow rate in the device.

The analysis of Equation (20) allows to calculate the gas flow velocity above the perforated shelf with the free cross-sectional area  $f_{cs} = \psi \cdot L_{sh} \cdot B_{dev}$ :

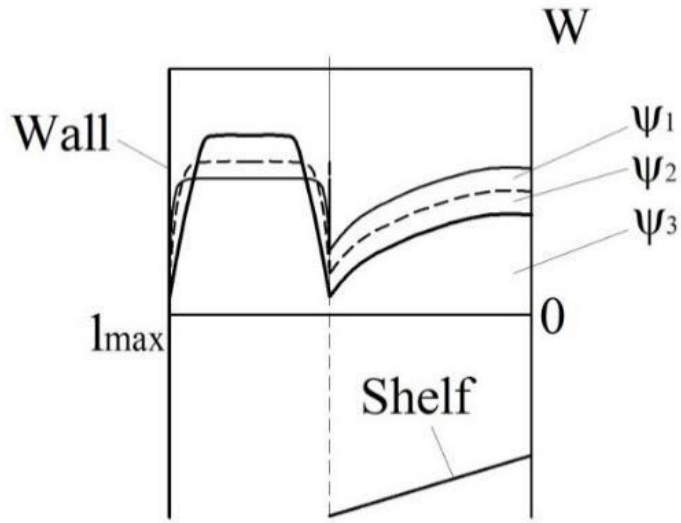
$$W_{cr1} \cdot \psi \cdot L_{sh} \cdot B_{dev} = \frac{2 \cdot \varphi \cdot \psi}{3 \cdot z \cdot \sqrt{\rho_{gas}}} \cdot B_{dev} \cdot \left( \sqrt{\Delta p_i^3} - \sqrt{(\Delta p_i - z \cdot L_{sh})^3} \right). \quad (22)$$

This ratio defines the pressure loss  $\Delta p_i$  when installed in the workspace of one shelf device. It is possible to vary the constructive parameters of the shelf, namely its length and perforation degree. It is also possible to obtain profiles of the vertical velocities of the gas flow in the space above the shelf and the outloading space according to the algorithm below.

Comparing the total flow rates in the perforation holes to the flow rates calculated through the total area of the shelf ( $W_{hol} \cdot \psi \cdot f_{sh} = \overline{W}_{hol} \cdot f_{sh}$ ), one can find the average velocity of the gas flow over the perforation holes in the vertical direction, taking into account Equation (15):

$$W_{gas} = \overline{W}_{hol} = \psi \cdot W_{hol} = \psi \cdot \varphi \cdot \sqrt{\frac{\Delta p_i - zX}{\rho_{gas}}}. \quad (23)$$

An analysis of this expression showed, first, that the local velocity of the gas flow above the holes in the vertical direction decreases linearly depending on the shelf perforation degree  $\psi$  and nonlinearly in the  $X$  direction along the shelf length to the outloading space (fig. 20).



$$\psi_i < 1; \psi_1 > \psi_2 > \psi_3 \text{ (diagram with pressure losses)}$$

Fig. 20. Vertical velocity profiles over the shelf and in the outloading space, depending on the shelf perforation degree  $\psi$  (qualitative distribution).

As a result of the free cross-section narrowing of the vertical channel, the inclined perforated shelf installation in the workspace of the shelf device causes a local increase in the velocity and turbulence of the gas flow in the outloading space and a change in the profile of gas flow velocities under the surface of the shelf and above it. As can be seen from fig. 21 (curves 1 and 2), a decrease in the value of the  $L_{cl}/L_{dev}$  ratio from 0.5 to 0.15 significantly increases the uneven distribution of the gas flow over the section of the workspace in the device in comparison with the installation of the perforated grid completely overlying the section of the workspace in the device (an analogue of the fluidized bed device (fig. 21, curve 4)), or the free channel (a pneumatic tube device (fig. 21, curve 5)). In this case, the width of the zone where the gas flow comes through the outloading space decreases, its absolute velocity and the profile of gas flow velocities in the workspace of the device is changed.

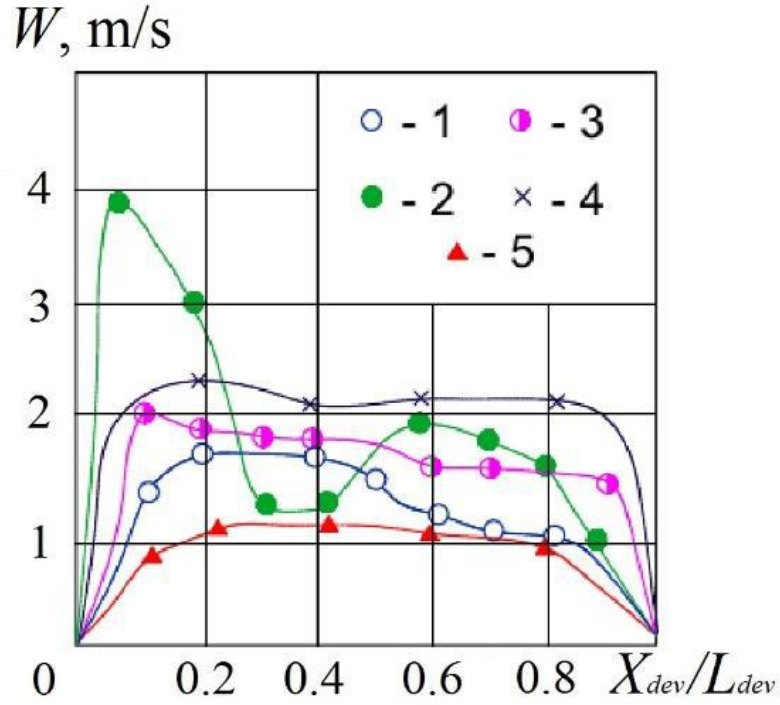


Fig. 21. The distribution of gas flow velocities along the section length of the device where the shelf is installed: 1— $L_{cl}/L_{dev} = 0.5, \psi = 15\%$ ; 2— $L_{cl}/L_{dev} = 0.15, \psi = 15\%$ ; 3— $L_{cl}/L_{dev} = 0.15, \psi = 30\%$ ; 4— $L_{cl}/L_{dev} = 0$ ; 5— $L_{cl}/L_{dev} = 1$ . Tilt angle of the shelf— $\gamma = 25^\circ$ . Gas flow velocity in the free cross-section—1.2 m/s.

If  $L_{cl}/L_{dev} = 0.5$  and the degree of the shelf perforation is 15% (Figure 4, curve 1) in the above-shelf space, the absolute values of the gas flow velocities are practically constant over the section of this space and reach a maximum only in the outloading space and above it. If  $L_{cl}/L_{dev} = 0.15$  (Figure 4, curve 2) the velocity profile has two maximum values: in the zone above the outloading space and at the middle level of the inclined shelf. This fact is explained by the differential “dividing” effect of the inclined shelf on the profile of gas flow velocities in or another one quantity through the outloading space and the holes in the inclined shelf. In the first case, the inclined shelf does not cause such a significant unevenness in the profile of gas flow velocities in the workspace of the device beyond its input point. In the second case, due to an increase in the resistance to the gas flow, caused by a sharp narrowing of the free cross-section in the device, significant swirlings arise at the inclined shelf edge. It defines the presence of a zone with

a reduced gas flow velocity in the space above the end of the shelf. An increase in the perforation degree of the inclined shelf to 30% (Figure 4, curve 3) levels out the unevenness of the velocity profile over the cross-section of the workspace in the device since the gas flow is redistributed into the holes of the shelf due to a reduction of the hydraulic resistance of the shelf to its access.

A comparison of the experimental (fig. 21) and theoretical velocity profiles (fig. 20) shows a sufficient coincidence between the nature of the gas flow velocities change along the cross-section of the workspace in the device. The absolute value of the gas flow velocity in the outloading space with a decrease in the  $L_{cl}/L_{dev}$  ratio from 0.5 to 0.3 grows insignificantly for a shelf with a perforation degree from 0% to 30% (fig. 22).

Under the conditions of the further decrease in the  $L_{cl}/L_{dev}$  ratio up to 0.15, the gas flow velocity in the outloading space increases by 2.5–3 times in comparison with the average gas flow velocity in the free cross-section of the device. With a decrease in the perforation degree of the shelf cross-section, this growth is more significant since the hydraulic resistance to the gas flow through the holes of the shelf contact is increased and the gas flow is redistributed towards the outloading space. The gas flow velocity in the outloading space reaches its maximum value at  $L_{cl}/L_{dev} = 0.15$  for shelves with a perforation degree from 0% to 30%. If  $L_{cl}/L_{dev} < 0.15$ , the gas flow velocity in the outloading space decreases since the hydraulic resistance to the gas flow through the outloading space is increased so much that most of the flow passes through the holes of the shelf. If the shelf contact has a perforation degree of 0% (solid shelf), there is no redistribution, and the gas flow velocity in the outloading space continuously increases with reduction of  $L_{cl}/L_{dev}$  ratio (fig. 22, curve 1).

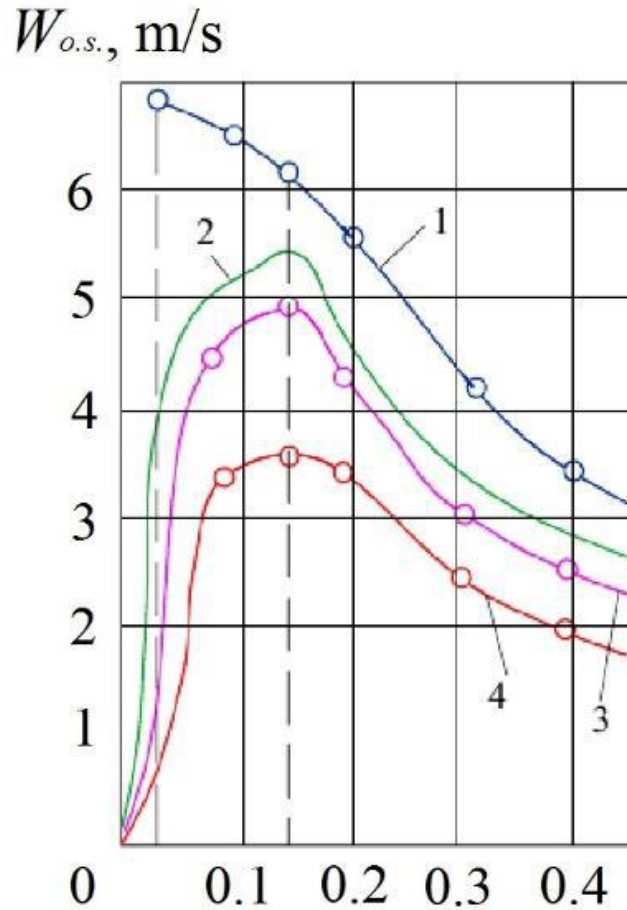


Fig. 22. The dependence of the gas flow velocity in the outloading space on the constructive parameters of the shelf. Shelf perforation degree  $\psi$ : 1–4—respectively, 0%, 5%, 15%, 30%. The tilt angle of the shelf— $\gamma = 25^\circ$ . Gas flow velocity in the free cross-section—1.65 m/s.

A change in the constructive parameters of the shelf has a significant effect on the uneven profile of gas flow velocities. It is reasonable to represent its quantitative measure by the dimensionless coefficient of the gas flow uneven distribution  $n$ , which is the ratio of the gas flow passing through the outloading space  $V_{o.s.}$  to its quantity in the holes of the shelf  $V$  (fig. 23).

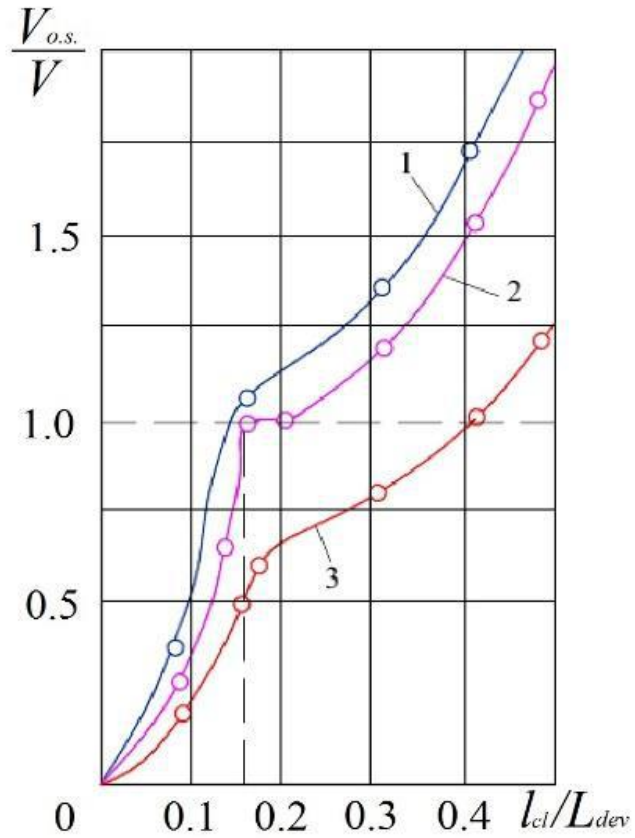


Fig. 23. The influence of the constructive parameters of the shelf on the uneven profile of gas flow velocities. Degree of the shelf perforation  $\psi$ : 1–3—respectively, 5%, 15%, 30%. The tilt angle of the shelf— $\gamma = 25^\circ$ . Gas flow velocity in the free cross-section—1.65 m/s.

If the coefficient of the gas flow uneven distribution is more than 1, the gas flow passes mainly through the outloading space, and if less than 1—through the holes of the inclined shelf. If the coefficient of the gas flow uneven distribution is 1, the flow is distributed in equal amounts both through the outloading space and through the holes of the shelf.

The special nature of the gas flow distribution determines the conditions for the emergence of various hydrodynamic modes of interaction between solid particles in the material and the ascending gas flow. It enables widely to influence the heat treatment efficiency (for example, cooling and drying) of granular and grained materials in devices with inclined perforated shelves.

At low gas flow velocities, the material continuously fed into the device with a flow rate of  $6 \text{ kg}/(\text{m}^2 \cdot \text{s})$  moves along the surface of the inclined shelf in the form of a rapidly “jumping” layer since the particles at the outlet of the supply pipe have sufficient inertia force. The porosity of such a layer reaches 0.8–0.85, and the concentration of material particles in it is  $20\text{--}30 \text{ kg/m}^3$  ( $0.15\text{--}0.2 \text{ m}^3/\text{m}^3$ ). Particles of the material after moving along the inclined shelf surface with a velocity of 0.2–0.3 m/s are inhibited at the device wall in the outloading space and are accumulated on the wall surface (fig. 24 a).

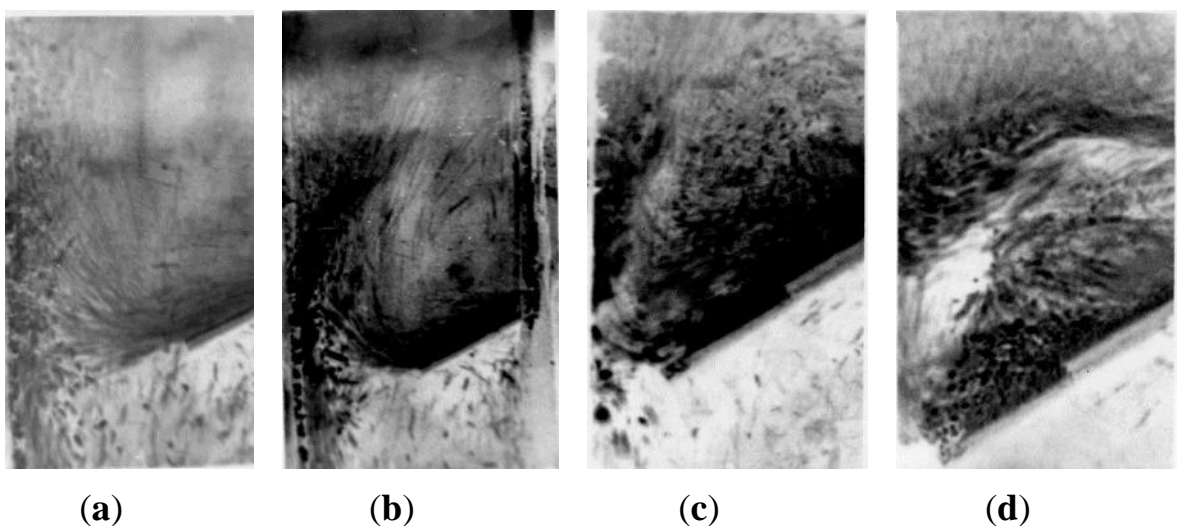


Fig. 24. Photographic image of hydrodynamic modes: (a) “gravitationally falling layer” mode; (b) “transitional” mode; (c) “weighted layer” mode; (d) “piston” mode.

The accumulated particles layer is blown by the ascending gas flow. Moreover, the layer mass due to the arrival of new portions of solid particles of material gradually increases. At a certain point in time, it exceeds the aerodynamic force of the ascending air flow, after which some of the particles are fallen down the device through the outloading space. In this nature of the motion of the material particles, both on the inclined shelf surface and the outloading space, the aerodynamic forces of the ascending flow do not provide sufficient resistance to the motion of the solid particles. The main part of the material moves in the form of a thin layer through the outloading space mainly by gravitational forces. Therefore, this nature of the motion of the solid particles in the material was called the “gravitationally falling layer” mode.

By increasing the gas flow velocity, its impact on the material layer grows. It begins to weigh particles both on the shelf contact surface and near the surface of the device wall in the outloading space (fig. 24 b). In this case, the porosity of the material layer moving along the surface of the inclined shelf decreases to 0.7–0.75, and the concentration of solid particles of the material increases accordingly to 80–150 kg/m<sup>3</sup> (0.25–0.3 m<sup>3</sup>/m<sup>3</sup>). This mode was called “transitional”.

If a certain velocity of the gas flow is reached, its effect on the material particles increases so much that their share in the upper part of the layer, breaks away from the wall surface. As a result of the breakaway of solid particles in the material, their concentration in this zone increases, the particles do not have time to get carried away by the gas flow to the upper part of the device and, losing their velocity, “fall” down onto the inclined shelf surface. Thus, a continuously circulating vortex layer of solid material particles is formed above the surface of the inclined shelf. Having reached a certain period, the formed circulating vortex layer of solid particles has a stationary state in its hydrodynamic structure and is characterized by a constant concentration of solid particles in the layer equal to 160–280 kg/m<sup>3</sup> (0.32–0.35 m<sup>3</sup>/m<sup>3</sup>). The porosity of such a layer is 0.65–0.68, which corresponds to the porosity of fluidized systems. At the same time, the material moves along the inclined shelf surface in the form of a dense layer blown by the gas flow, and in the form of a weighted intensely circulating layer in the zone above the outloading space (fig. 24 c). The velocity of material particles motion on the inclined shelf surface in this mode is reduced to 0.05–0.15 m/s.

The above mechanism demonstrates the transition of the hydrodynamic mode of the “gravitationally falling layer” of the material into the “weighted layer” mode given the “transition” mode. The velocity at which such a transition occurs is called the critical velocity of the initial weighing. The empirical dependence of the type defines the critical velocity of the initial weighing:

$$\text{Re}_{crit} = \text{Re}_{o.s.} [1.19 \cdot \lg(100 \cdot \psi) + 0.005] \left( \frac{L_{cl}}{L_{dev}} \right), \quad (24)$$

$$W_{crit} = \frac{\text{Re}_{crit} \cdot v}{d_p}, \quad (25)$$

where  $L_{cl}$  is the distance between the end of the shelf and the wall of the device, m;  $L_{dev}$  is the length of the cross-section side in the device, m;  $\psi$  is the perforation degree of the shelf, %;  $W_{crit}$ —critical velocity of the initial weighing, m/s;  $d_p$  is the average diameter of particles being weighed, m;  $v$  is the kinematic coefficient of the gas flow viscosity,  $\text{m}^2/\text{s}$ ;  $\text{Re}_{o.s.}$ —Reynolds criterion in conditions of particle hovering in a gas flow;  $\text{Re}_{o.s.} = W_{o.s.} d_p / v$ ;  $W_{o.s.}$ —medium velocity in conditions of particle hovering, m/s.

The “piston” mode for weighing material particles occurs in the workspace of the device with a further increase in the air flow velocity (fig. 24 d). This mode does not work. It is characterized by the maximum gas flow velocity.

The influence of the gas flow velocity on the interphase heat transfer process intensity is represented by the dependence  $\text{Nu} = f(\text{Re})$  (fig. 25).

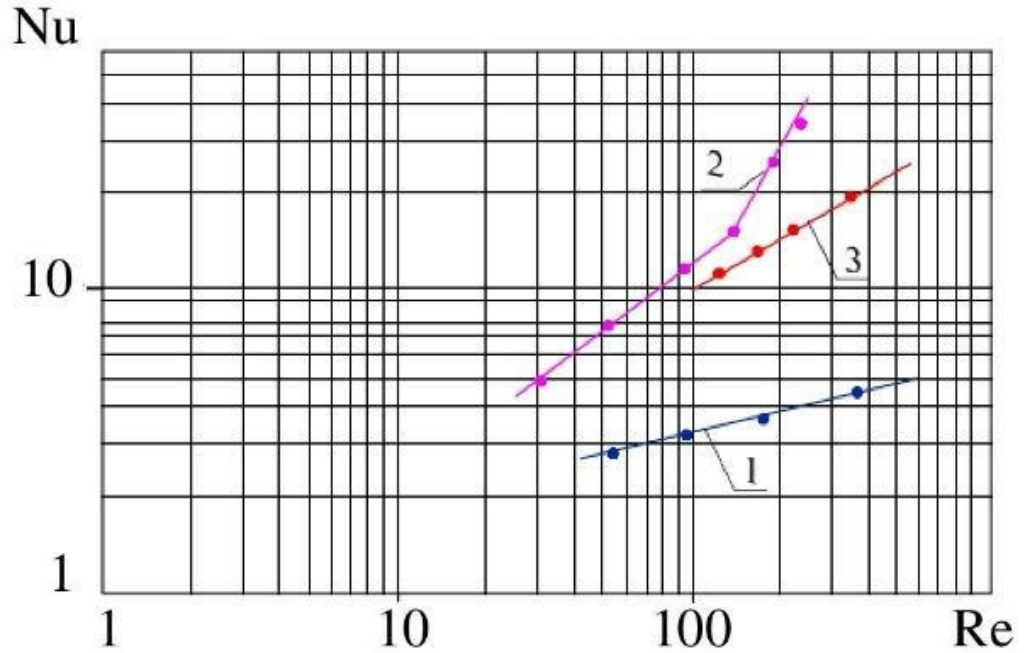


Fig. 25. The effect of gas flow velocity on the interphase heat transfer intensity:  
1—“gravitationally falling layer” mode; 2—“weighted layer” mode; 3—the fluidized bed on a horizontal grid.

One can see from the graph (Figure 8, line 1) that the interphase heat transfer intensity between the gas flow and particles for the “gravitationally falling layer” mode increases slightly with an increase in the gas flow velocity in the free cross-section of the device, at  $40 < \text{Re} < 600$ . It is proved by the fact that the particles of material coming from the loading nozzle move along the surface of the shelf with a sufficiently high velocity, the contact time of the particles with gas jets coming from the holes of the shelf is small. Owing to the insufficient contact time of the rapidly moving layer of material with the gas flow, the Nusselt criterion values obtained for the interphase heat transfer conditions on the inclined shelf surface under conditions of the “gravitationally falling layer” mode implementation in the workspace of the device come into the  $\text{Nu} < 5$  area.

The empirical correlation for the “gravitationally falling layer” mode is the following

$$\text{Nu} = 1,5 \cdot \text{Re}^{0.2} \text{ (if } 40 < \text{Re} < 600\text{)}, \quad (26)$$

where the Nusselt criterion  $Nu = \alpha \cdot d_p / \lambda_g$ ;  $\alpha$ —heat transfer coefficient from the surface of particles to the gas flow,  $\text{W}/(\text{m}^2 \cdot \text{K})$ ;  $\lambda_g$ —gas heat (thermal) conductivity coefficient,  $\text{W}/(\text{m} \cdot \text{K})$ ; Reynolds criterion  $Re = W \cdot d_p / v$ ;  $W$ —gas flow velocity in the free cross-section,  $\text{m}/\text{s}$ .

The “weighted layer” mode initially (at  $Re = 30–170$ ) is characterized by a gradual increase in heat transfer intensity, and then (at  $Re > 170$ ) a significant increase in interphase heat transfer intensity is observed as a result of the material layer formation blown by the gas flow on the inclined shelf surface (fig. 26, line 2). This situation is explained by the improvement of the conditions for “washing” particles with a gas flow, “opening” of their surface, and also due to additional turbulization of the boundary film as a result of an increase in the relative velocity of neighboring particles. In the weighted material layer in the area above the outloading space, the active heat transfer surface increases due to intensively circulating material particles throughout the entire weighted layer space. In the weighted layer mode, the most intensifying effect is exerted by a gas jet entering the weighted layer of material through the outloading space at a sufficiently high velocity. Due to the expansion of the gas flow at the exit from the space of the outloading gap, intense interaction is ensured over the entire area of the weighted layer in the filtration mode. When the material is unloaded, the lower part of the weighted layer partially overlaps the outloading space. It causes a slight increase in the gas flow velocity in this zone and its part is redistributed into the holes of the shelf. In this case, the uniform filtration mode of the material layer by the gas flow is replaced by the gas jet “breakthrough” through the material weighted layer over the outloading space. Therefore, such a variable mode defines the pulsating nature of the material particles interaction with the gas flow, not only in the layer of material weighted over the outloading space, but also in the layer moving along the inclined shelf surface. It increases the phase contact intensity, and, accordingly, the heat transfer coefficient in the weighted layer mode in comparison with the fluidized bed (fig. 26, line 3).

The experimental studies enabled to identify the “active” heat exchange zone of the shelf unit - the outloading space zone.

The empirical correlation for the “weighted layer” mode is the following:

$$\text{Nu} = 0.38 \cdot \text{Re}^{0.73} \text{ (if } 30 < \text{Re} < 170\text{)}, \quad (27)$$

$$\text{Nu} = 0.0045 \cdot \text{Re}^{1.73} \text{ (if } 170 < \text{Re} < 300\text{)}. \quad (28)$$

Comparing the dependence, which is typical for the weighted layer on the inclined perforated shelf (fig. 25, line 2) with the dependence, which is peculiar for the fluidized bed (fig. 25, line 3), we can see that the interphase heat transfer intensity in the former case is a bit higher.

It is difficult to identify the true residence time of solid particles in the weighted layers with different structures. That is why the authors propose a calculation method for estimating the average residence time of particles in a layer weighted above a shelf.

As can be seen from the trajectories of solid-phase motion in the photographs (fig. 25), the weighted layer can be divided into two zones: the solid particle motion zone on the surface of the shelf and the particle motion zone in the overshell space.

For the first zone, the residence time of the particles is calculated by the formula:

$$\tau_1 = \frac{L_{sh}}{u_p \cdot (1-\beta)^m} = \frac{L_{dev} - \frac{L_{cl}}{L_{dev}}}{u_p \cdot (1-\beta)^m}, \quad (29)$$

where  $u_p$  is the velocity of solid particles motion on the shelf surface, m/s;  $\beta$ —the volume concentration of the solid phase in the weighted layer,  $\text{m}^3/\text{m}^3$ ;  $m$ —the experimental coefficient;  $m = 4.4\text{--}4.5$ —for the “weighted layer” mode;  $m = 10\text{--}10.2$ —for the “gravitationally falling layer” mode.

The following empirical correlation is proposed to find the volume concentration of the solid phase in the weighted layer:

$$\beta = n \cdot G_{ex}^{0.95} \left( \frac{W}{W_{o.s.}} \right)^{0.6}, \quad (30)$$

where  $G_{ex}$  is the mass flow rate concentration, kg/kg;  $G_{ex} = G_p/G_{gas}$ ;  $G_p$ —mass flow rate of the material, kg/s;  $G_{gas}$ —mass flow rate of gas, kg/s;  $W$ —velocity of the gas flow in free cross-section, m/s;  $W_{o.s.}$  is the velocity of medium diameter particles, m;  $n$  is the experimental coefficient;  $n = 0.25\text{--}0.35$  for the “weighted layer” mode;  $n = 0.1\text{--}0.15$ —for the “gravitationally falling layer” mode.

There is no weighted layer in the space above the shelf for the “gravitationally falling layer” mode, as can be seen from the photograph (fig. 24a). Therefore, the second zone is typical only for the “weighted layer” mode (photograph, fig. 24 c). When particles pass along the shelf length, they meet with a gas jet, formed by the outloading gap. Particles with a velocity less than the velocity of the gas jet are carried up into space above the shelf. The velocity of the gas jet decreases in height. The particles with a velocity greater than the velocity of the gas are lowered down to the shelf surface. Only small particles are carried out by the gas flow from the device. Thus, in the second zone, the particles move up the trajectory to the upper boundary of the weighted layer and downward trajectory to the surface of the shelf. Then the residence time of the particles is calculated as the following:

$$\tau_2 = \frac{L_{tr}}{\vartheta_r} = \frac{2 \cdot k \cdot B_{dev}}{\vartheta_r}, \quad (31)$$

where  $L_{tr}$  is the length of the trajectory, m;  $\vartheta_r$  is the pulsation velocity of the solid particle, m/s;  $k$  is the experimental coefficient;  $k = (1.5\text{--}3) \cdot B_{dev}$ .

The pulsation velocity of a solid particle in a weighted layer is determined by the empirical dependence:

$$g_r = bW, \quad 0 < W < 3.5 \text{ m/s}, \quad (32)$$

where  $b$  is the experimental coefficient;  $b = 0.06$  (defined according to the regression with correlation coefficient of 0.844).

The calculations show that for the “weighted layer” mode with a gas flow velocity of 2.4 m/s in a free cross-section, the velocity of particles with average diameter of 2 mm is 10–12 m/s, the flow mass concentration of 3 kg/kg, the volume concentration of solid phase in the weighted layer  $0.34 \text{ m}^3/\text{m}^3$  and the particle velocity on the surface of the shelf is 0.1 m/s, the residence time of the particle for the first zone is  $\tau_1 = 5.73\text{--}5.97$  s. For the second zone, at a pulsating velocity of particles in the layer of 0.14 m/s, the residence time is  $\tau_2 = 2$  s. The total estimated residence time of the particles in the weighted layer  $\tau_{\Sigma} = 7.73\text{--}7.97$  s. The experimental residence time of the particles in the layer (calculated as the ratio of the material amount in the weighted layer to its mass flow rate) is  $\tau_{ex} = 7.72$  s. For the gravitationally falling layer mode, the estimated time at a particle velocity of 0.25 m/s and a volume concentration of the solid phase in the layer above the shelf of  $0.15 \text{ m}^3/\text{m}^3$  is  $\tau_1 = 1.12\text{--}1.15$  s, and experimental  $\tau_{ex} = 1.16$  s. The calculation results (Table 1) show that the residence time of the particles in the layer increases with the increase of the solid phase volume concentration in the layer and the number of shelves.

Table 3. The residence time of solid particles in a shelf unit.

Mode; Concentration $\text{m}^3/\text{m}^3$	$\beta$ , Shelves, s	The Residence Time of Particles with Number of				
		1	2	3	4	5
Weighted layer; 0.3	7.2	12.4	17.6	23.0	28.0	
Weighted layer; 0.35	9.2	16.4	24.0	31.0	38.0	
Gravitationally falling layer; 0.1	1.3	2.5	3.8	5.1	6.4	
Gravitationally falling layer; 0.2	4.2	8.4	12.7	16.9	21.0	

According to the comparative tests (Table 4) the shelf cooler-pneumoclassifier in terms of the cooling coefficient and the small fraction extraction degree exceeds pneumatic tubes devices, and units with fluidized and weighted layers, in which the specific cooling air flow rate to achieve the same cooling efficiency is 30–50% higher.

The temperature of the material in the device with one shelf (if  $L_{cl}/L_{dev} = 0.5$ ) decreases from 90 to 65–70 °C. This insignificant cooling degree is explained by the short residence time of the material moving along the inclined shelf in the gravitationally falling layer mode. At the same time, as a result of the small concentration of material particles in the workspace of the device and the close contact of the particles with the air jet, a small fraction is intensively extracted from the product. The highest dusting degree is achieved with the shelf perforation degree of  $\psi = 5\%$ . If the air flow velocity in the free cross-section of the device increases from 2.4 to 3.7 m/s, the extraction degree of the fraction of less than 1 mm in ablation is 30–60%, and the product fraction of 1–1.6 mm is not more than 1.5–2%.

Table 4. Test results of a shelf cooler.

Material	Specific Productivity on the Material, $\text{kg}/(\text{m}^2 \cdot \text{s})$	Content of the Extracted Fractions Less Than 1 mm, %			Cooling Coefficient, $K_{cool}$	The Degree of Extraction, $\varepsilon_m, \%$	Specific Air Flow Rate, $\text{m}^3/\text{k g}$	Hydraulic Resistance, kPa
		Initially	In Ablation	In Undershooting				
Ammophos	6	20	97.5	10	0.69	73	0.4	0.5–1.5
Superphosphate	6	40	100	26.2	0.6–0.65	50	0.4	0.5–1.5
	8	40	98	12.6	0.64–0.71	79	0.7	1.8–2.0

The cooling degree of the material on the shelf with a perforation degree of 15% and  $L_{cl}/L_{dev} = 0.5$  increases significantly and reaches a maximum. If the specified optimal design parameters and air flow velocity in the cross-section of the device is 2.4 m/s, the “weighted layer” mode is implemented on the shelf, in which the particles are cooled more effectively, reaching a final temperature of 40–45 °C. As a result of the longitudinal mixing effect in this mode, the extraction efficiency of the small fraction is reduced to 20%.

The advantage of the shelf cooler-pneumoclassifier is the possibility to separate and to cool wide fractional composition materials without clogging grids and at low hydraulic resistances not exceeding 1.5 kPa. Thanks to the pulsating outloading with the flow of the air share between the shelf perforation and the outloading gap and the intense phase contact in this space, a clear pneumatic classification is provided at high specific loads, reaching 15–20  $\text{kg}/(\text{m}^2 \cdot \text{s})$  significantly exceeding the specific loads of 0.1–1.5  $\text{kg}/(\text{m}^2 \cdot \text{s})$ , at which fluidized bed coolers-separators work.

In the granular mineral fertilizer technology, cooling is used to stabilize the structure of the granules. Thus, drum coolers are used, which reduce the temperature of

NPK fertilizer granules from 60–80 to 30 °C. The granules are also cooled using fluidized bed coolers. A single-stage fluidized bed cooler for cooling doubled superphosphate provides cooling of granules from 85 to 40 °C with air at a temperature of 20 °C at a fluidization rate of 1.6 m/s, as well as cooling diammonium phosphate from 85 to 30 °C. Therefore, according to the data in Table 2, the performance of the developed shelf cooler is fully confirmed.

Table 5 presents the testing results of the shelf dryers, which have significant advantages since the material is simultaneously separated and dried in such devices.

Table 5. Testing results of the shelf dryer.

Material	Content of the Extracted Fractions Less than 0,1 mm, %			Extract ion Degree , $\varepsilon_m$ , %	The Humidity of the Material, %			Specific Productivity on the Evaporated Moisture, kg/(m <sup>3</sup> ·h)
	Initia lly	In Undershoo oting	In Ablat ion		Initi al	Undershoo oting	Ablat ion	
Fine-grained potassium chloride	7.5–10	1.2–5.5	60–80	80–90	6.1	0.1	0.06	420–460
Coarse-grained potassium chloride	4.5–10	2–5	58–65	70–80	7.0	0.14	0.1	520–1170

Thus, the content required in the dust-free product of a fraction of fewer than 100 µm in size equal to 1–2% is achieved for fine-grained potassium velocities at a flow

velocity of 1.44 m/s, and coarse-grained 1.34 m/s. If the flow velocity is more than 1.5 m/s in the coarse-grained potassium chloride, a fine-dispersed fraction is practically absent. The ablation of the fine-dispersed fraction of the material into cyclones does not exceed 6.5–10.8%, and the content of a fraction of more than 100  $\mu\text{m}$  in it is 3–5%. The indicated results were achieved with specific loads on the section of the device in the material equal to  $10 \text{ kg}/(\text{m}^2 \cdot \text{s})$ , the hydraulic resistance of 700–1500 Pa, and specific gas flow velocity of 0.12–0.14  $\text{m}^3/\text{kg}$ . For fluidized bed dryers, the ablation of the fine-dispersed fraction up to 7% is ensured at a gas velocity of 1.8–2.3 m/s. In this case, the specific gas flow rate is 0.41–0.52  $\text{m}^3/\text{kg}$ , the hydraulic resistance is 1500–2500 Pa.

In the potassium chloride production technology, fluidized bed dryers provide drying of the product from an initial moisture content of 3–9% to a final moisture content of 0.1%. Therefore, according to the data in Table 3, the developed shelf dryer's performance is fully confirmed.

To define the optimal number of experiments and the highest accuracy degree and reliability of the obtained results, as well as for the processing of these results, methods of mathematical statistics were used.

Two types of measurement errors—random and systematic—may occur during the experiment conducting.

A random error reduces the accuracy of experiment results. An analysis of this type of error is possible by using the root-mean-square deviation  $\sigma$ , calculated by the following equation:

$$\sigma = \sqrt{\frac{\sum_{i=1}^n (\bar{x} - x_i)^2}{n-1}}, \quad (33)$$

where  $\bar{x}$  is the arithmetic mean value;  $x$  is the single parameter value;  $n$  is the number of measurements.

The maximum possible error of a single measurement,  $\Delta$ , was determined by the three sigma rule:

$$\Delta = 3 \cdot \sigma. \quad (34)$$

The bilateral confidence interval of the arithmetic mean value  $\varepsilon$  was determined by the following function, provided that this parameter is located in the confidence interval with the probability not less than 95%:

$$\varepsilon = t \cdot \frac{\sigma}{\sqrt{n}}, \quad (35)$$

where  $t$  is the Student's criterion.

The root-mean-square error of indirect measurements is calculated as:

$$\sigma_y = \sqrt{\sum_{i=1}^n \left( \frac{\partial y}{\partial x_i} \Delta x_i \right)^2}, \quad (36)$$

where  $y = f(x_1, x_2, \dots, x_n)$ .

The accuracy of the obtained regression equations is determined by the least-squares method.

The systematic measurement error had an identical effect on all parameters that were controlled during the experiment. All measurement devices were calibrated by calibration instruments by comparing their accuracy with that declared in the technical documentation in order to exclude the above error. Connection between measurement devices and controllers was provided with a maximum error of processing signals within 1.5%.

Creation of graphical dependences was carried out by differential methods of mathematical analysis and integral calculus. Reliability of the obtained experimental results is due to application of time-tested methods in practice.

1. Due to the creation of an active hydrodynamic mode to weigh solid particles in a layer, a multistage fluidized bed device with inclined perforated shelves provides efficiency to carry out heat-mass transfer processes.
2. Changes in the constructive parameters of the inclined shelf (the width of the outloading space and the shelf perforation degree) identify the different nature of the gas flow distribution between the holes of the shelf and the outloading space.
3. Various hydrodynamic modes during operation of the device were revealed: the “gravitationally falling layer” mode and the “weighted layer” mode. The first mode is effective in carrying out pneumatic classification processes, and the second—in cooling and drying of granular materials.
4. The study of interphase heat transfer showed a higher intensity of heat transfer in the weighted layer on an inclined perforated shelf compared to a traditional fluidized bed on a horizontal gas distribution grid.
5. The theoretical model enables to present the gas flow velocity profiles depending on the length and perforation degree of the shelf contact, as well as to estimate the residence time of material particles in the workspace of the device.
6. Further research will point to develop the mathematical model of the weighted layer hydrodynamics on an inclined perforated shelf. The corresponding scientific and methodological approaches based on using artificial neural networks for parameter identification of the proposed mathematical model will be developed.

## **5 EXPERIMENTAL-INDUSTRIAL IMPLEMENTATION OF THE TECHNOLOGY FOR PRODUCING NANOPOROUS LAYERS ON AMMONIUM NITRATE: THE FINAL DRYING STAGE IN MULTISTAGE DEVICES**

*This section is prepared in according to data [5] and references in this work.*

The ammonium nitrate, used as a component of industrial explosives, must have a developed network of nanopores on the surface for the liquid fuel (for example, diesel distillate) successfully to access the near-surface layers and the core of the granule. It is called a porous ammonium nitrate which is an integral part of the ANFO industrial explosive.

The main methods of obtaining porous ammonium nitrate (PAN) are presented in various works, for example. The ordinary ammonium nitrate granule humidification with its subsequent heat treatment, implemented in a vortex granulator, should be distinguished among other methods. This method has the following advantages:

1. Absence of pore-forming and modification additives in the formation of the porous structure in the granule.
2. Absence of phase changes in the granule and the formation of new compounds.
3. High strength of granules due to the minimum number of heat treatment cycles.
4. A developed network of twisting nanopores on the granules' surface due to a properly selected humidifier (for example, the water solution of ammonium nitrate).
5. Sufficient oxygen in the granule to detonate ANFO.

However, given the hydroscopic property of PAN granules (as well as any ammonium nitrate in general), it is essential to ensure a low value of residual moisture in the granules. This indicator is not normative (in contrast to the strength of the granule and retentivity and absorptivity concerning the diesel fuel distillate), but it influences the ANFO quality.

Excessive humidity of PAN granules leads to the following structural defects and a decrease in quality indicators:

1. Insufficient absorptivity of the granule.
2. Caking during storage and transportation.
3. Loss of strength.
4. Violation of the structure of nanopores.

Fig. 26 demonstrates the disturbance of the nanopores structure during storage of undried PAN. Several parts of the surface are "smoothed"; the pores disappear. This process leads to the fact that there are obstacles to the penetration of diesel distillate into the core of the granule. The relative porous surface area decreases, and the diesel fuel distillate flows from the granule already at the saturation stage (not to mention the storage and transportation of ANFO)

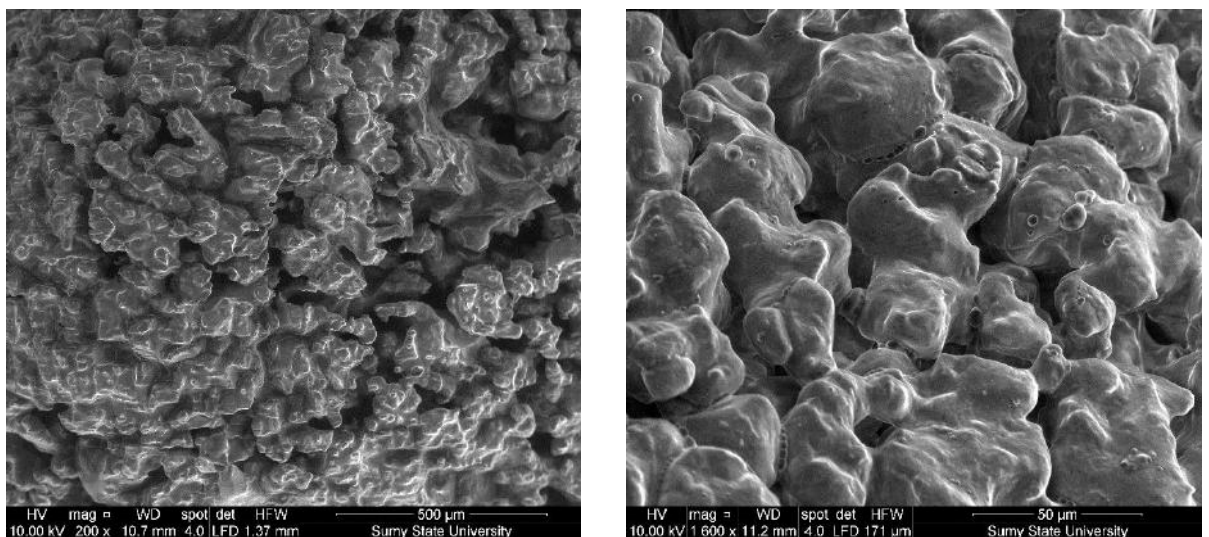


Fig. 26. Disturbance of the PAN granule nanoporous structure with its excess humidity.

Therefore, the study proposes an improved scheme for PAN production, which includes an additional final drying stage.

Drying methods are diverse in the way of realization, organization of flow, instrumentation, the use of extra stages, etc. The data analysis from the above sources and data enables an improved design of the drying unit - a multistage gravitational shelf dryer.

It is necessary to solve two problems for the successful implementation of the improved method within the framework of this work:

1. To model the heat treatment and dehydration of PAN.
2. To confirm the efficiency of the final drying stage to form a developed nanoporous structure of the PAN granule.

The scheme of the experimental stand for the final drying stage of the PAN is shown in fig. 27.

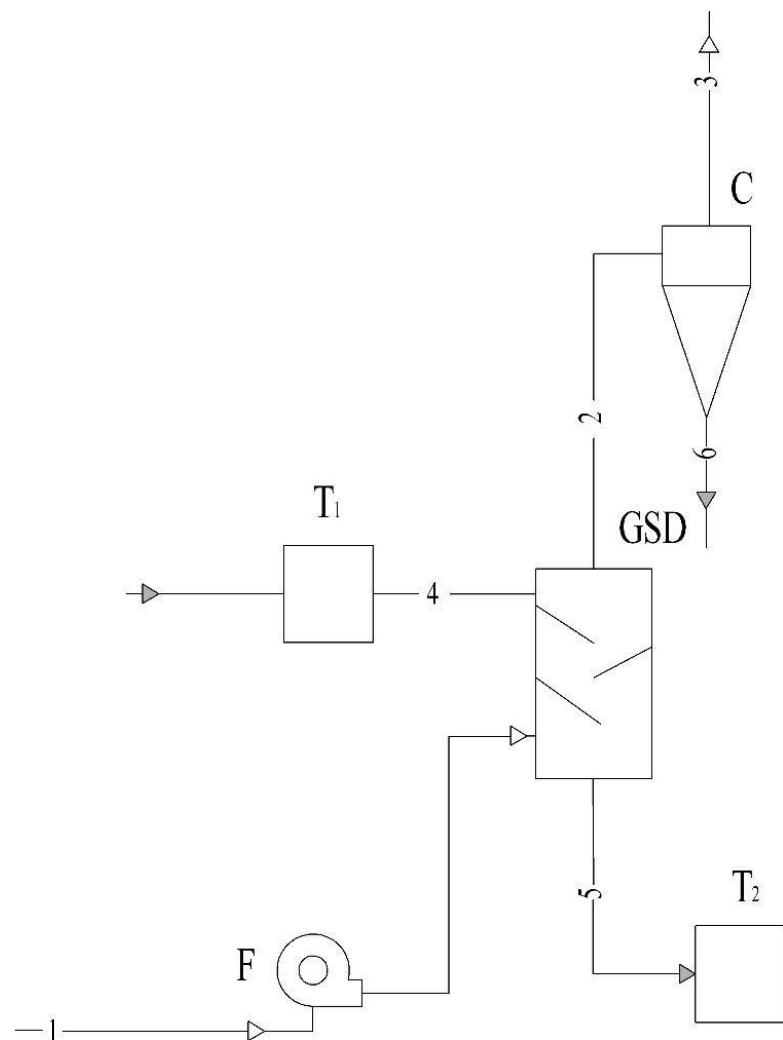


Fig. 27. Schematic diagram of the experimental stand for the study of shelf devices: F – fan; GSD – gravitational shelf unit; C – cyclone; T1, T2 – containers (tanks); 1 – drying agent; 2 – waste drying agent; 3 – purified gas; 4 – PAN; 5 – PAN after final drying; 6 – fine particles

The surface morphology of the granules is studied by scanning electron microscopy using a SEO-SEM Inspect S50-B instrument.

The Converter Image tool, with its interface in fig. 28, is investigated to analyze the scanning electron microscopy results (pore size, shape, relative porous surface area, etc.). This tool enables to modify images to determine the surface relief and detailed study of the pore structure.

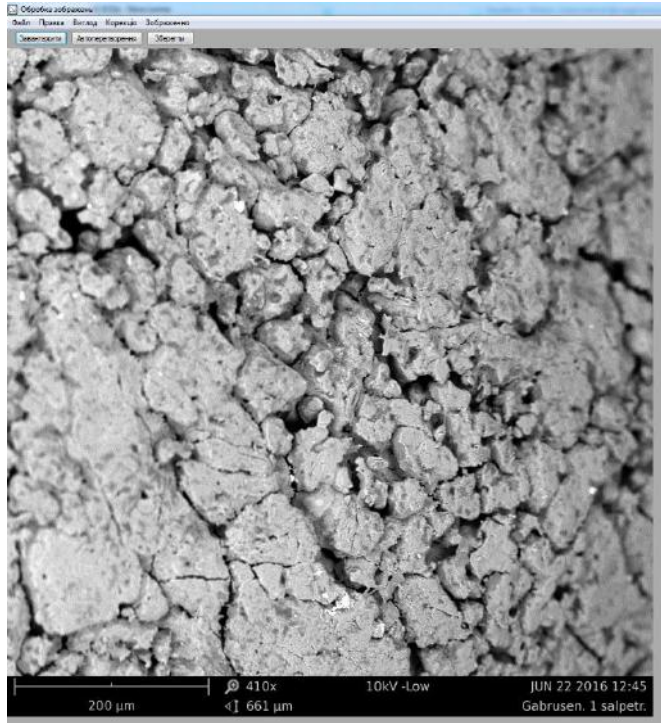


Fig. 28. The interface of the author's program for studying the nanoporous surface morphology of granules with the initial results of microscopy (the interface language is Ukrainian)

When considering the drying process kinetics of a single spherical particle, interphase heat exchange process between its surface and the drying agent flow is observed at the first level as well as heat transfer inside.

When the nature of thermal conductivity inside the particle affects the moisture removal kinetics, the calculation is based on the equations of internal heat and mass transfer:

$$\left. \begin{aligned} \frac{\partial t_m}{\partial \tau} &= a_{id} \left[ \frac{\partial^2 t_m}{\partial r^2} + \frac{2}{r} \frac{\partial t_m}{\partial r} \right] + \frac{\varepsilon^* r_{ph}}{c_p} \frac{\partial U_m}{\partial \tau} \\ \frac{\partial U_m}{\partial \tau} &= k \left[ \frac{\partial^2 U_m}{\partial r^2} + \frac{2}{r} \frac{\partial U_m}{\partial r} \right] + k \sigma^* \left( \frac{\partial^2 t_m}{\partial r^2} + \frac{2}{r} \frac{\partial t_m}{\partial r} \right) \end{aligned} \right\}, \quad (37)$$

where  $t_m$  – temperature of the material;  $U_m$  – relative humidity of the material;  $\varepsilon^*$  – phase transformation criterion;  $\sigma^*$  – thermogravitational moisture transfer coefficient;  $a_{td}$  – thermal diffusivity coefficient;  $r_{ph}$  – specific heat of phase transition;  $r$  – the current radius of PAN granules;  $c_p$  – heat capacity of the PAN granule;  $k$  – potential conductivity coefficient.

According to the mass transfer equation, the drying process calculation has some peculiarities since an interconnected heat and mass transfer process occurs in the drying objects: moisture removal and simultaneous heating of the wet material. There is a relationship between these processes since the mass transfer coefficients depend on the temperature, and heat - on the moisture in the material.

Given that at each stage, the material is dried in a limited range of humidity and is thermolabile, it is also advisable to assume the analogy of gradient mechanisms of heat and mass transfer. Then the system of equations (28) is as follows:

$$\left. \begin{aligned} \frac{\partial t_m}{\partial \tau} &= a_{td} \left[ \frac{\partial^2 t_m}{\partial r^2} + \frac{2}{r} \frac{\partial t_m}{\partial r} \right] \\ \frac{\partial U_m}{\partial \tau} &= k \left[ \frac{\partial^2 U_m}{\partial r^2} + \frac{2}{r} \frac{\partial U_m}{\partial r} \right] \end{aligned} \right\}, \quad (38)$$

Using one of the system equations (38) as one of the author's describing methods proposed to calculate the drying kinetics, makes it possible to replace the second equation with an empirical approximation. Thus, the temperature-humidity feature of the material closes the system of heat and mass transfer equations. For drying process calculation in the concentration zones, in this case, it is necessary to know the thermophysical properties of the dispersed material. Moreover, one can use a similar temperature-humidity approximation to define the mass transfer coefficient and mass transfer properties.

Currently, there are many theoretical solutions of heat and mass transfer differential equations for dispersed systems that can be dried. All of them describe the heating process of particles under given third kind initial and boundary conditions in equations (29).

We consider one of the most common exponential models through changes in temperature and humidity of the particle depending on its current radius and drying time:

$$\frac{t_{(r,\tau)} - t_{dr.in}}{t_{dr.in} - t_{m.in}} = 1 - \sum_{n=1}^{\infty} A_n \frac{\sin \mu_n \frac{r}{R}}{\mu_n \frac{r}{R}} \exp(-\mu_n^2 Fo_t), \quad (39)$$

$$\frac{U_{m.in} - U_{(r,\tau)}}{U_{m.in} - U_{dr.in}} = 1 - \sum_{n=1}^{\infty} A_n \frac{\sin \mu_n \frac{r}{R}}{\mu_n \frac{r}{R}} \exp(-\mu_n^2 Fo_u), \quad (40)$$

where  $t_{(r,\tau)}$  – the temperature of the particle in its current radius at a given time;  $t_{m.in}$  – the initial temperature of the PAN granules, which are getting dried;  $t_{dr.in}$  – the initial temperature of the drying agent, °C;  $U_{m.in}$  – the initial moisture content of the PAN granules, which are getting dried;  $U_{(r,\tau)}$  – the humidity of the particle in its current radius at a given time;  $U_{dr.in}$  – the initial humidity of the drying agent;  $R$  – the peculiar size of the dispersed material;  $Fo_t$  – Fourier test for heat transfer during drying process;  $Fo_u$  – Fourier test for mass transfer during drying process;  $A_n$ ,  $\mu_n$  – constant coefficients and roots of the characteristic equation, the values of which are in the relevant tables.

The root of characteristic equations (39)-(40)  $\mu_n$  is a Biot criterion function

$$\mu_n = f(Bi), \quad (41)$$

calculated by the following formula:

$$Bi = \frac{\alpha \cdot R}{\lambda}, \quad (42)$$

where  $\alpha$  – heat transfer coefficient;  $\lambda$  – thermal diffusivity coefficient.

When considering this functional dependence, the features of the heat transfer process, determined by the limit values of the Biot criterion, are considered:

$$0 < Bi < \infty, \quad (43)$$

If  $Bi \rightarrow 0$  the small dispersed material will have the maximum thermal diffusivity, if  $Bi = \infty$  the material of the maximum size will have the maximum heat transfer coefficient.

Based on the limit values of the Biot criterion for the drying process, it is necessary to use it within the specified limits to find the root of the characteristic equation (30)  $\mu_n$ .

The heat transfer coefficient  $\alpha$  for determining the Biot criterion is obtained from experimental data obtained by the authors. Depending on the Biot criterion, the root of the equations (39)-(40)  $\mu_n$  is determined on the graph.

One should note that solutions (39) - (40) in the form of series are found quickly. Starting with some value of the Fourier criterion, calculation accuracy of 1-2%, acceptable in engineering practice, can be achieved thanks to the first two or three members in the series. In this case, the contribution of the first member of the series is not less than 96%, i.e., the error will not exceed 3-4%. Thus, given the conditions

$$\left. \begin{array}{l} r = R, \\ Fo \geq 0,7 \end{array} \right\}, \quad (44)$$

from the equation (39), the heating kinetics of the particle is determined by the exponential function:

$$\frac{t_{surf} - t_{m.in}}{t_{dr.in} - t_{m.in}} = 1 - A_n \cdot \frac{\sin \mu_n}{\mu_n} \cdot \exp(-\mu_n^2 \cdot Fo_t), \quad (45)$$

where  $t_{surf}$  – the temperature of the PAN granule surface;

Given the value of the Fourier test, the equation (45) is as follows:

$$\frac{t_{surf} - t_{m.in}}{t_{dr.in} - t_{m.in}} = 1 - A_n \cdot \frac{\sin \mu_n}{\mu_n} \cdot \exp(-\mu_n^2 \cdot \frac{a_{id} \cdot \tau_h}{R^2}), \quad (46)$$

where  $\tau_h$  – heating time.

The exponential nature of the surface temperature change in the dispersed particle according to equation (46) is shown in the graphs (fig. 29).

Analysis in Fig. 29 shows that the material is heated with different intensities at a constant radius of the particle, depending on its thermophysical properties. The particles with similar thermophysical properties are heated more intensely when their radius decreases.

Given the active mixing of particles in the layer, the drying process kinetics is described by the balance equations of heat and moisture transfer in the fluidized bed of solid particles:

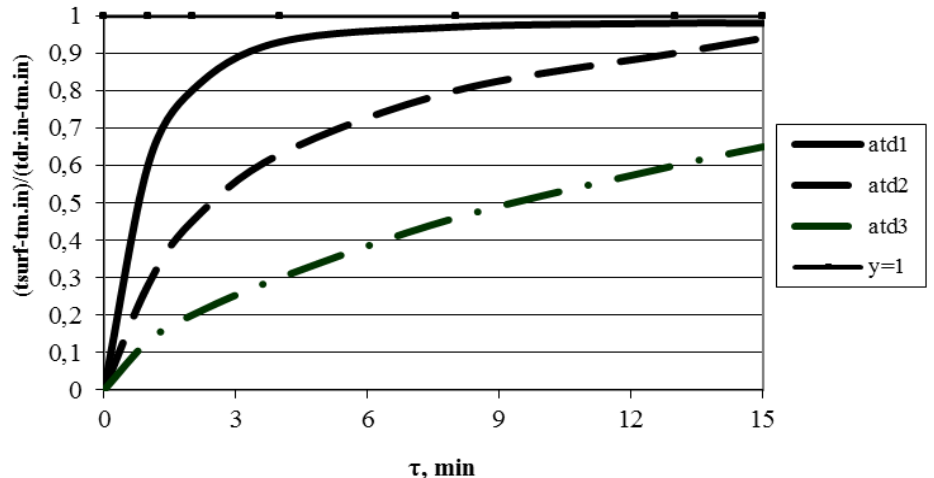
$$\begin{cases} G \cdot c_p \cdot \rho_p \frac{dt_m}{d\tau} = \alpha \cdot F_{gr} (t_{dr} - t_m) \\ \rho_p \frac{dU_m}{d\tau} = \beta \cdot F_{gr} (U_m - U_{dr}) \end{cases}, \quad (47)$$

where  $G$  – flow concentration (as the ratio between mass flow rates of solid and gas phases);  $\rho_p$  – density;  $U_m$  – current humidity of the material;  $t_m$  – current temperature of the material;  $t_{dr}$  – the current temperature of the drying agent;  $\beta$  – mass transfer coefficient;

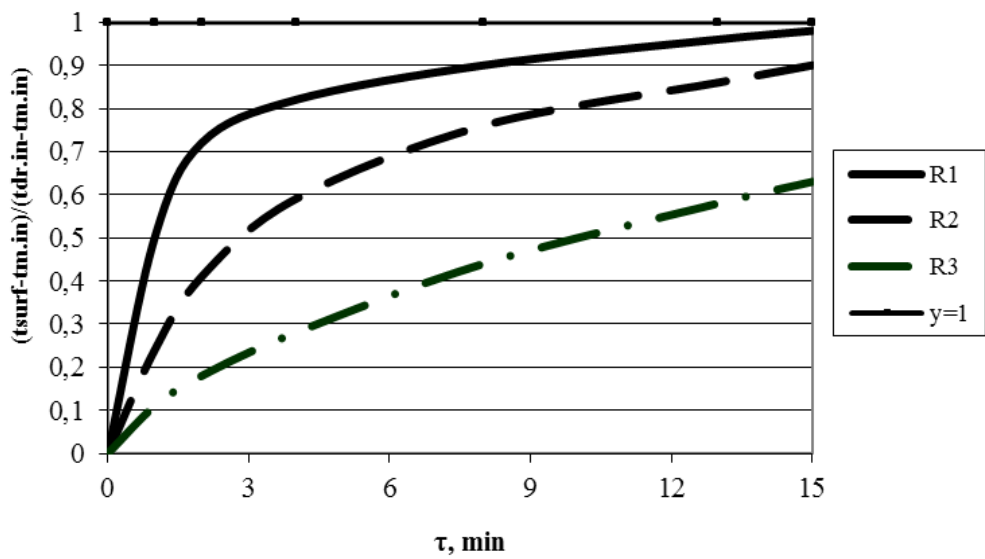
$F_{gr}$  – the specific surface area of the PAN granules in the device  $F_{gr} = \frac{6(1-\varepsilon)}{d}$ ;  $\tau_{dr}$  – drying time of the material.

After integration of the equation (47), we obtain:

$$\begin{cases} \frac{t_{dr.in} - t_m}{t_{dr.in} - t_{m.in}} = \exp\left(-\frac{\alpha \cdot F_{gr}}{G_s \cdot c_p \cdot \rho_p} \cdot \tau_h\right) \\ \frac{U_m - U_{dr.in}}{U_{m.in} - U_{dr.in}} = \exp\left(-\frac{\beta \cdot F_{gr}}{\rho_p} \cdot \tau_{dr}\right) \end{cases}, \quad (48)$$



a



b

Fig. 29. Qualitative nature of intensity curves of the material heating: a – if  $R = \text{const}$  depending on their thermophysical properties ( $a_{id1} > a_{id2} > a_{id3}$ ) ; b – if  $a_{id} = \text{const}$  depending on their thermophysical properties ( $R_1 < R_2 < R_3$ ) .

A linearization defines the kinetic features of these exponential curves. Thus, equations (48) show that the heating rate of a material with a peculiar particle size  $d$  is a parameter  $K_t$ :

$$K_t = \frac{a}{G \Psi_p \Psi_p} \frac{6(1 - \varepsilon)}{d}, \quad (49)$$

The first equation of the system (48), considering the replacement of the corresponding parameters in the left part of this equation, will be as follows

$$\frac{t_{dr,in} - t_m}{t_{dr,in} - t_{m,in}} = \exp(-K_t \tau_h), \quad (50)$$

or after logarithmation

$$K_t \tau_h = -\ln \frac{t_m - t_{m,in}}{t_{dr,in} - t_{m,in}}, \quad (51)$$

Thus, after linearization, the heating kinetics model becomes convenient for processing the statistical data and determination of kinetic parameters (fig. 29 a). Table 6 demonstrates the data for the construction of the following graphical relationship.

Table 6. Data of the kinetic parameter for the material heating

Value $-\ln \frac{t_m - t_{m,in}}{t_{dr,in} - t_{m,in}}$	Heating time $\tau_h$ , min
0	0
1,2	4,5
1,0	9,0
1,92	12
3,4	15,3
2,7	18
4,5	23,4
0,9	2,1
2,5	15
0,4	3
4,5	22,2

This graph shows that the kinetic parameter  $K_t$  is the tangent of the tilt angle of the line, approximating the experimental points in the coordinates of time and dimensionless temperature.

It is reasonable to investigate the change in material humidity according to a similar solution (50) with the appropriate replacement of temperatures by humidity, to find the drying time of the dispersed particle.

The linearized graph of drying kinetics in time and humidity coordinates is represented in fig. 30 b. Table 7 demonstrates data for the construction of the following graphical relationship.

Table 7. Data of the kinetic parameter  $K_u$  for the material drying

Value $\frac{-\ln \frac{U_m - U_{dr.in}}{U_{m,in} - U_{dr.in}}}{K_u}$	Drying time $\tau_{dr}$ , min
0	0
1,2	4,5
2,0	9,0
1,8	12,0
3,5	15,3
2,9	18,0
4,5	23,4
0,1	2,1
2,2	15,0
0,4	3,0
3,4	22,2

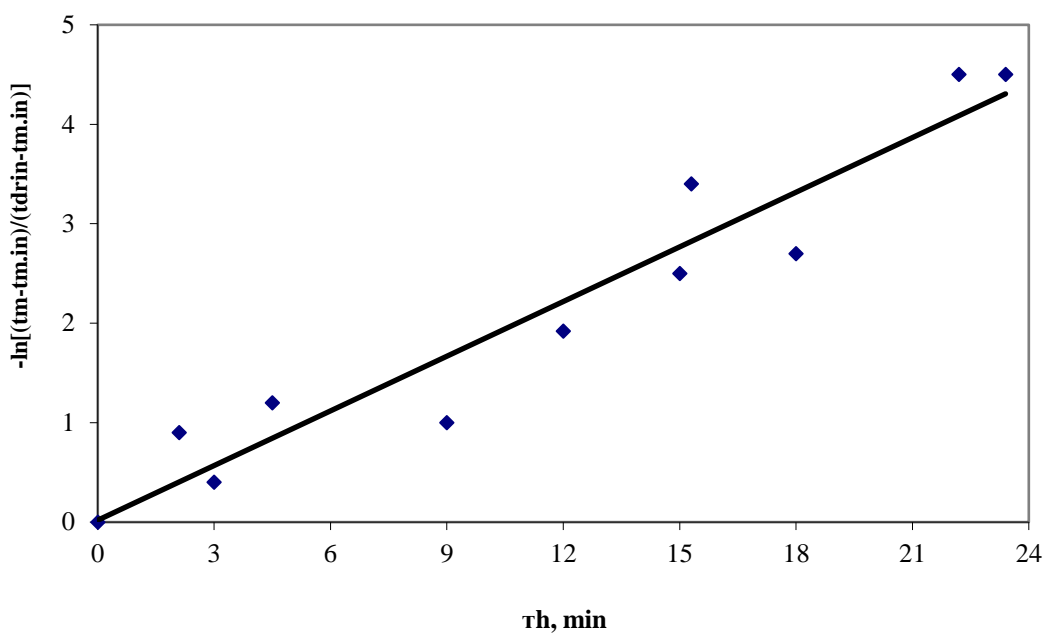
According to the analogy of heat and mass transfer processes, the linear approximation equation of the humidity change is like

$$K_u \tau_{dr} = -\ln \frac{U_m - U_{dr.in}}{U_{m,in} - U_{dr.in}}, \quad (52)$$

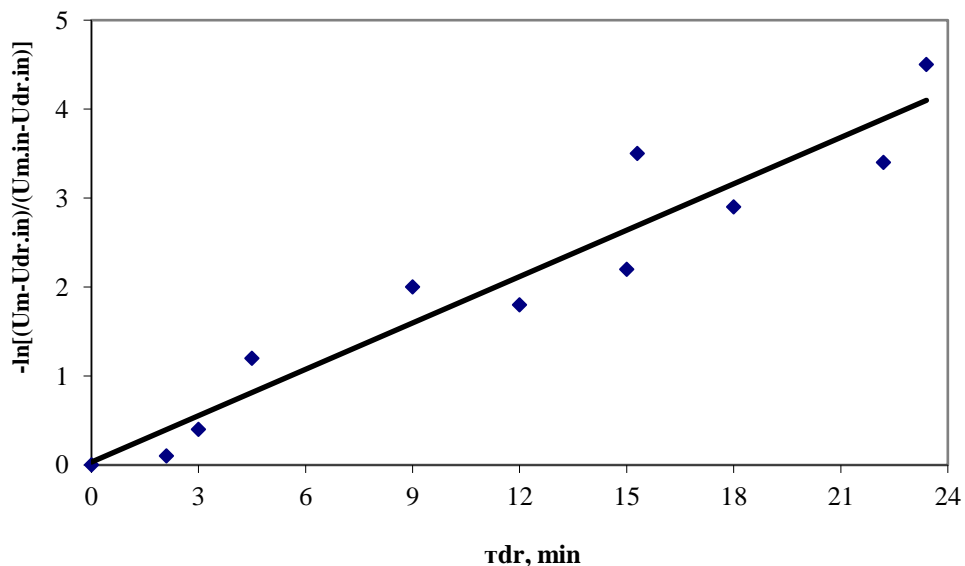
where  $K_u = \frac{\beta \Psi F_{gr}}{\rho_p}$  – kinetic parameter of moisture transfer.

Based on the initial humidity of the material, the drying agent and the required technological humidity of the material, the drying time is calculated

$$\tau_{dr} = -\frac{1}{K_u} \ln \frac{U_m - U_{dr.in}}{U_{m,in} - U_{dr.in}}, \quad (53)$$



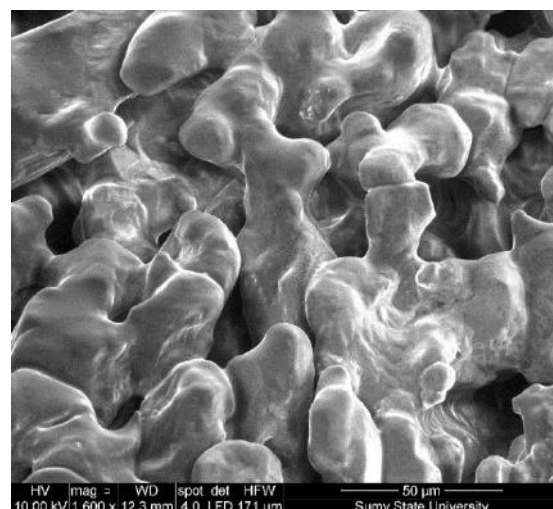
a



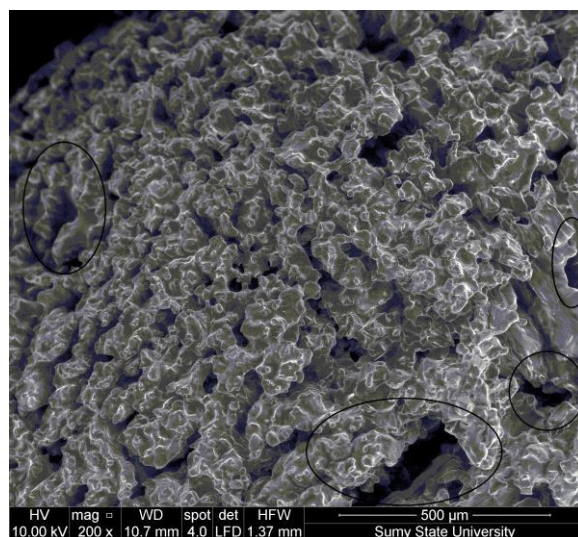
b

Fig. 30.. Graph of the kinetic parameter: a – for heating of the material ( $K_t$ ); b – for drying of the material ( $K_u$ )

There are many studies regarding the surface morphology of the PAN granule to confirm a developed network of nanopores on the surface of the granules after the final drying stage. The PAN granule is taken as a sample for comparison after humidification and heat treatment in the vortex granulator (fig. 31). The sample of PAN granules after the vortex granulator has a network of shallow nanopores. Some of the pores are cavities on the surface and cannot transport diesel fuel distillate deep into the granule (fig. 31a). Being humidified, the liquid will flow out of these cavities. The retentivity of the granule (if there are many such pores) will be low and will not provide a regulatory indicator.



a



b

Fig. 31. PAN granule after humidification and heat treatment in a vortex granulator (a) and "mechanical" pores on its surface (b)

Although the number of such cavities is about 10% of the total surface area, this index should be reduced to 3-4%. In this case, these cavities will not significantly affect the retentivity of the granule. One should also note that there are "mechanical" pores - faults and cracks on the PAN granules after the vortex granulator, caused by the internal temperature stresses and during vaporization in the heat treatment process (fig. 31b). The "mechanical" pores will not disappear after the final drying. However, their relative number may decrease due to the formation of new nanopores.

Another disadvantage of this sample is the number of twisting micropores (in the nanometer range), making 30-40% of the total number of nanopores. There are also many mesopores (up to 25%). The rest of the pores are macropores. Besides, the pores are predominantly rectilinear on the surface of the PAN granules. It facilitates the penetration of diesel fuel distillate into the granule. However, it reduces the leakage of this liquid influenced by the external forces (starting from gravity). This pore size distribution and pore shape do not significantly affect the ANFO quality preparing this industrial explosive directly on site. However, the long-term storage or transportation to the blasting places through such pores lead to the leakage of the diesel fuel distillate. Besides, these pores can cause the caking of PAN granules since the moisture easily penetrates the near-surface layers and destroys the surface.

Thus, after the final drying stage, it is necessary to increase the number of micropores, and eliminate the cavities substituting them with a network of deep twisting pores.

We consider the nanoporous surface structure of the PAN granules after the final drying stage in a multistage gravitational shelf unit (fig. 32). There are twisted and deep nanopores of different sizes on the surface. One should note the increase in pore depth compared to the PAN sample after the vortex granulator. The granule surface structure is changed in direction of reducing the number of cavities and replacing them with deep pores, increasing the tortuosity of the nanopores, their number and relative area of the porous surface.

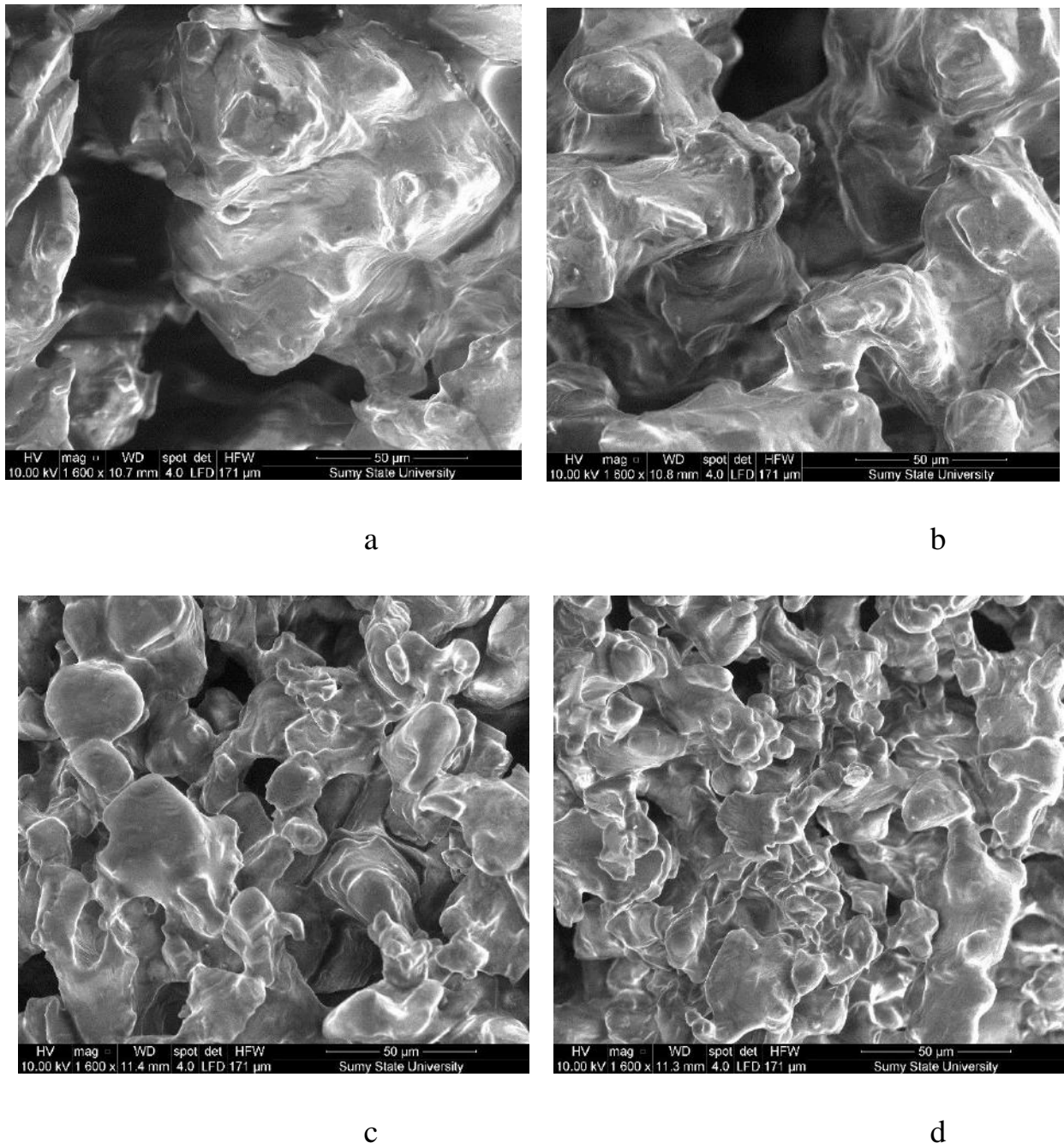


Fig. 32. PAN granule after the final drying stage: a - "mechanical" pores; b - macropores; c - mesopores; d - micropores

The data below show the study regarding the properties of the samples.

1. The method of obtaining the sample: humidification and heat treatment in a vortex granulator.

Strength of the granule, kg / granule - 0.43.

Absorptivity, % –12.2.

Retentivity, % - 8.5.

The relative number of "mechanical pores", % - 14.

Number of nanopores, % (micropores / mesopores / macropores) - 40/25/35.

Relative number of cavities, % - 10.

The relative area of the porous surface, % - 70.

2. The method of obtaining the sample: humidification and heat treatment in a vortex granulator + final drying

Strength of the granule, kg / granule - 0.43.

Absorptivity, % - 13.

Retentivity, % - 9.1.

The relative number of "mechanical pores", % - 10.

Number of nanopores, % (micropores / mesopores / macropores) - 60/30/10.

Relative number of cavities, % - 6.

The relative area of the porous surface, % - 77.

Analysis of these data enables us to draw the following conclusions:

1. After the final drying, the strength of the granules does not decrease since a new cycle of heat treatment does not occur, and the granule continues to dry at the same temperature.

2. The absorptivity value increases since instead of cavities on the granule, there are deep nanopores, which allow the diesel fuel distillate to penetrate deep into the granule.

3. The retentivity value increases since the number of twisting deep micropores increases. These micropores allow the diesel distillate to penetrate deep into the granule and stay securely there.

4. The relative number of mechanical pores decreases since the total number of micropores / mesopores / macropores increases.

5. Some cavities on the surface of the granules are replaced by nanopores of different sizes.

6. The ratio of micropores / mesopores / macropores changes increasing micropores.

7. The relative surface area of the porous surface increases slightly but the porous surface structure undergoes significant changes.

## **6 DRYING MACHINES WITH COMBINED HYDRODYNAMIC REGIMES**

*This section is prepared in accordance to data [6] and references in this work.*

For a theoretical description of the drying process in a shelf dryer, a mathematical model is proposed, consisting of three consecutive levels. The time for drying the dispersed material to the required final moisture content is determined at the first level. The second level of the model is devoted to describing the hydrodynamics of the process; the residence time of particles in the apparatus is determined, which is compared with the drying time from the first level. At the third level, a recurrent calculation of removing moisture from the material in the volume of the entire apparatus is carried out, the efficiency of each stage of the apparatus and the optimal design parameters of the dryer are determined.

By varying the design parameters of the shelf (angle of inclination, the gap between the end of the shelf and the wall of the apparatus, the free section area and the diameter of the perforation holes of the shelf), it becomes possible to determine their optimal values to achieve maximum drying efficiency at each stage of the apparatus.

Due to changes in the design parameters of the shelf contacts of the dryer, the necessary hydrodynamic conditions for the movement of material on each shelf of the cascade are provided. Note that when designing a gravity shelf dryer, it is necessary to ensure uniform contact of the drying agent with the dispersed material on each shelf of the dryer. Achieving this uniformity makes it possible to adjust the residence time of the particles on the shelves, taking into account their physical and chemical properties. Any uneven contact of the drying agent with the dispersed material can lead to underheating (with insufficient drying) or overheating with undesirable destruction of particles and reducing its consumer qualities.

The distribution of the gas flow in the working space of the gravitational shelf dryer at different initial velocities in the drying agent inlet is shown in fig. 33.

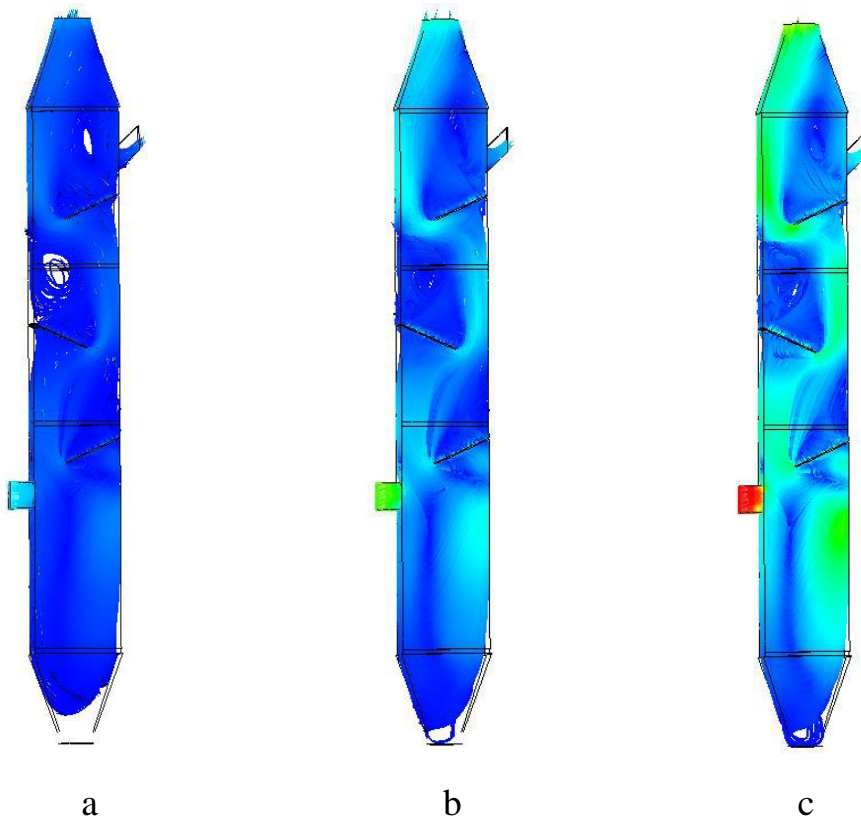


Fig. 33. The distribution of the gas flow in the working space of the gravitational shelf dryer: a –  $V=3$  m/s; b –  $V=8$  m/s; c –  $V=15$  m/s

The nature of the distribution of the gas flow rate at the stage of the shelf dryer under other conditions of experimental studies (design of the shelf and the flow of gas flow) does not change qualitatively. Peculiarities of the gas flow velocity field distribution depending on the initial conditions of the experiment are given below.

Analysis of the results of the experiment on the distribution of the speed of the gas flow at different stages of the dryer depending on the height of their installation with the same design of each stage showed that:

- the distribution of the velocity of the gas flow becomes more uniform with increasing value of the discharge gap;

Diagram of the gas flow velocity for shelf contact of one structure quantitatively changes its profile. This is due to the redistribution of gas flow in the cross-section of the dryer in height, and with height, it becomes more uniform.

When installing in the volume of the dryer shelf contact with different values of the free cross-section (increase in the free cross-section), the following picture is observed:

- the level of speed of movement of a gas stream on a shelf contact is partially leveled;
- there is a decrease in the peak velocity of the gas flow in the discharge gap;
- plot of the velocity of the gas flow in the transition from the shelf contact to the discharge gap has a smoother character.

Reducing the angle of the shelf contact at a constant value of the gap makes its features in the diagram of the distribution of the velocity of the gas flow:

- there is a decrease in the peak velocity of the gas flow on the shelf, the plot is aligned;
- the peak speed of the gas flow in the discharge gap decreases;
- the zone of the maximum speed of the gas flow in the discharge gap expands with the alignment of the plot.

The diagram of the distribution of the velocity of the gas flow with increasing consumption has the same qualitative law but is characterized by the following distinctive features:

- smoothing of the peak in the middle of the shelf contact;
- equalization of speed along the length of the shelf contact;
- the peak velocity of the gas flow in the discharge gap has a more pronounced character.

Diagrams of the distribution of the gas flow velocity make it possible to determine the zones of gravitational motion of the dispersed material, its soaring in the apparatus, separation, and possible removal. To fully describe the hydrodynamics of the movement of the dispersed material, determine the trajectory of its movement and residence time in the volume of the dryer and the impact on these parameters of the shelf contact design and gas flow rate, it is necessary to investigate the basic modes of movement of the dispersed material.

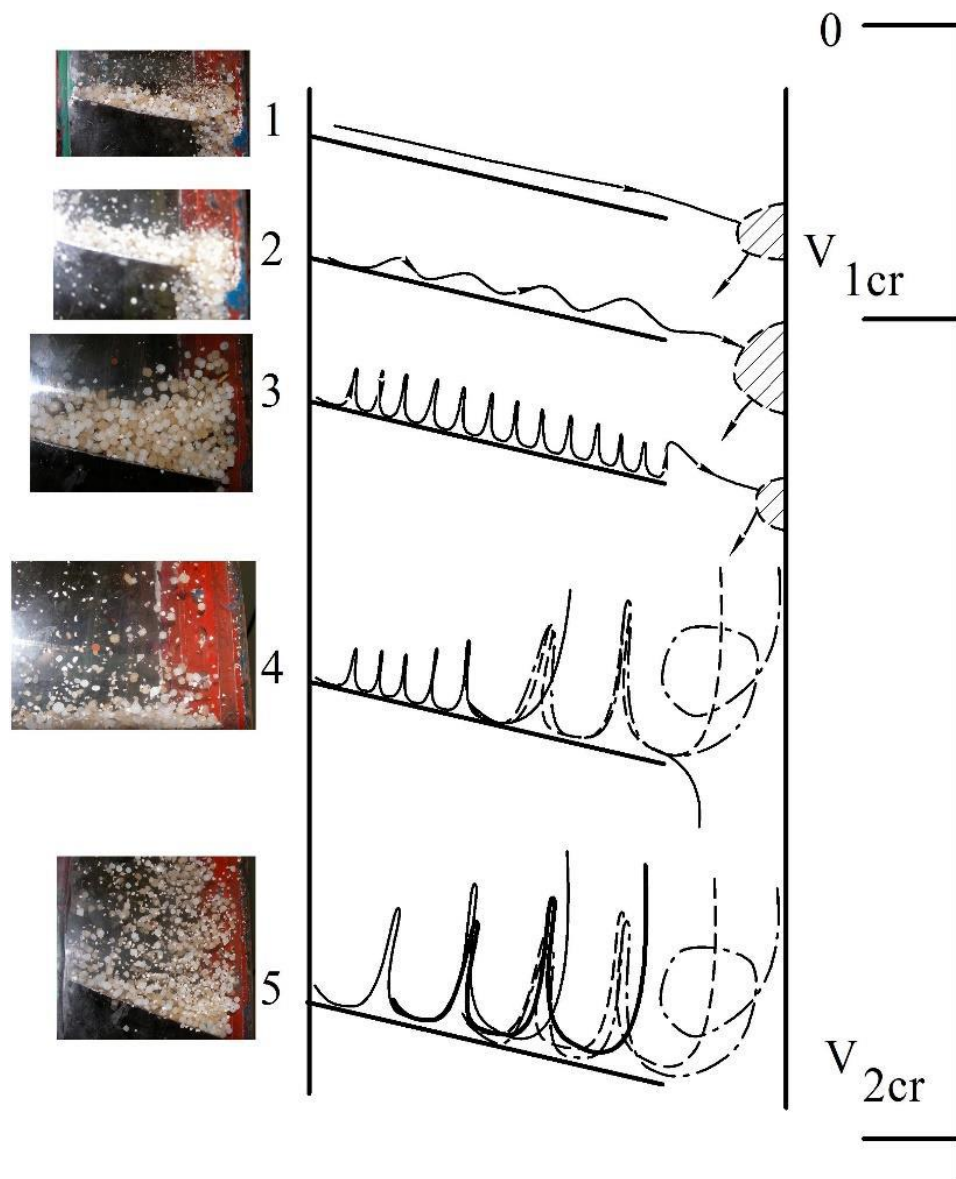


Fig. 34. Operating modes of a multistage gravitational shelf dryer: 1- the gravitational falling layer mode of the dispersed material; 2 - the first transitional mode; 3 - the dryer's operation in the weighted layer mode of the dispersed material; 4 - the second transitional mode; 5 - the dryer's operation in the dispersed material ablation mode

It should be taken into account that the design of the shelf and the peculiarities of its location in the working space of the dryer affect the gas flow rate in the overhead space.

This speed is decisive when choosing the mode of movement of dispersed material. The range of existence of the fluidized bed is determined by the first critical velocity  $V_{ck1}$

(the gas flow rate that corresponds to the beginning of fluidization) and the second critical velocity  $V_{ck2}$  (the gas flow rate that corresponds to the beginning of material removal from the dryer).

As a result of the experiment, as well as on the basis of earlier studies by the authors, a general pattern of changes in the nature of the movement of dispersed material on the shelf was obtained (fig. 18).

Each of the modes is characterized by the peculiarities of the movement of dispersed material, as well as the residence time of the material on the shelf, depending on the degree of the constraint of the flow (the relative content of the dispersed phase in the volume of the apparatus) (fig. 19).

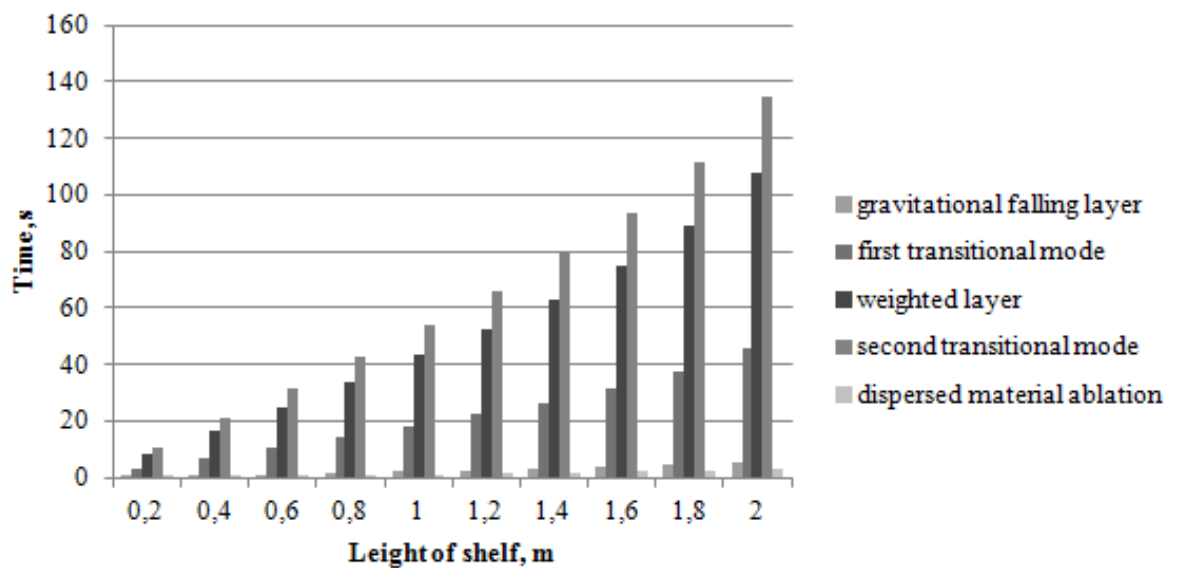


Fig. 35. The residence time of the material on the shelf

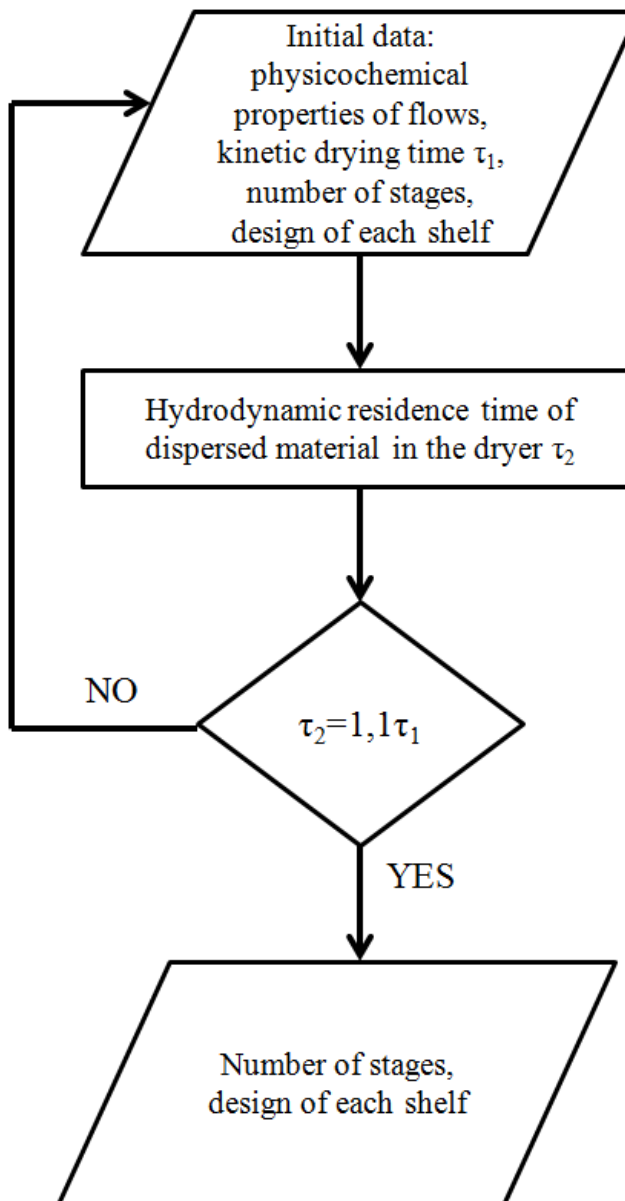


Fig. 36. Algorithm for engineering calculation of a gravitational shelf dryer (large-block model)

Optimization of the shelves' design, their placement features, and the number of stages in the dryer is carried out according to the criterion of the minimum required "hydrodynamic" residence time of the dispersed material. This time should not exceed by more than 10% the calculated drying time. This approach makes it possible to achieve minimum energy costs and ensure the preservation of the strength (and, in some cases, specific properties, such as, for example, seed germination) properties of the dispersed material.

Based on the obtained results an algorithm for engineering calculation of a gravitational shelf dryer is proposed (fig. 37).

It should be noted that the engineering calculation algorithm can be implemented in two ways:

- determination of the design of the dryer, taking into account the provision of the required residence time of dispersed material;

- determination of the design of each stage to ensure the heating time of the dispersed material, the drying time in the constant speed mode and the drying time in the decreasing speed mode.

The second option is more efficient because it allows dividing the dryer into separate zones and a differentiated contact of dispersed material with a drying agent with different temperature and humidity potential is provided.

The research results allowed us to propose new designs of shelves, which allow providing the required residence time of the material in the dryer (fig. 37).

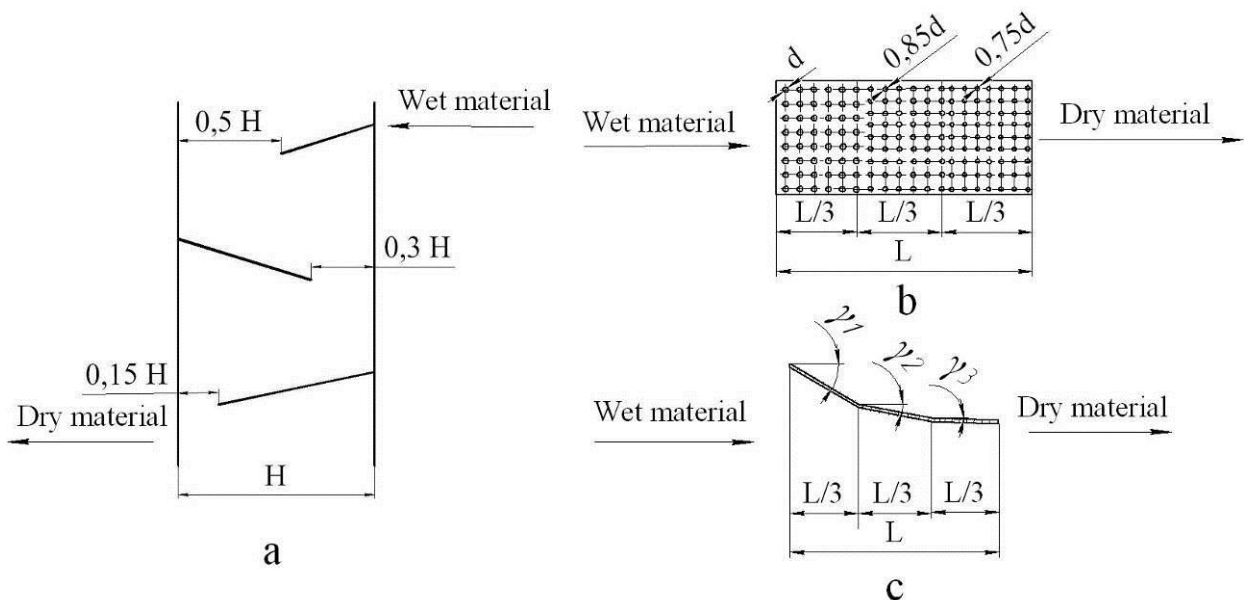


Fig. 37. Constructions of shelves of multilevel gravitational shelf dryer: a – shelf with different gap on height of dryer; b – sectioned shelf with variable perforation of sections; c – partitioned sections shelf with constant perforation and variable angle of inclination;  $d$  – diameter of hole of perforation;  $L$  – length of the shelf;  $H$  – width of device;  $\gamma_i$  – angle of inclination of shelf section to horizon.

The use of inclined perforated contact shelves of the above structures allows to creation at each stage of the dryer, such a hydrodynamic situation in which there is an alignment of the plot of the speed of the drying agent along the shelf, its action remains constant in all areas of the shelf. This causes the process of compensation of the action on the dispersed material of inertial forces and rolling on an inclined surface, braking of the dispersed material on an inclined perforated contact shelf, its uniform movement in the suspended layer and long-term contact with the drying agent.

It is possible to implement the proposed constructive solutions (in addition to the design of the dryer, which is shown in fig. 16) in various designs of dryers-classifiers (fig. 38).

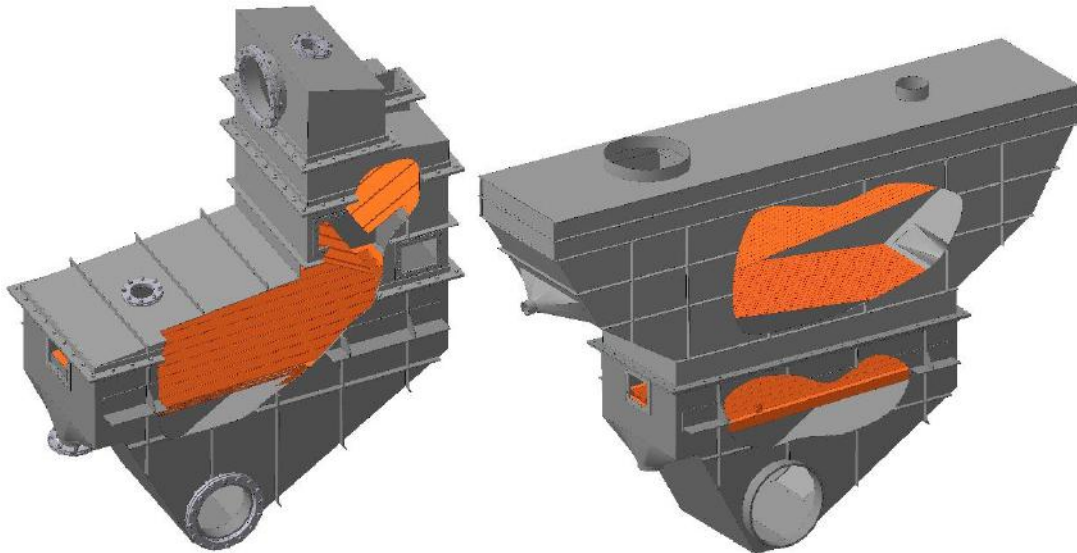


Fig. 38. Constructions of dryers-classifiers

The proposed designs of multistage shelf dryers (in accordance with the model material used in the experiments) can be implemented in industrial drying installations (fig. 39).

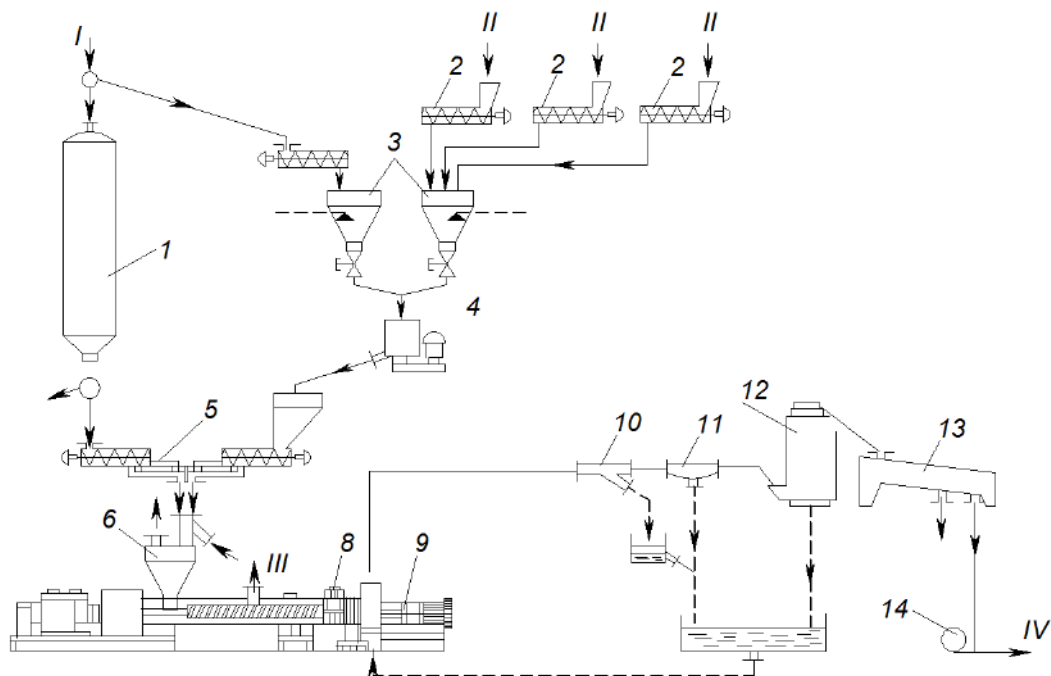


Fig. 39. Technological line of the unit for production of the stabilized and painted polypropylene and polyethylene: 1 – silo for powdered polypropylene; 2 – screw conveyors; 3 – bucket batchers; 4 – high-speed mixer; 5 – the tape batcher; 6 – bunker; 7 – extruder; 8 – the starting valve; 9 – granulator; 10 – damper; 11 – water separator; 12 – dryer; 13 – vibrating sieve; 14 – pneumatic transport; I – polypropylene; II – supplements; III – waste gases; IV – dried polypropylene

One of the most important principles of designing new designs of convective dryers is compliance with energy efficiency requirements because this type of equipment is characterized by sufficiently high values of energy consumption per unit mass of grain product, which is dehydrated. A promising direction to reduce energy costs for creating a flow of high-temperature drying agent in the apparatus is the development of advanced equipment designs with internal partitioning of the working space using shelf contacts.

The engineering calculation method of such devices is based on the results of theoretical and experimental studies of hydrodynamic parameters of flow motion and kinetics of dehydration of granular materials.

Based on the results of modeling the kinetics of the drying process of a single granular particle, the required time of its dehydration in the flow of the drying agent with the specified characteristics is determined. The theoretically and experimentally hydrodynamic characteristics of the flow of drying agent and dispersed material allow determining the time of its stay in the apparatus depending on the design of shelf contacts and technological parameters of the process. At the stage of analysis of the laws of the kinetics of the process of dehydration of the dispersed material on the cascade of shelves, the optimal organization of the flow is determined, which will provide the minimum energy costs at the required final humidity of the product.

As a result of optimization calculation of the gravity shelf dryer according to the initial data established by the customer of the industrial equipment, it becomes possible to define its following design characteristics:

- the number of shelf contacts in the dryer;
- the angle of inclination of the shelf contacts to the horizon;
- the size of the gap between the end of the shelf contact and the wall of the dryer (or the length of the shelf contact);
- the area of the free section of the shelf contact.

The design characteristics of shelf contacts at each stage of the dryer may differ due to the physicochemical characteristics and strength of the granular material, its stability under long-term exposure to high-temperature drying agent, as well as minimizing energy consumption for the dehydration process.

## **7 FLUIDIZED BED IN GRAVITATIONAL SHELF DRYERS: OPTIMIZATION CALCULATION**

*This section is prepared in according to data [7] and references in this work.*

Implementing a fluidized bed in heat-mass transfer processes has become widespread due to the undoubted advantages of such a hydrodynamic system. At the same time, there are often difficulties in devices with a fluidized bed providing the required hydrodynamic regime. In this regime, the dispersed phase is predicted to spend in the device the estimated time needed to complete the process. In this case, a significant advantage of devices with a fluidized bed is the ability to control the residence time of the dispersed phase in the workspace of the device. Despite the variety of granulation and drying devices multistage devices with vertical sectioning of the working space did not receive a wide distribution for drying. The effectiveness of such devices has been proven by the example of various classifiers and granular devices, which confirms the relevance of their further implementation in the drying technology. The authors of this work attempted a theoretical description, experimental studies of the fluidized bed configuration, and the conditions for the implementation of heat-mass transfer processes in other devices with the directed motion of the dispersed phase - vortex granulators.

The article aims to form an algorithm for calculating the hydrodynamic parameters of the flow in devices with inclined shelves for the implementation of heat treatment and dehydration processes. The research results will complement the general algorithm for the engineering calculation of shelf units, which authors begin to study in the research.

The authors use the hypothesis of the possibility to control the motion trajectory and the residence time of the dispersed phase in the dryer's workspace thanks to its directed transfer mechanisms. The joint solution of the basic equations of flow motion hydrodynamics, the kinetics of change of the temperature-humidity features in the interacting flows, and the growth rates of granules will allow inventing a rational design of the workspace, heat transfer agent's optimum flow rate and its temperature-humidity features in a shelf dryer. The calculation is carried out by the optimization criterion of the

“minimum” hydrodynamic “residence time of the dispersed phase in the workspace of the device”.

Hydrodynamic” time should be equal to “kinetic” time - the period during which the temperature and moisture content features of the dispersed phase should acquire a normative value. This paper presents an algorithm for calculating the "hydrodynamic" residence time of dispersed particles in a shelf dryer's working space. At the same time, the drying operating temperature was maintained in the dryer, which, for example, for granules of porous ammonium nitrate was 105-110 °C.

There are multiphase flows of different nature. The following types of multiphase flows should be distinguished. In the first case, the considered volume is filled with the substance of one phase. The substance of another phase occurs in the form of discrete particles (solid phase) or bubbles (gaseous phase) where the volume rate of the substance of the other phase is low (up to 10% of the total volume). In the second case, the considered volume is partially filled with liquid and partly with gas, which does not mix and the free surface separates them from each other. In the most difficult case, substances of different phases can mix (dissolve / stand out from solution), and the volume rate of the substance of another phase is large (over 10 % of the total volume). Various approaches are used to model these multiphase flows.

In the case under consideration, the dispersed phase motion trajectory applies to the dispersed particle model. The substance forming the main phase is assumed to be a continuous space, and its flow is modeled (depending on the flow turbulence degree) by the Navier – Stokes or Reynolds equations and the flow continuity. The substance in the flow in the form of discrete particles does not form a continuous medium. Individual particles interact with the flow of the main phase and with each other discretely. The Lagrange approach is used to model the motion of the particles of the dispersed phase. It means that the motion of the separate particles of the dispersed phase influenced by forces from the side of the main phase flow, is controlled.

It should be noted that there is a constrained motion of particles (discrete particles, a solid phase, occupies a volume greater than 10 % of the total space in the device) in the

industrial model of a shelf dryer. In this case, the calculation model should be supplemented with a block that allows defining how the particles' residence time changes (increases) in the dryer if the volume of particles increases more than 10 %.

The fraction composition of particles (distribution by size), the motion of which is modeled in this work is shown in fig. 40.

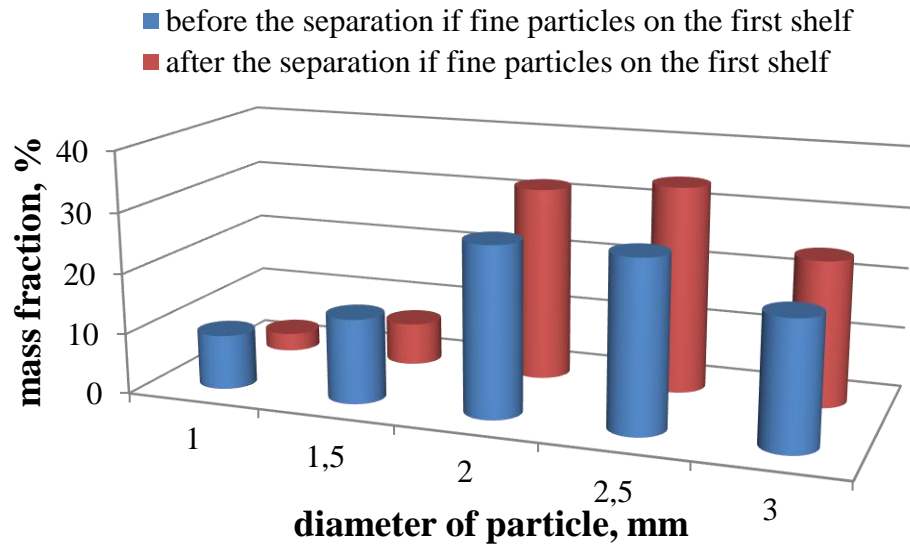


Fig. 40. The fraction composition of particles

The previous experimental studies demonstrate that the gas flow in the shelf dryer is turbulent. Direct modelling of the turbulent flows by calculation of the Navier – Stokes equations written for instantaneous velocities is complicated. Besides, not instantaneous, but time-averaged velocity values attract attention. For the analysis of turbulent flows, the Reynolds equation and the continuity of the flow are used:

$$\frac{\partial}{\partial \tau} (\rho_{cf} \overline{u_{cfi}}) + \frac{\partial}{\partial x_j} (\rho_{cf} \overline{u_{cfi} u_{cfj}}) + \frac{\partial}{\partial x_i} (\rho_{cf} \overline{u'_{cfi} u'_{cfj}}) = - \frac{\partial p}{\partial x_i} + \frac{\partial}{\partial x_j} \left[ \mu_{cf} \left( \frac{\partial \overline{u_{cfi}}}{\partial x_j} + \frac{\partial \overline{u_{cfj}}}{\partial x_i} \right) \right] + f_i, , \quad (54)$$

$$\frac{\partial \rho_{cf}}{\partial \tau} + \frac{\partial}{\partial x_j} (\rho_{cf} u_{cfj}) = 0, \quad (55)$$

where  $\overline{u_{cf1}}, \overline{u_{cf2}}, \overline{u_{cf3}}$  – time-averaged velocities of carrier phase,  $\overline{u'_{cf1}}, \overline{u'_{cf2}}, \overline{u'_{cf3}}$  – pulsation component of velocities of carrier phase.

In equations (54) and (55) the simplified equations are used,  $i, j = 1 \dots 3$ , the summing up to over the same indices are assumed,  $x_1, x_2, x_3$  - coordinate axes,  $\tau$  - time. The  $f_i$  term expresses the action of mass forces.

In this system of 48 equations, the independent sought parameters are 3 velocity components  $u_{cf1}, u_{cf2}, u_{cf3}$  and pressure  $p$ . The density  $\rho_{cf}$  of the gas, at velocities up to about 0.3 of the Mach number, can be assumed to be constant.

As the boundary conditions, the adhesion condition is set on all solid walls (the velocity is zero), the distribution of all velocity components in the inlet section, and the first derivatives (in the direction of flow) of the velocity components in the outlet section are equal to zero. Besides, the direct interest is the distribution of the velocity along the length of the device in space above the shelf, where the motion of dispersed particles occurs.

The range of existence of a fluidized bed in a shelf device is limited by such two boundary conditions or two critical gas flow (carrier phase) velocities: (i) the first critical velocity or the velocity of the start of fluidization; (ii) the second critical velocity or the velocity of the start of ablation. The values of these velocities depend on the size (diameter) of the dispersed phase, the flow rate of the carrier phase, and the velocity in the overhead space of the device (depends on the value of the free section of the shelf, its tilt angle, length, etc.).

Let us assume that the dispersed phase particles have a spherical shape. The forces influencing this particle are caused by the difference between the particle velocity and the flow velocity in the main phase and the displacement of the main phase by this particle. The equation regarding the motion of such a spherical particle is as follows:

$$m_{df} \frac{du_{df}}{d\tau} = 3\pi\mu_{df} dC_{cor} (u_{cf} - u_{df}) + \frac{\pi d^3 \rho_{cf}}{6} \frac{du_{cf}}{d\tau} + \frac{\pi d^3 \rho_{cf}}{12} \left( \frac{du_{cf}}{d\tau} - \frac{du_{df}}{d\tau} \right) + F_e \quad (56)$$

Here  $m_{df}$  - the mass of the particle,  $d$  - the diameter of the particle,  $u_{df}, u_{cf}$  - velocity;  $\rho_{df}, \rho_{cf}$  - density;  $\mu_{df}$  - the dynamic viscosity of the substance in the main phase,  $C_{cor}$  - its viscous resistance coefficient;  $F_e$  - an external force which is directly acting on a particle (for example, gravity, aerodynamic drag, centrifugal force etc.); index  $df$  refers to the dispersed phase, index  $cf$  refers to the carrier phase.

According to Stokes's law, the first term on the right-hand side of equation (49) expresses the deceleration of the particle as a result of viscous friction against the flow of the main phase. The second term is the force applied to the particle due to the pressure drop in the main phase surrounding the particle caused by the main phase flow's acceleration. The third term is the force required to accelerate the main phase's weight in the volume displaced by the particle.

Let us consider the dependence of the ascending velocities profile on the structural features of the inter-shelf space, namely, the length of the shelves, the degree of their perforation and the installation angle  $\gamma$ . The ascending velocities profile will have a peculiar peak in the inter-shelf space with no perforation (fig. 41).

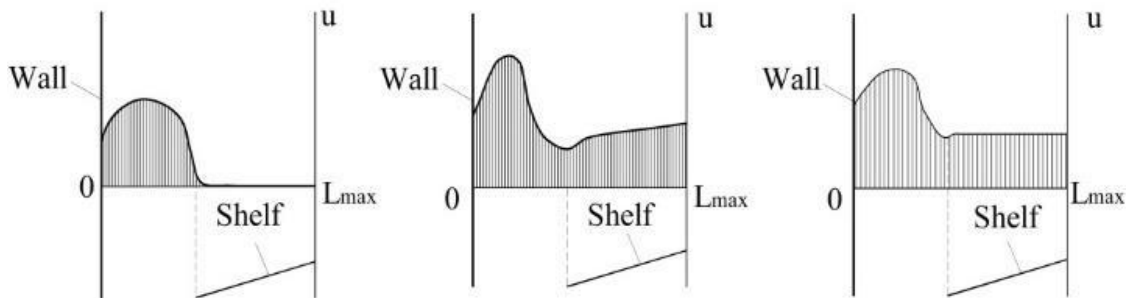


Fig. 41. Gas flow velocity profiles: a – non-perforated shelf; b – perforated shelf with constant length perforation; c – perforated shelf with variable length perforation

In the presence of perforation, the peak decreases according to the increase in the drying agent's flow rate through the sectioning shelves holes (Fig. 24 b). Optimization of the ascending velocity profile can be achieved not only by changing the outloading gap and the tilt angle of the shelves, but also by varying the perforation degree along the shelves (Fig. 24 c).

When establishing shelf contacts with different outloading gap, the epure of the gas flow velocity distribution has the following features:

- the distribution of the gas flow velocity has the descending nature from the wall of the device to the end of the shelf contact. It is caused by the length difference of the pressure under the shelf contact and above it;

- when reducing the ratio of the current length to the length of the shelf  $X/L$ , starting from the middle of the shelf contact, there is an intense decrease in the gas flow velocity, caused by the creation of swirls in the outloading gap. Reducing the outloading gap size leads to an increase in the intensity of swirls at the end of the shelf contact, which disrupts the ascending motion of the gas flow;

- the minimum velocity value of the gas flow at the shelf contact is greater, the smaller the outloading gap value is.

The results analysis regarding the gas flow velocity distribution at different stages of the dryer depending on their height with the same design of each stage showed that:

- the distribution of the gas flow velocity becomes more uniform with the increasing value of the outloading gap;

- the epure of the gas flow velocity for shelf contact of one structure quantitatively changes its profile. It is caused by the gas flow redistribution in the dryer's cross section in height, and with the height it becomes more uniformed.

When installing shelf contact with different values of the free cross-section (the free cross-section increase) in the dryer, the following situation is observed:

- the level of the gas flow motion velocity is partially leveled on a shelf contact;
- there is a decrease in the peak velocity of the gas flow in the outloading gap;
- the epure of the gas flow velocity in the transition from the shelf contact to the outloading gap has a smoother character.

Reduction of the shelf contact angle at a constant gap  $X/L$  puts its features in the epure of the gas flow velocity distribution:

- there is a decrease in the peak velocity of the gas flow on the shelf, the epure is leveled;

- the peak velocity of the gas flow decreases in the outloading gap;
- the zone of the gas flow maximum velocity in the outloading gap is expanded with the alignment of the epure.

The epure of the gas flow velocity distribution with increasing consumption has the same qualitative law, but is characterized by the following distinctive features:

- smoothing of the peak in the middle of the shelf contact;
- leveling of the velocity along the length of the shelf contact;
- the peak velocity of the gas flow in the outloading gap is more expressed.

Epures of the gas flow velocity distribution enable to define the gravitational motion zones of the dispersed material, its soaring in the device, separation, and possible ablation. It is necessary to investigate the basic modes of the dispersed material motion to describe the hydrodynamics of the dispersed material motion, identify its motion trajectory and residence time in the dryer and the impact on these parameters of the shelf contact construction and gas flow rate.

Analysis of the previous studies in the two-phase flows modelling field, which consist of gas as a dispersion phase and dispersed particles, shows that one of the most promising ways to calculate the motion of particles is the so-called trajectory method. In modelling, the constrained motion of particles with large (0.5–5 mm) diameter can be based on the Lagrangian model of force analysis of particle motion using differential equations of motion which have already been used to describe hydrodynamic conditions of dispersion phases in the workspace of the shelf device. At the same time, for the case of granules motion in the workspace of the device, the application of the trajectory method is complicated by the following:

- polydispersity of the system;
- constrained motion of granules in the shelf device.

Thus, the trajectory method with highly accurate results can be used only if there is a software that allows one to export a theoretical model of the single particle motion and to take into account the degree of flow constraint.

In this work, the software product Ansys Fluent is used to export the original mathematical model, to calculate the granules trajectories and the distribution law of the polydisperse system in the workspace of the shelf device taking into account the concentration of the dispersed phase (the flow constraint).

Results visualization of the polydisperse system motion modelling in fig. 42 (relative content of the dispersed phase in the workspace  $\psi = 0.2$ ).

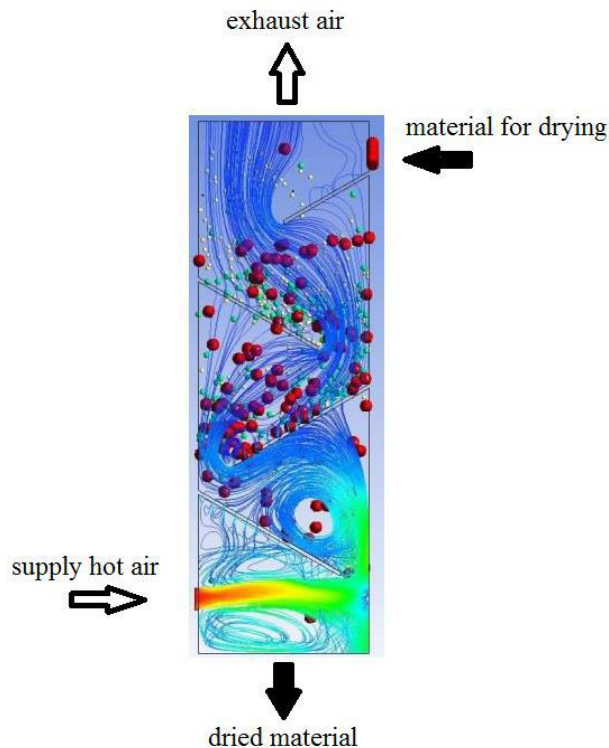


Fig. 42. Visualization of results of the poly disperse system constrained motion modelling in the shelf device

The methodology for carrying out this stage in the research allows inserting the calculated number of granules of a certain size as initial data (analog of the polydisperse system's fractional composition) and the total number of granules (analog of the degree of dispersed flow compression). With the help of this technique it becomes possible to define the dispersed phase trajectories and refine the empirical constraint coefficient  $m$  to calculate the constrained motion time.

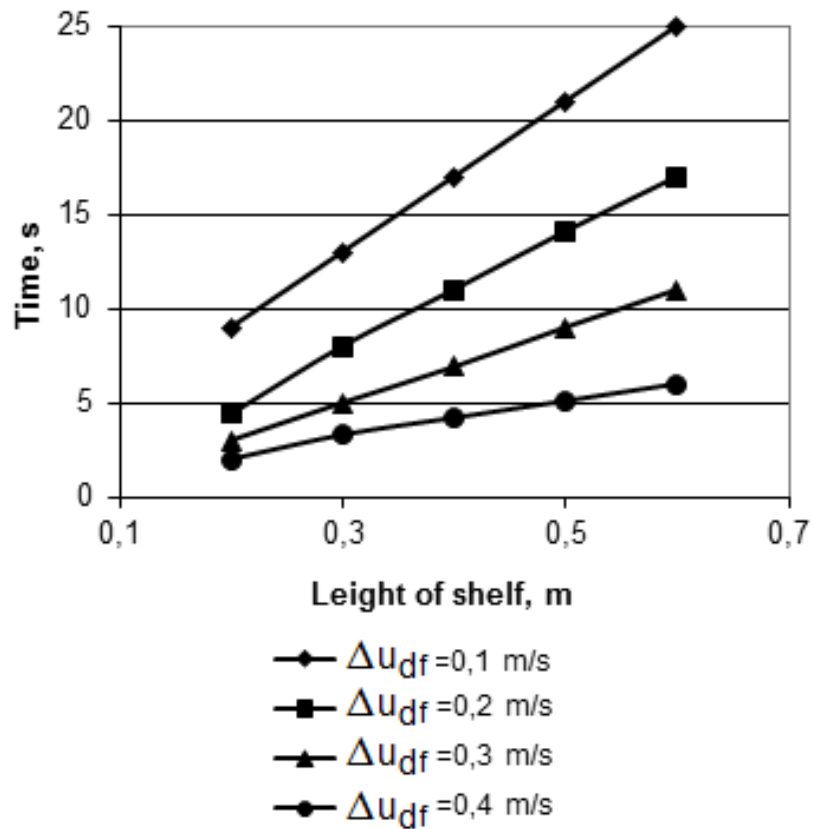


Fig. 43. The residence time of the particle on the shelf (free motion):  $d_p = 2 \text{ mm}$ ;  $\psi = 25\%$ ,  $\gamma = \gamma_0 + (11-13)^\circ$

Figs 43–46 show data for calculating the residence time of dispersed material on the shelf in free and constrained mode, and an example of comparing data for determining the residence time of dispersed material in the constrained mode according to the theoretical model, experimental data and computer modelling data.

Data from Fig. 26 show that the results of computer modelling give a higher value of the residence time of the dispersed phase on the shelf in the device. It is explained by the inhibition of particles not only due to the action of neighboring particles, but also due to the creation of a vortex gas flow zone at the end of the shelf.

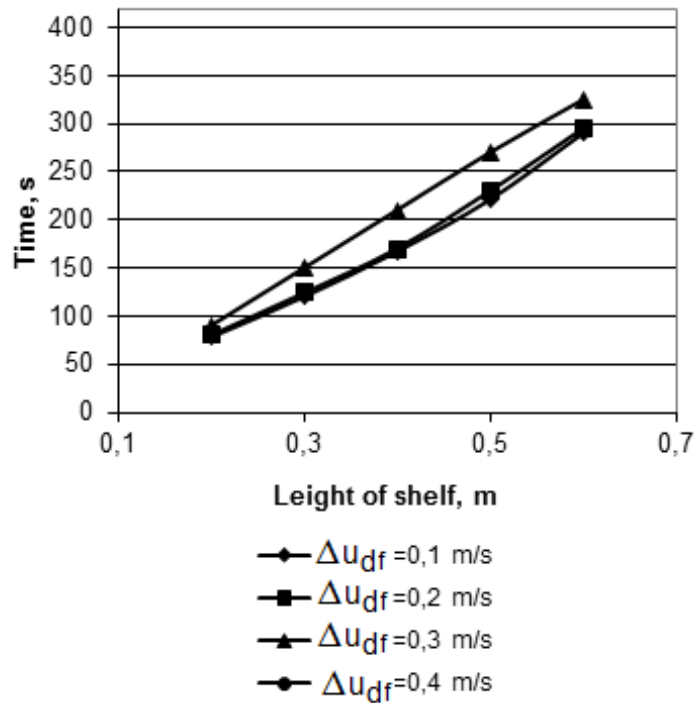


Fig. 44. The residence time of the particle on the shelf (constrained motion):  $d_p = 2$  mm;  $\psi = 25\%$ ,  $\gamma = \gamma_0 + (11-13)^\circ$ ,  $\delta = 0.6$

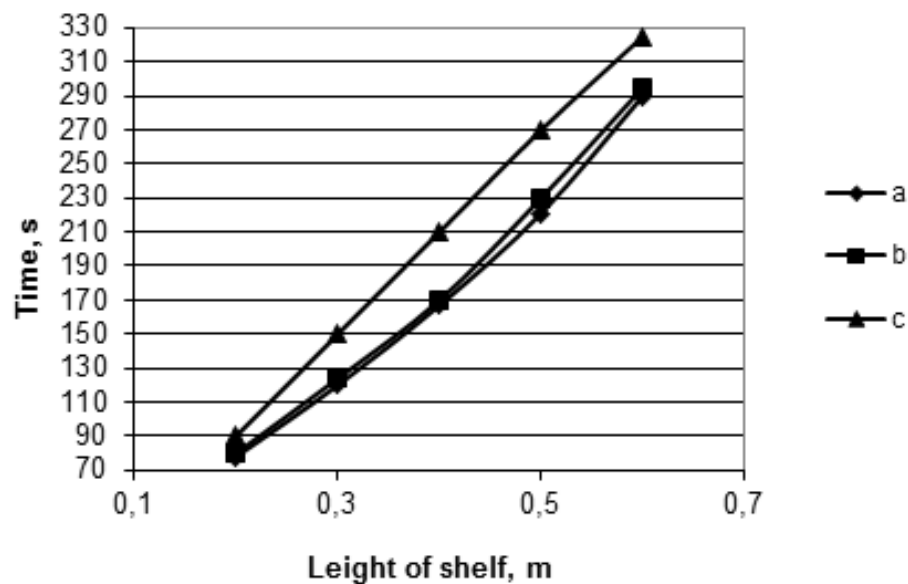


Fig. 45. The residence time of the particle on the shelf (constrained motion):  $d_p = 2$  mm;  $\psi = 25\%$ ,  $\gamma = \gamma_0 + (11-13)^\circ$ ,  $\delta = 0.6$ ,  $\Delta u_f = 0.2$  m/s; a – data from the theoretical calculation; b – data of the experimental studies; c – data of the computer modelling

## **8 ANALYSIS OF PARAMETERS AND OPERATING MODES OF DRYERS IN TERMS OF MINIMIZING THE ENVIRONMENTAL IMPACT**

*This section is prepared in according to data [8] and references in this work.*

Drying is a new process involving both heat and mass transfer, with the driving force being enthalpy and concentration differences. Fluidized bed dryers (FBD) are the most commonly used dryers than other dryers in industries. Fluid bed dryers show reasonable drying rates in the solids handling industries. Fluid bed drying to dry grain immediately after harvest is an effective alternative to on-farm drying for farmers in developing countries. The reasons for the adaptation of fluidized bed dryers are higher heat transfer between gas and solids, good contact with wet particles, good solids circulation rate, high capital cost reduction and fast drying with satisfactory product quality compared to other traditional dryers.

It is significant to examine the energy consumption and energy efficiency of FBD. The thermodynamic analysis is the critical study of the system design for energy analysis and optimization. FBD energy expertise does not provide comprehensive information on the process based on the first thermodynamic law. In this regard, the analysis of exergy as the maximum useful work that can be extracted from a system under standard environmental conditions should have the potential to describe a working system following the second thermodynamic law.

It is essential to emphasize that in the case of the same temperature and exergy rate of the dried material and the fluidizing/drying medium (SHS) in mechanical vapor recompression – fluidized bed dryers (MVR–FBD) system, this process is going without energy recovery. Simultaneously, the self-heat recuperative fluidized bed dryers (SHR–FBD) system provides heat recovery, including the sensible heat of the dried material and the condensate. Hence, higher energy efficiency could be earned from the SHR–FBD system employing air as a fluidizing/drying medium. SHR–FBD system utilizing air as fluidizing/drying medium can reduce the drying energy consumption compared to hot air

drying with conventional heat recovery or MVR–FBD system using SHS as fluidizing/drying medium. Numerically, the developed SHR–FBD system can reduce the energy consumption to about 15 % and 75 % of that required in hot air drying with conventional heat recovery and MVR drying technologies.

According to the Sustainable Development Goals until 2030, one of the promising areas is introducing energy-saving technologies. This approach is especially crucial in the case of the development of new or improvement of existing drying units. Simultaneously, the modification of design and operating parameters must meet the indicators of economic efficiency and environmental safety. Assessment of the environmental and economic efficiency of the technology enables to choose the most appropriate option in terms of these two components. The economic effect is based on developing innovative energy-saving technologies, particularly with heat and energy recovery. The ecological effect is related to the decreasing of technogenic load on the environment by the pollutants emissions-reducing and renewable energy sources.

In comparing grain drying equipment about the impact on the environment, modern foreign grain dryers have a relatively small impact on the indicators (volumes) of harmful substances emissions into the atmosphere. Most Ukrainian enterprises have outdated equipment that needs updating and improvement. There is an essential issue of grain processing with the least economic and environmental losses and environmental pollution.

The main problem with the drying of low-rank coal (LRC) is the energy intensity of the process related to the water's high latent heat. Although a conventional heat recovery (CHR) dryer allows using waste stream heat, it still consumes significant energy due to the inability to recover large amounts of latent water heat. Until now, this technique has been applied to drying systems using both non-condensable and condensable drying media.

The utilization of high amounts of energy in the drying industry makes the drying process one of the most energy-intensive operations with great industrial significance.

Thus, one of the most significant challenges of the drying industry is to reduce the cost of energy sources for good quality dried products.

A self-heat recuperation (SHR) technology that effectively recovers latent and sensible heat has been developed to enhance more energy-saving have developed a drying system based on SHR technology with a dryer applying countercurrent heat exchanger type utilizing air as a drying medium. They presented a great possibility of SHR application to the drying process. A state-of-the-art SHR technology is developed based on the concept of exergy recuperation. The SHR system's description is on the exergy recuperation through compression, heat exchange, and heat pairing for each sensible and latent heat.

In one study the authors designed the fluidized bed drying process for energy saving and economical LRC drying. The proposed technique uses an exergy recovery module to remove freezing water based on heat recovery technology, a heat integration module to remove antifreeze water, and a cooling module to cool the hot particles LRC. A fan is used instead of an expensive compressor for removing the freezing water to reduce capital costs.

Table 7 compares energy consumption per ton of LRC for three different energy-efficient fluidized bed drying processes. The steam recompression dryer (SRD) consumed the most electricity to compress steam, namely 80 kW, while the CHR consumed half that amount.

Table 7 – Comparison of energy consumption per ton of LRC in different drying systems

		<b>Proposed process</b>	<b>VRC</b>	<b>CHR</b>
Heat exchange amount Q1	kW	341	341	341
Recovered energy	kW	323.7	331	69
Electrical energy	kW	40.5	80.0	-
Amount of extracted steam	kW	53	-	272
Total energy consumption Htot	kW	174.5	240	272
Energy efficiency	%	51.2	29.6	20.2
$\eta = 1 - H_{tot} / Q_1 \times 100$				
Ratio	-	0.64	0.88	1

In conventional low-temperature dryers, water is removed from the air by condensation. The air is cooled to below the dew point and then heated to the drying temperature. The dried air is then used for drying, but the overall energy efficiency is below 50 %. For example a group of scientists applied a heat pump for air dehumidification to enhance the performance. However, compared to the conventional dryer, the result did not significantly affect energy efficiency and drying time. Some authors proposed combining a vacuum-freeze dryer and a convective air dryer in two successive stages. This system could be a potential option because the product quality is maintained. The result with an energy efficiency of 50–60 % is only meant as an alternative for vacuum-freeze dryers.

Simulation studies of single- and multi-stage zeolite drying for the temperature range 50–90 °C showed that it is possible to achieve energy efficiency of 75–90 %, and in particular configurations, for heat recovery, the efficiency may go up to 120. For low-

temperature drying in the range 10–50 °C, heat recovery possibilities differ from medium temperature drying in multi-stage zeolite dryers

Another aspect is that in medium-temperature drying, the dehumidified air requires additional heating, while in low-temperature drying, air cooling may be required after drying. Both factors result in lower energy efficiency for multi-stage desiccant dryers. The exergy and energy analysis of dryers of different designs and different bed materials have been investigated. In particular, a study carried out with two steam drying processes with and without steam recirculation showed that the energy is significantly reduced by up to 90% with traditional drying with heat recovery.

Therefore, when drying wood particles using a fluidized bed dryer for the domestic industry, the dryer must be optimally designed for the target amount of wood particles, and the air circulation rate must be appropriate for that dryer size (fig. 46).

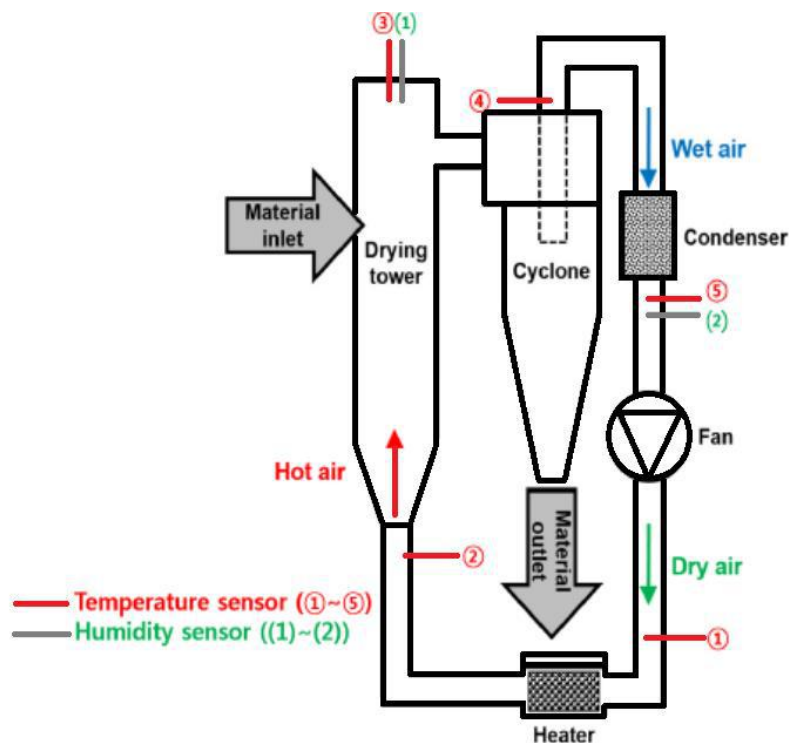


Fig. 46. Fluidized bed dryer for wood particles

The correlation between initial moisture content in rice and energy consumption, energy utilization rate (EUR) and exergy efficiency was found based on energy and exergy analysis of fluidized bed drying. The higher temperature of the drying air led to an increase in energy consumption, thus increasing the energy utilization rate and reducing the exergy losses led to the rise in the exergy efficiency and, therefore, an increase in the efficient use of the available energy in the drying air. However, only 31–37 % of the exergy is used to dry rice, indicating that the remaining exergy can be used.

The bibliometric method was used in this study as an effective approach to meta-analysis (fig. 47) of an investigated scientific problem. As a quantitative analysis, this method lets collect the results from previous studies, structure them according to the required parameter, and, based on generalized information, highlight problem areas and unsolved problems. The bibliometric analysis helps avoid carrying out a multifactorial experiment, often presented as a problematic scientific task, due to the generalization of other researchers' results regarding the drying efficiency for given system parameters. This study focuses more on the overall statistical characteristics of the literature and citation analysis used to identify highly cited papers and references. Citation analysis based on keyword search determines the importance of specific research and identifies the topics that receive the most attention in this field.

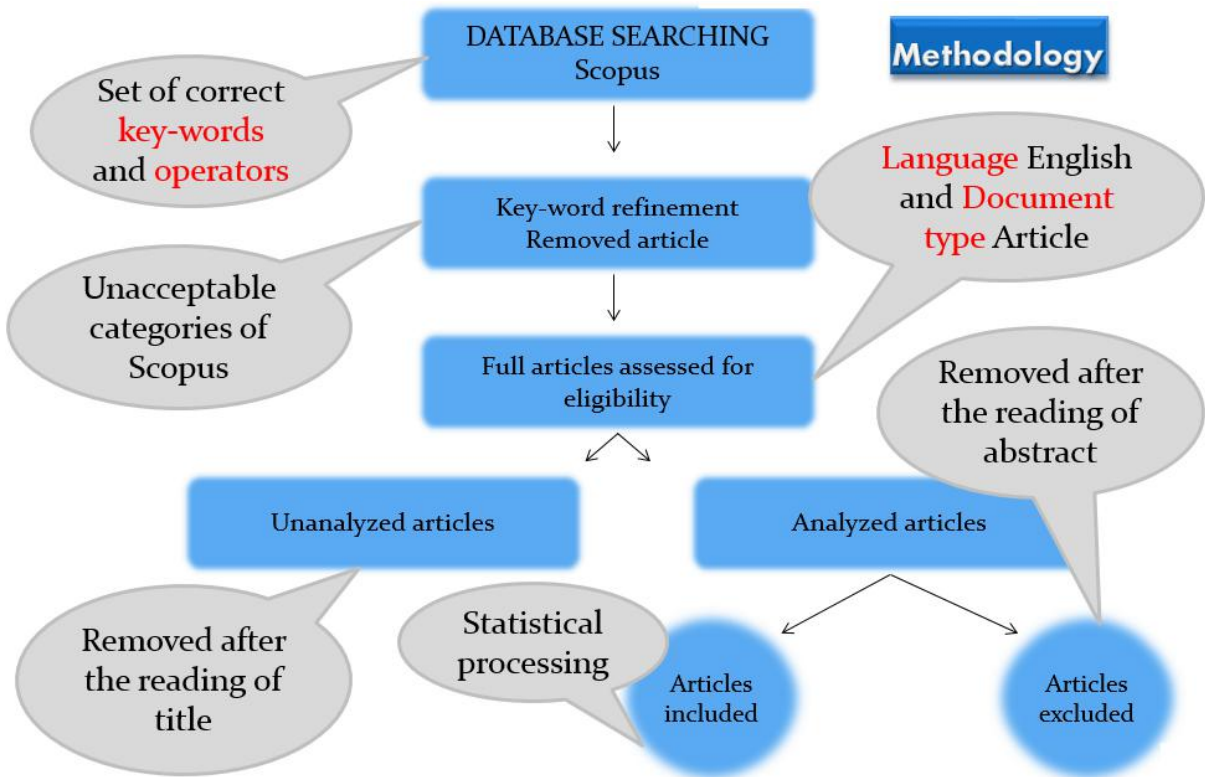


Fig. 47. A methodology of meta-analysis process

Therefore, keyword analysis is used to explore research topics and hotspots in this field. Moreover, this study also uses other indicators, particularly, impact factors, to evaluate the impact of journals and H-index to assess the scientists' research output. The main advantage of the h index is that it combines the measurement of quantity and influence in a single concise and useful indicator. In the bibliometric analysis, the essential software tools include CSV and VOSviewer used for visual analysis that can compile bibliographic data from the Scopus and Web of Science.

The data in this study come from the Scopus. The Scopus database provides comprehensive, multi-disciplinary citation data and is the primary data source for bibliometric analysis. Fig. 3 shows the research framework of this study. The search fields used in this study are TITLE-ABS-KEY, which contains titles, abstracts and keywords. The specific search form is TITLE-ABS-KEY = ((“fluidized bed dry\*” OR “multi-stage dry\*” OR “vertical sectioning dry\*”) AND (“energy efficiency” OR “energy utilization” OR “ecological safety” OR “energy analysis” OR “exergy analysis”)). The document type

(DOCTYPE) is an article, the search language is English, the time is a period (2014-2020), and the search time is July 29, 2020. A total of 124 documents were obtained. All data were exported in full records and cited references type for bibliometric analysis.

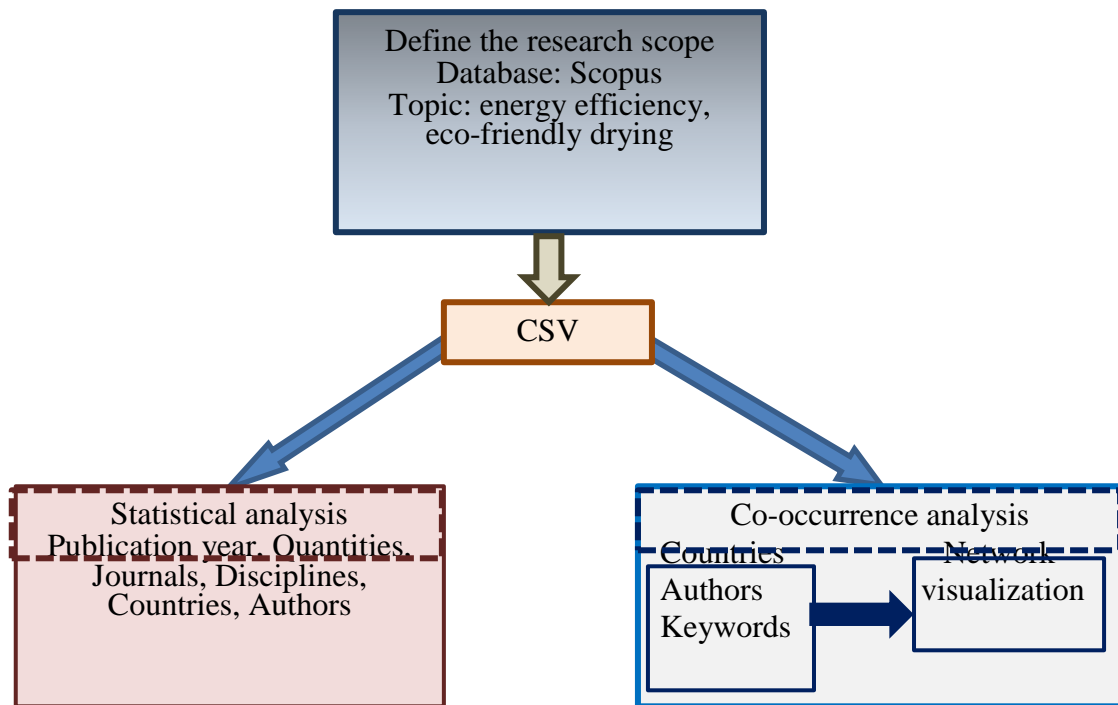


Fig. 48. A flowchart of systematic bibliometric review

Multi-stage small-sized drying plants can meet the criteria of environmental and economic efficiency in the following cases. First, their implementation through the transition to energy-saving technologies gives a financial benefit. Secondly, such technologies should provide a reduction in economic tax, as well as environmental and economic damage. The prevented damage in the case under study is achieved by introducing environmental protection measures to avoid air pollution with dust.

Economic indicators define the total cost of natural resources used in production, the cost of natural resources per unit of output, the amount of payment for environmental pollution by emissions, effluents, waste, etc., the cost of environmental measures and compensation. Environmental indicators describe the level of harmful effects on the environment due to the extraction of natural resources and environmental pollution by

emissions, effluents, waste. Environmental indicators also include the amount and concentration of harmful substances in emissions, effluents and waste, and the probability of accidental emissions, effluents, and wastes during production. The material and energy balance equations determine the quantitative, cost and relative indicators of natural resource use and environmental pollution.

According to the sustainable development goals and tasks for Agenda 2030 implementation at the national level, it is globally relevant to substitute such minerals as coal or natural gas used in electricity production with renewable energy sources. Biogas solutions are often highlighted as a cornerstone of bio-based circular economy and represent a strategic means of simultaneously managing waste and producing renewable energy, fuels and biofertilizer while increasing the valorization of raw biowastes in a decarbonization setting.

The methodology for substantiating the ecological and economic efficiency of dryers includes: 1) to manage the design and operating parameters of the investigated dryers to reduce dust emissions to the level of standard indicators; 2) to find the ways and means of heat and energy recovery; 3) to assess the use of renewable energy sources, including the integrated planning of the placement of dryers and bioreactors within the same facility.

The keywords usually reflect the author's purpose and interest in the research field. In this study, we can identify research hotspots in the area of multi-stage shelf fluidized bed dryers through the frequency and clustering analysis of keywords. Fig. 4 shows the occurrence network of the main keywords. The size of the circle indicates the frequency of the keyword. The larger the circle, the more frequently it appears. The line between two circles represents the co-occurrence links between two keywords.

Fig. 49 demonstrates that the keywords that appear more frequently include some general keywords, such as energy efficiency, energy utilization, energy and exergy analysis because these keywords are included in the search terms. Therefore, we separate

these keywords and focus on concrete research subject to analyze the specific research topic.

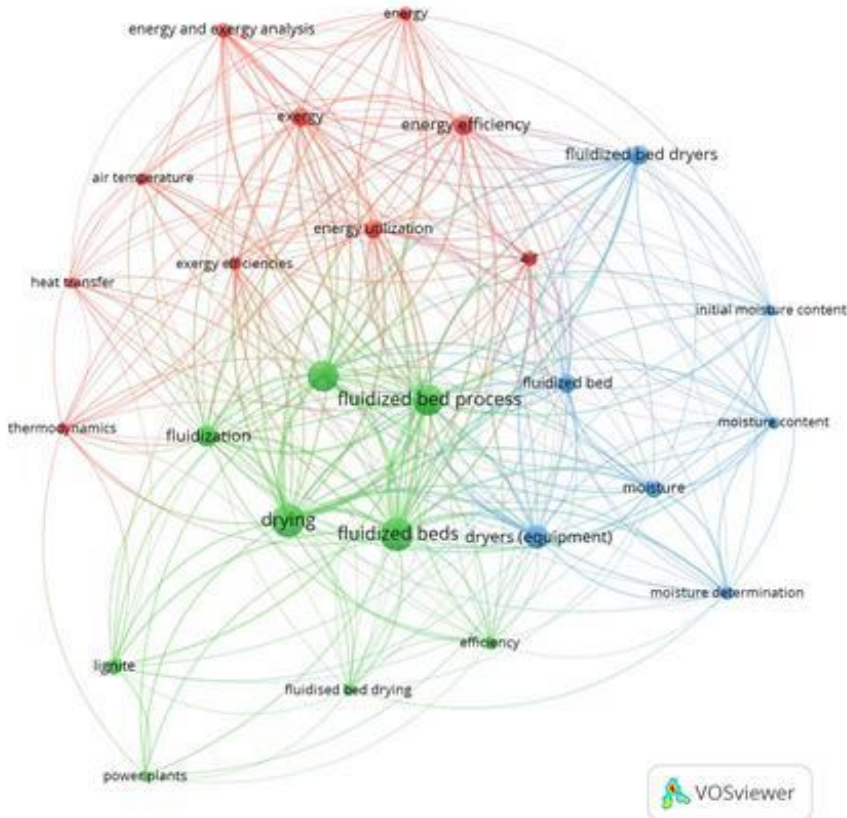


Fig. 49. The occurrence network of the most frequently used keywords (frequency > 5)

The publications in this field has increased significantly over the past decade; India and Iran are the most influential countries.

The heat transfer calculations of condensation and adsorption dryers are based on a minimum temperature difference of 10 °C. The analysis showed that in the conventional condenser dryer systems (see fig. 50), the dryer's exhaust air can heat the cooled air from the condenser. For the adsorption dryers, the exhaust air from the regenerator and adsorbent leaving the regenerator can be reused to heat the air, sent to the regenerator before heater 1.

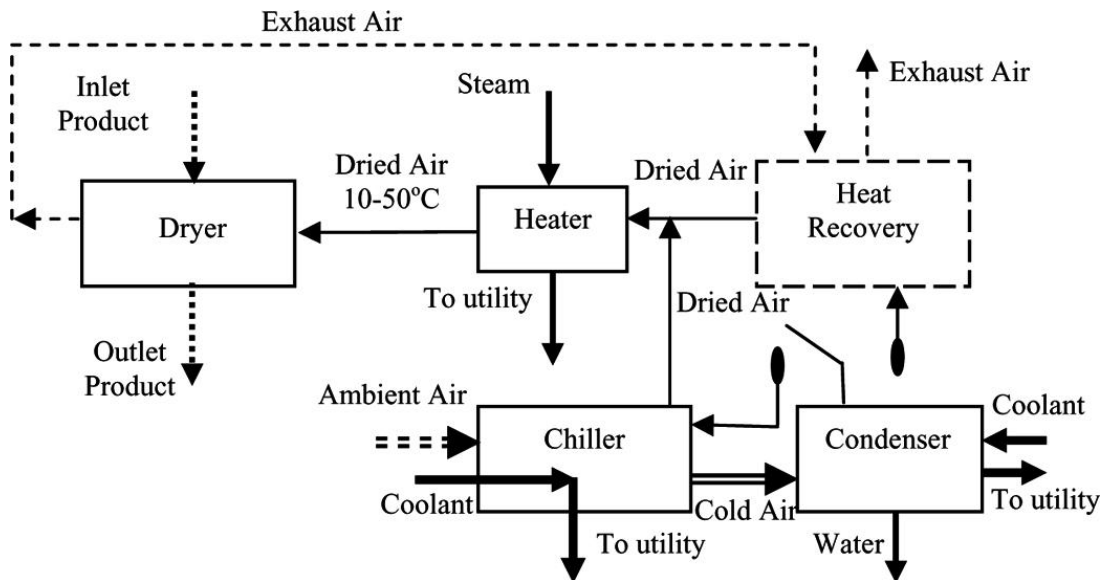


Fig. 50. Low-temperature condensation dryer

Increasing the operating temperature and the number of stages leads to an increase in the desiccant dryer's energy efficiency. The number of stages significantly impacts energy efficiency at dryer inlet temperatures of 30 °C and below. This temperature provides significant heat recovery from the exhaust air from the regenerators (hot 2). The improvement is negligible for three stages and temperatures of 40 °C and above, so a three-stage dryer seems to be the most economically promising. Only hot streams with high temperatures are used for heat recovery.

A zeolite dryer is useful for drying at inlet temperatures below 30 °C because the air supplied to the dryer has low water content, resulting in a high drying driving force. At 40–50 °C, the multistage alumina column dryer does not require refrigeration, whereas the zeolite system must be refrigerated for these conditions. As a result, the columnar clay has an advantage over zeolite for these drying temperatures.

Fig. 51 demonstrates the main convective drying intensification methods in the part of the external and internal heat and mass transfer. It is not always expedient and justified from an economic point of view to use all methods at once; therefore, they successfully resort to mathematical modeling methods to solve such problems.

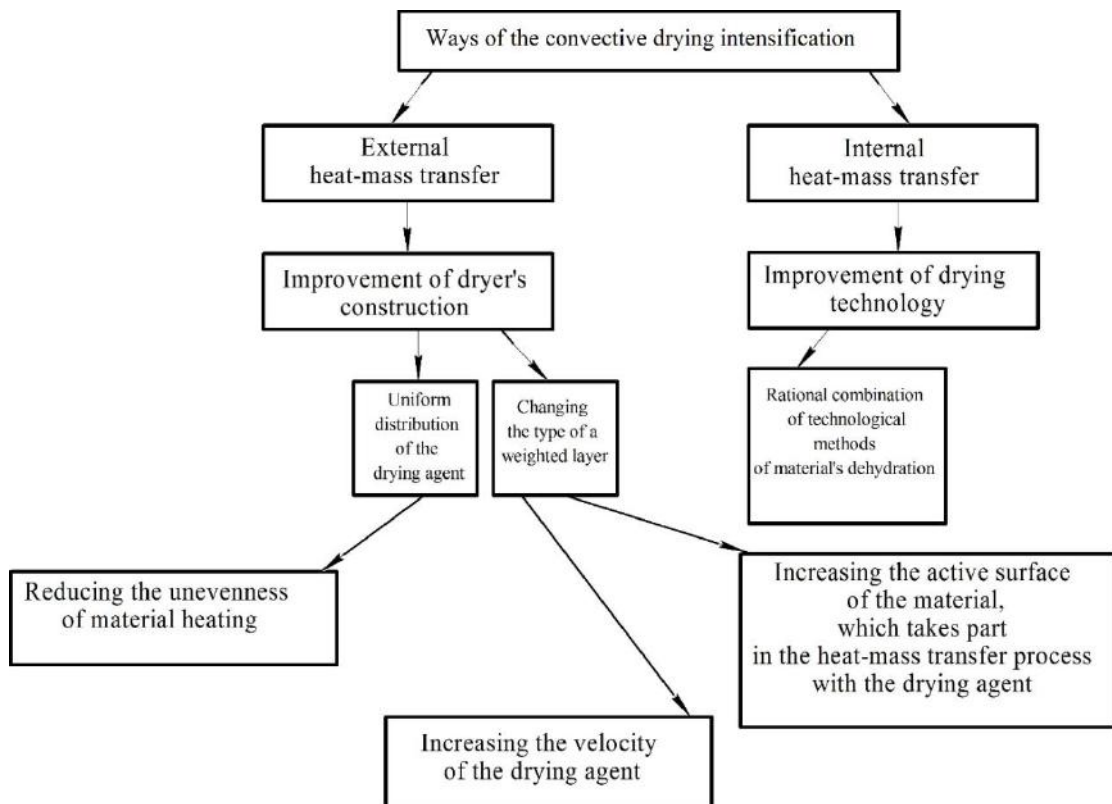


Fig. 51. Ways of the convective drying intensification (for dispersed materials)

The mathematical model allows optimization calculation of the time the dispersed phase stays in the free and constraint motion regime at every stage of the shelf dryer. The software product enables to vary the length of the shelf, its open intersection and tilt angle, and relative content of particles in the device to achieve the required time the material stays in the device.

The design of the dryer (changing the type of the weighted layer) and drying technology (a rational combination of technological methods for dehydrating the material, in particular, the choice of a way to organize the drying agent's motion) is an extremely urgent scientific problem to improve the environmental safety of the process, in particular, to reduce dust emissions.

Pneumatic unloading. Electronically controlled pneumatic unloading proved itself in practice, especially when drying corn. Large quantities of product are discharged promptly at short intervals. Thus, the product slides down the drying column continuously, even with a crude product. This function corresponds to the multiple shutter

function, which closes and opens the areas between roofs. The gaps between the moving parts of the unloading mechanism are easily adjusted to dry grain of different sizes. Since environmental protection is significant, legal limit values and regional conditions require the most modern dust protection systems.

Dust reduction with pneumatic valve control. The pneumatic exhaust valves are closed when the product is discharged to prevent dust from being emitted during the movement of the product in the grain column. The response times of the valves are adjusted on the dryer control panel. Advantages: low energy consumption of the entire system; especially suitable for continuous maize drying with the heat recovery system.

Dust cleaning system centrifugal separator STELA works as a multistage centrifugal separator (fig. 52). A centrifugal fan draws in dusty air from the dryer and directs it into the vortex chamber (1). There it is set in rotational motion. Thanks to the centrifugal force, dust particles are removed from the walls using a peeling tongue and a weak air stream. Then they are fed in the last part of the spiral into the secondary cyclone section (2). The main flow of air leaving the vortex chamber enters through the cylindrical partitions system (3) in the opposite direction of movement. In this way, the trapped dust particles are thrown out. The cone (5) of the secondary cyclone separator is bent 90 °; dust is emitted through it. Through the central pipe (4), the cleaned airflow returns to the main flow.

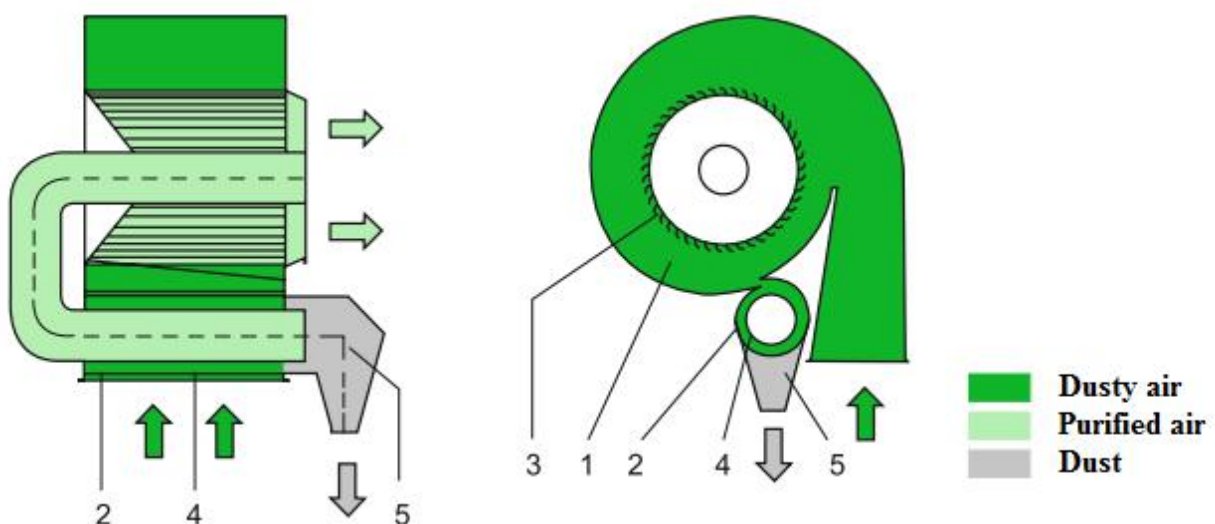


Fig. 52. Construction of centrifugal separator STELA

A support device is provided on the cone shape for direct completion of dust into hoods for utilization. For further transport of this dust, the air pressure is dumped using a sluice shutter. This centrifugal system's advantages could be presented as follows: the newest technology, especially for removing corn peel and grain dust; the final dust content depends on the product and remains much lower than the established limits (max. 20 mg/m<sup>3</sup>).

This method intensity can be organized by the contact surface gain of the grain with the heat-transfer agent in the device with a fluidized bed. Qualitative indicators of seeds such as high growth energy and germination are provided at the heat-transfer agent's temperature around 70 °C and the velocity of 1.6 m/s. A subsequent rising of the heat-transfer agent's temperature up to 80 °C and a velocity up to 1.8 m/s reduces the seeds' quality with increasing time of dehydration more than 250 s. The temperature of the heat-transfer agent plays a decisive role in the drying process of productive seeds. It is necessary to sustain the temperature at a level of not more than 70 °C to ensure high germination and seed growth features.

The recirculation drying scheme has some disadvantages, including an increase in the recirculation rate with an increase in the initial bulk of the grain; a decrease in the dryer's performance when the air temperature drops and, as a result, the grain is cooled. Along with the mine, column-type grain dryers are widely used, in which the layout is modular. In these dryers, the grain is moved by gravity from top to bottom between two perforated walls exposed to the cooling liquid in the longitudinal direction. Column dryers provide a higher specific coolant flow (no grain removal) than mine. Due to the free movement of grain in the columns, the probability of stagnation is reduced. The most famous producers of column dryers are American companies: Mathews Company, Delux, Sukup, Farm Fans (USA) and others.

The main disadvantage of column-type grain dryers is the uneven drying of the grain thickness of the layer. We offer the following method to increase the drying uniformity: to change the direction of movement of the coolant relative to the grain layer; to change

the position and nature of the movement of the layers adjacent to the walls. Bed material and its features play an essential role in drying studies and energy analysis. Studies have been made using different bed materials that belong to food and agricultural products in several types of dryers.

Authors found that exergy losses grow with increasing stage bottom angle height, wall temperature, solids flow rate and decrease with an increase in the air speed and drying time. The exergy efficiency grows with an increase in the wall temperature of the stages, air speed and drying time and decreases with an increase in the lower corner's height and the flow rate of solid particles.

Multi-stage gravitation shelving devices and devices for granulation and drying in the vortex fluidized bed have been proved as efficient equipment with high indicators of specific productivity. By changing the cross-sectional area of drying units by the height of the device (installation of shelves with varying degrees of perforation in multi-stage gravitation shelving devices and working space of conical shape in devices with vortex fluidized bed), there is the possibility of carrying out the granules classifying process into the size with the separation of fine and commodity fractions.

Dividing the drying space with shelves of different designs allows to create different conditions for the movement of material in each section. Depending on the initial and final fractional composition of the granules, each shelf can act as a classifier. Besides, the change in the shelf design at each stage ensures the specified residence time of each fraction in the working space of the dryer.

Therefore, the optimal selection of perforated shelf construction allows stabilizing the fluidized bed of granules due to the next actions:

- reduction of granules ablation from the top shelf of the cascade (under conditions of separation of the small non-commodity fraction of granules);
- control the residence time of particles in the dryer's workspace depending on the initial and necessary final features of the product;

– reduction of the vortex structures formation in the gap between the end of the shelf and the dryer's case.

A fluidized bed dryer unit was developed and successfully tested for drying of the wheat grains. The drying features of wheat were evaluated in the fluidized bed dryer for various operating characteristics. The effects of dimension ratio, heat-transfer agent's temperature, and drying process period on the dryer performance were determined. Thus, there are the following conclusions:

- the fluidized bed dryer unit has worked well as an exceptional tool for drying of wheat grains, as well as having the potential to dry other organic and non-organic products;
- the lowest moisture content of wheat reached 16.3 % db at the ratio of the dimensions of 2 m/m, the temperature of drying agent 200 °C, and the drying process period of 1 h;
- the drying velocity ranged between 7.0 % and 4.3 % moisture points per hour;
- the highest overall drying velocity reached 0.117 %/min at the ratio of the dimensions of 2 m/m, the drying agent's temperature of 200 °C and the drying process period of 1 h;
- the dryer efficiency reached 63.2 % at the ratio of the dimension of 4 m/m and the drying agent's temperature of 200 °C;;
- two correlations between the wheat moisture content and the dryer efficiency as functions of the dimension ratio, the drying temperature and the drying process period were developed with the corrected determination factor of 0.91 and 0.88, respectively.

Introducing multi-stage dryers from the working space sectioning by perforated shelves ensures the achievement of environmental safety criteria. In addition to the specified design parameters, a convective fluidized bed drying method is used. Thus, ecological and economic efficiency is achieved by the selection of design and operating parameters. The complex application of countercurrent and/or combined modes of the drying agent's interaction with the product ensures decreased material carryover and dust

emissions. The efficiency is also increased by the optimal way of introducing the drying agent into the workspace of the device and its reuse. According to the principles of low-waste technologies, the drying agent's potential can be reused by recuperating heat and energy and utilizing harmful substances. The development of mechanisms and approaches to control a two-phase flow movement is based on vertical sectioning of the working space. Ensuring the minimum required drying time remains essential from the standpoint of environmental and economic efficiency, which becomes possible due to the rational organization of the drying agent's movement and dispersed particles.

Controlling the dryers' design and the number of shelves envisioned to provide the material residence time calculated to achieve the desired moisture content directly addresses the problem of reducing dust and pollutant emissions in the waste gases. Such preventive measures are of higher priority than the "on the pipe" methods in the environmental actions to reduce the ingredient pollution in the atmosphere. The latter includes using a jet device to clean exhaust gas, a vortex separator for separating dust from exhaust gases. Small-sized modular units containing dust utilization and heat recovery units comply with the concept of full use of material flows (fine phase, dust) in terms of environmental safety.

The proposed drying units with the described design and operating parameters provide a reduction in the cost of designing and operating an additional unit for cleaning exhaust gases from dust to normal values (for this type of installation – the maximum permissible concentration is not more than  $50 \text{ mg/m}^3$ ).

In a proposed way, the developed approach to substantiating the ecological safety of the investigated dryers reduces the technogenic load on the environment by reducing air pollution, water bodies, reducing the generation of waste and the use of natural resources.

Conducted bibliometric analysis related to the energy and exergy efficiency of multi-stage shelf dryers with vertical sectioning of workspace showed a network of the main keywords and made it possible to highlight unsolved problems.

The rational design of the working space and the coolant's optimal flow rates and temperature and humidity characteristics within the gravity shelf dryer are the main approaches to the ecological and economic efficiency of the investigated devices.

Within the specified temperature of the coolant, electric heating is most expedient. However, it is advisable to propose electricity production not from non-renewable natural resources but from alternative ones – biogas obtained from production and consumption waste to reduce the technogenic load on the environment. So, the investigated dryers have significant technological advantages; therefore, compliance with environmental safety requirements remains essential, the solution of which is being investigated within the framework of this work.

## **9 MODELING OF EROSION OF CONSTRUCTION MATERIALS IN THE WORKING SPACE OF MULTISTAGE CONVECTIVE DRYERS**

The introduction of new technologies for drying wet materials (in some cases – moistened at the stages of preliminary preparation to obtain special properties of materials) in the known methods is based on the improvement of technological, environmental, and economic characteristics of the target process and the creation of new designs of dryers and forms of flow organization in the working space of the devices.

In the drying process, the vast majority of dispersed (granular) materials of inorganic (e.g., fertilizers) and organic origin (e.g., seeds of cereal, sunflower, etc.) are dehydrated. The drying process of dispersed materials is carried out in devices with different designs depending on the drying method. The choice of method and hardware design of the drying process depends on the type of dispersed material to be dried, as well as the temperature and humidity parameters of the dispersed material and the drying agent.

Convective drying processes in devices with a weighted layer as a kind of drying methods have become widespread in the technology of dehydration of dispersed materials. Due to the contact of the drying agent (for example, heated to a certain air temperature) with the dispersed material, a developed mass transfer surface is created. In addition to the direct interaction between the streams of dispersed material and the drying agent, each of the streams comes into contact with the dryer's structural elements. In this case, one of the defining stages of the general algorithm for calculating the dryers is selecting construction materials that will ensure the stability of the dryer in operation and will not affect the properties of the dispersed material, except for changes in moisture content. The dryer's main element with the weighted layer, which is studied in the article, are perforated contact shelves (shelf contacts), directly removing moisture.

The selection of material for shelf contacts of the gravity shelf dryer is the task to be solved using the research presented in this article. The study is based on computer

simulation of erosion wear of shelf contacts in interaction with dispersed material of plant origin or granular ammonium nitrate with special properties (so-called porous ammonium nitrate).

Previous results present the research of modular grain dryers produced by leading foreign manufacturers and Ukraine companies. According to the manufacturers and real samples of modular grain dryers, the analytical review and analysis of the design allows to state that for the manufacture of their main parts used stainless steel.

According to the industry standard's general technical requirements, the main parts for dryers with rotating drums must be made of construction carbon steel.

The American manufacturer of engineering equipment FEECO International offers various materials for construction shells of rotary dryers. This list includes carbon and stainless steel, Hasteloy, Inconel, and other alloys, depending on the customer's technological requirements. Chinese manufacturer of industrial rotary dryers Hengxing produces equipment for drying minerals and construction materials. As a shell material, they use carbon steel or stainless steel grade 304.

Scientists designed and manufactured a tunnel dryer in two modes of operation with an aluminum drying chamber for indoor and outdoor use. The choice of the aluminum sheet was justified by its high corrosion resistance, availability, ductility, ductility, lightweight and average cost.

Scientists presents the design, construction, and analysis of a mixed solar dryer's characteristics for crops. The choice of material for each part of the dryer was based on the following requirements: functionality, manufacturability, cost and reliability. Following these requirements, silica, glass, aluminum, and wood were proposed for the drying chamber parts; for solar collector parts it includes low carbon steel, rubber, and organic glass Perpex.

Thus, domestic and foreign companies-manufacturers of dryers traditionally use carbon, construction, and stainless steel for the manufacture of basic parts, which ensure compliance with the technological requirements (temperature, pressure, durability, etc.).

Instead, scientists are working on a solution to reducing energy and material costs during drying in devices of various designs and improving existing ones. One way to reduce the size of dryers and reduce their cost is the use of non-ferrous metals and non-metallic materials.

Erosion is a complex phenomenon that depends on many parameters. Particle parameters may include the following:

- shape or angularity of particles (angular particles cause greater erosion than spherical particles);
- particle size (erosion rate  $ER = (d_p)^n$  with  $0,3 \leq n \leq 2$ );
- hardness of particles ( $ER = H_p$  with  $H_p < 700$  HV).

On the other hand, flow parameters have a stronger effect on erosion because they determine particle concentration, particle impact angle, and impact velocity. Other parameters that affect erosion are surface hardness and multiphase effects [9].

Progress in understanding erosion due to solid particles has been achieved by using computational fluid dynamics (CFD), which allows to accurately model the flow of fluid and the trajectory of particles through pipelines and bends. After calculating the impact velocity and the angle of the particles in contact with the surface, empirical correlations can be applied to quantify the erosion rate.

The authors [10-13] found that the empirical correlations of erosion include the angle of impact, impact velocity, particle diameter, particle mass, and collision frequency connected to it.

A typical erosion model has the following general form (the default erosion fluid dynamics model in Ansys Fluent):

$$ER = \sum_{p=1}^{N_{trajct}} \frac{\dot{m}_p C(d_p) f(\alpha) v_p^n}{A_{face}}$$

where  $\dot{m}_p$  – the mass flow rate of particles,  $f(\alpha)$  – the impact angle function,  $C(d_p)$  – the particle diameter function,  $v_p$  – the particle impact velocity,  $n$  – the velocity exponent.

Particle impact angle, impact velocity and mass flow rate are calculated directly using CFD. However, the impact angle function, the particle diameter function and the velocity index must be supplemented as input to the solver.

In addition to the typical ones, three corresponding erosion correlations have been added to Ansys Fluent in Ansys 18: Finnie, Oka and McLaury.

The Finnie erosion model is more suitable for plastic materials, where erosion varies depending on the angle of impact and speed. The Oka model provides a more realistic correlation, including the effect of the wall material's hardness. The McLaury erosion model was designed to predict the rate of erosion of solids in water; it was mainly used in sludge streams.

Thus, each erosion model must be calibrated empirically for a particular flow scenario, so the appropriate flow conditions for each model should be considered before using any erosion model.

The choice of construction materials for the manufacture of chemical equipment should be based, first, on the specifics of their operation. The indicators of working conditions of materials include operating temperature, pressure, environment and its concentration.

Secondly, it is very important to consider the following main properties of the material: physical (thermal expansion, thermal conductivity), mechanical (strength, elastic properties), chemical (corrosion resistance, chemical inertness), technological (weldability, etc.).

Third, the physicochemical properties of materials can change under the influence of operating conditions. Among the main factors of influence are pressure (from deep vacuum to excess values), temperature regime (from liquid nitrogen temperature to melting of iron ore), types of corrosion (chemical, thermal, atmospheric), high mechanical loads in aggressive environments.

As the temperature rises, the material may creep, which limits its ability to withstand the load. The phenomenon of creep can lead to oxidation, destruction or

decomposition of the material with a change in its chemical composition, making it unsuitable for further use. Fig. 53 shows the dependence of strength on the maximum service temperature at which each class of materials can be used.

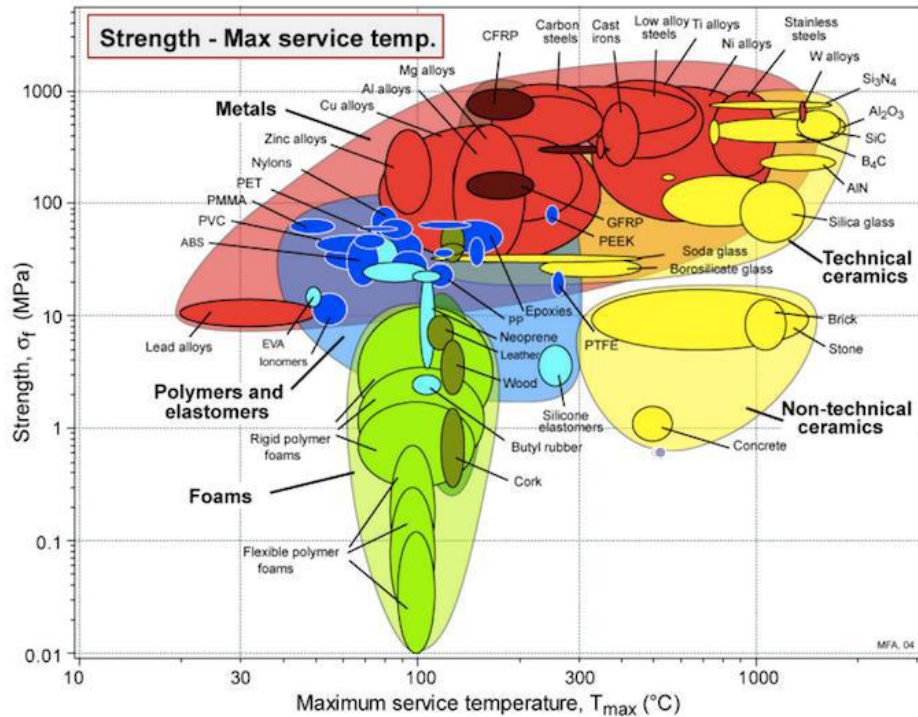


Fig. 53. Dependence of strength  $\sigma_f$  on the maximum service temperature  $T_{\max}$  for different classes of materials

The dependence of the change in yield strength under static loads or elastic properties (modulus  $E$  and Poisson's ratio  $\mu$ ) on the service temperature is the most important characteristic for steels and alloys. Fig. 54 shows the linear thermal expansion  $\alpha$  from the Young's modulus  $E$  for different classes of materials. The regions' contours show the temperature stress caused by the change in temperature ( $^{\circ}\text{C}$ ) in a constrained sample. They determine the characteristic  $\alpha E = C$  [MPa/K] (constant thermal stress,  $^{\circ}\text{K}$ ). The value of the constant  $C$  increases towards the upper right.

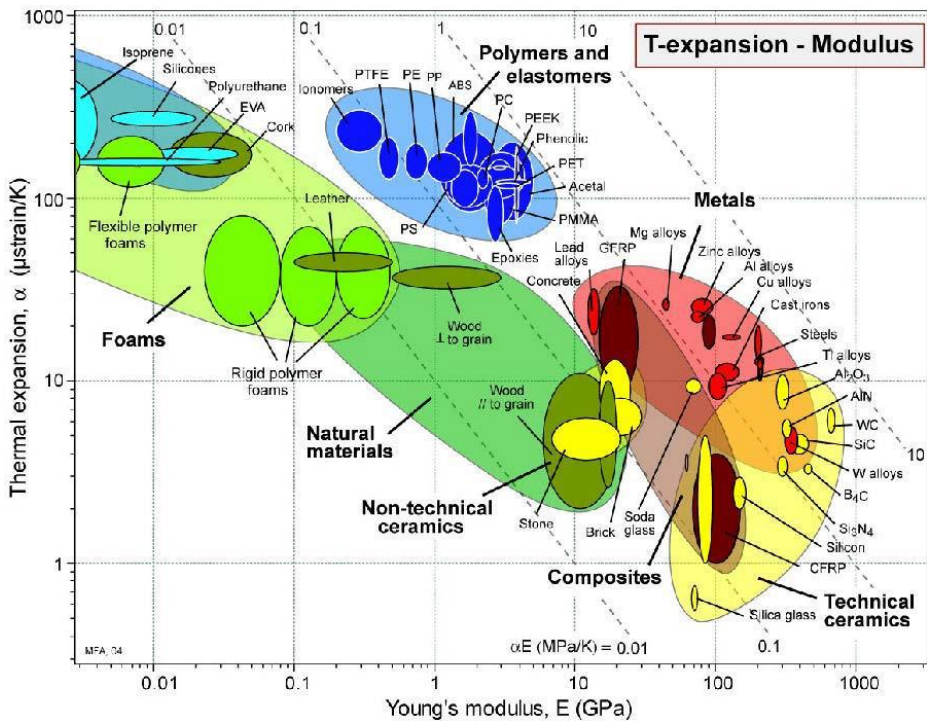


Fig. 54. Dependence of linear thermal expansion  $\alpha$  on the Young's modulus  $E$  for different classes of materials.

Therefore, construction materials for chemical industrial equipment must meet the following requirements:

- enough corrosion resistance in an aggressive environment at a certain technological process concentration of reactive compounds, temperature range, pressure level;
- enough mechanical strength under the same conditions, considering additional loads from its weight, wind, method of installation, support area;
- the possibility of obtaining strong welds resistant to breakage and mechanical loads in extreme conditions;
- availability of the material in terms of cost and prevalence;
- safe and easy disposal after service life or recyclability.

Polymers have attractive properties (excellent corrosion resistance, lightweight, ease of manufacture and installation), making them competitive materials for use in various chemical processes. Also, polymer structures require less maintenance than metal structures.

The following thermoplastics have been used as corrosion-resistant: fluorocarbon polymers, acrylics, nylon, chlorinated polyester, polyethylene, polypropylene, polystyrene and polyvinyl(chloride). Fluorocarbon polymers have extraordinary chemical resistance and show good elastic properties in a wide range of temperatures (fig. 54). Therefore, they are used for the manufacture of various parts (sealer, linings, tubing, hose, belting, fabrics, caulk, adhesives, dampeners, etc.).

When choosing a construction material, it is necessary to anticipate the extreme conditions and apply them to all components. Material composition and temperature deviations can have a significant effect on the corrosion rate.

Although carbon and stainless steels are commonly used construction materials, non-metallic and lined or plastic process equipment is increasingly used. A wide range of plastics is available for use as construction materials and can be used in areas such as the treatment of inorganic salt solutions where metals are unsuitable. The use of plastic pads is widespread in chemical equipment – tanks, pipes and drums. However, their use is limited to moderate temperatures, and they are generally unsuitable for use in abrasive working conditions. The most used plastics include PVC, PTFE and polypropylene.

Thus, plastics soften at high temperatures and swell under prolonged exposure to the environment; from this point of view, metals are superior. One of the ways to effectively use high corrosion resistance of plastics is to combine them with metal structures in the form of protective coatings, pads, etc.

The research was carried out for a multistage convective shelf dryer with vertical partitioning of the working space in the technology of obtaining porous ammonium nitrate. This drying unit is an apparatus of continuous action. Drying of materials is carried out in a constant temperature mode: from initial temperature and on the achievement of the maximum temperature, it remains invariable. The drying agent reduces its temperature along the height of the device after contact with the dispersed material at each stage of the dryer.

The selection of optimal materials was carried out for internal devices – perforated shelves, which can perform the functions of a heat exchange surface and provide conductive drying of dispersed materials.

After analyzing the above review of the use of classes of construction materials for the manufacture of basic parts of drying units of different types, the basic principles and criteria for selecting materials for chemical equipment, two research materials were selected for the experiment - traditionally used corrosion-resistant steel 12H18N10T and chemically inert polymer PTFE.

The drying process of ammonium nitrate and wheat using different shelf materials (steel and PTFE) considering gravity was simulated in the ANSYS software complex.

Initially, a three-dimensional dryer model (fig. 55, a) was created based on the discrete phase model (DPM) in Ansys Fluent software to detect the rate of erosion on walls caused by fine solids. A complete model of a gravity shelf dryer was considered. \

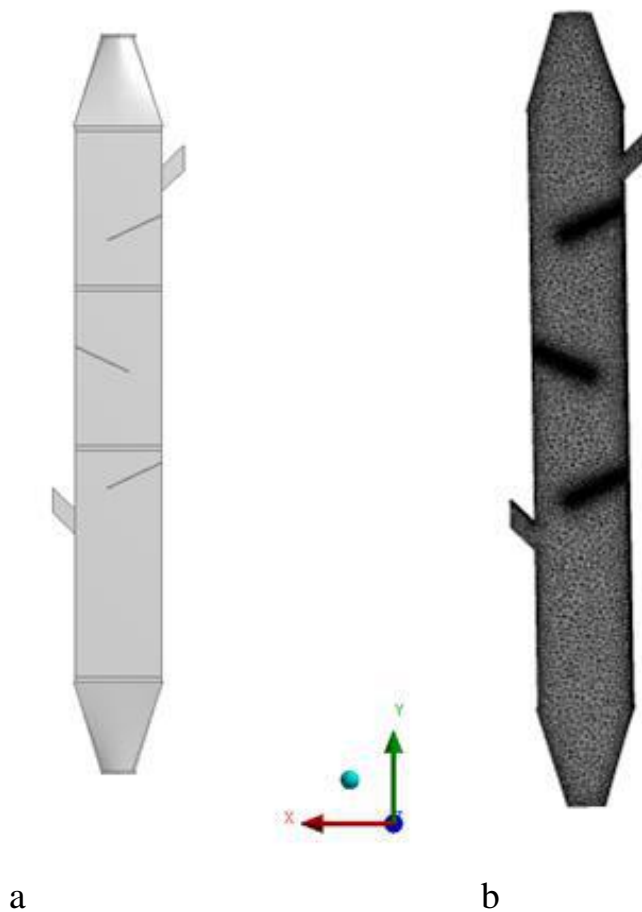


Fig. 55. Creation of 3D-model (a) and calculation grid (b) of the dryer.

The calculated grid of the compaction model is created in the program ANSYS Meshing (fig. 55, b). As a result, the estimated grid has approximately 7,5 million elements. The calculation grid in the wall layers was condensed. The quality of the grid was controlled by the dimensionless parameter  $y^+$  on the walls of the shelf dryer, which varied in the range from 20 to 50 for the  $k-\varepsilon$  model of turbulence; growth rate; the coefficient of proportionality and orthogonality of the model grid. The problem was considered in a static formulation taking into account gravity. The model uses two inputs and two outputs (13, 14); ammonium nitrate, wheat 15 kg/h are fed to the inlet 13; hot air ( $O_2$ ) is supplied to the rectangular pipe 14 for drying nitrate 130 °C and for wheat at 70 °C at a speed of 0,2 m/sec.

For a branch pipe 7 for removing the drying agent and the connected conical frame 8, which is equipped with a branch pipe 9 for removing the dried material, the limit conditions of atmospheric pressure (1 atm) were set.

The calculation of particle trajectories is conditional. The program simulates the track from the center of each element on the injection surface. The track is the most probable trajectory not of one particle, but of the whole group of particles, which entered the calculation zone through the area of the face of the corresponding cell. That is, if there are ~ 100 cells at the input boundary, then only ~ 100 trajectories will be calculated and constructed. The number of particles that will be physically «injected» every second into the calculation zone can be found by the formula:

$$N_{\Sigma} = \frac{\dot{m}}{\rho_p \cdot V_p}$$

where  $\dot{m}$  – consumption of particles for a certain period of time,  $V_p = 4/3\pi r^3$  – particle volume,  $\rho_p$  – density of particle material (ammonium nitrate, wheat).

During the calculation, the effect of particles on the inclined contact shelf 10 for different materials was considered.

As a result of the simulation the problem of drying of dispersed material in the Ansys Fluent software package was solved:

1. «Discrete Particle Model» from the model tree was enabled, and the Erosion/Accretion model on the «Physical Models» tab was activated.
2. Particle injections, particle diameter, injection rate, and flow rate were determined.
3. The coefficients of normal and tangential reflection of particles on the wall were established.
4. Models of erosion on the wall with the DPM tab were selected: Generic Fluent (fig. 56-59, a), Finnie (fig. 56-59, b), McLaury (fig. 56-59, c) and Oka (fig. 56-59, d).
5. After starting the flow during one iteration, particles were isolated and the erosion rate on the participating surface was calculated.
6. The contours of the erosion rate on one of the shelves of the dryer for different wall materials (PTFE and steel) for different drying materials (ammonium nitrate and wheat) were displayed (fig. 56-59).

Analysis of fig. 56 and 57 showed that for drying ammonium nitrate PTFE is superior to steel in terms of erosion resistance. In general, there is a much smaller amount of eroded polymer material in the plane of the shelf (fig. 56, 57, a). The localization of traces of erosion near the holes is noted, which is a predictable phenomenon. The calculation of additional erosion correlations (figs 56, 57, b-d) confirmed the proportional distributions of the impact areas of the nitrate erosion particles on the surface of the experimental materials.

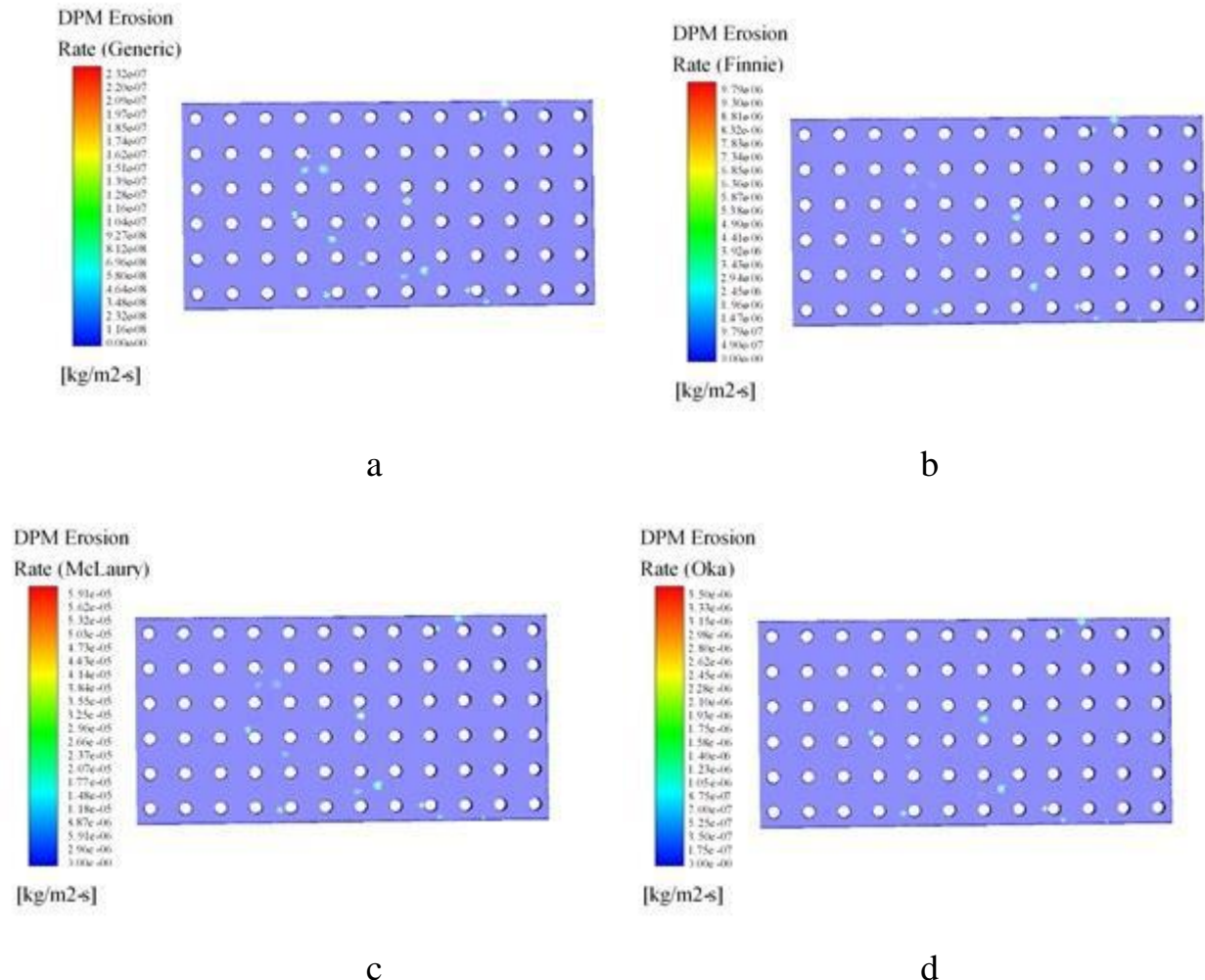


Fig. 56. Contour graphs of DPM erosion rate in Ansys Fluent, shelf material – steel, drying material – ammonium nitrate.

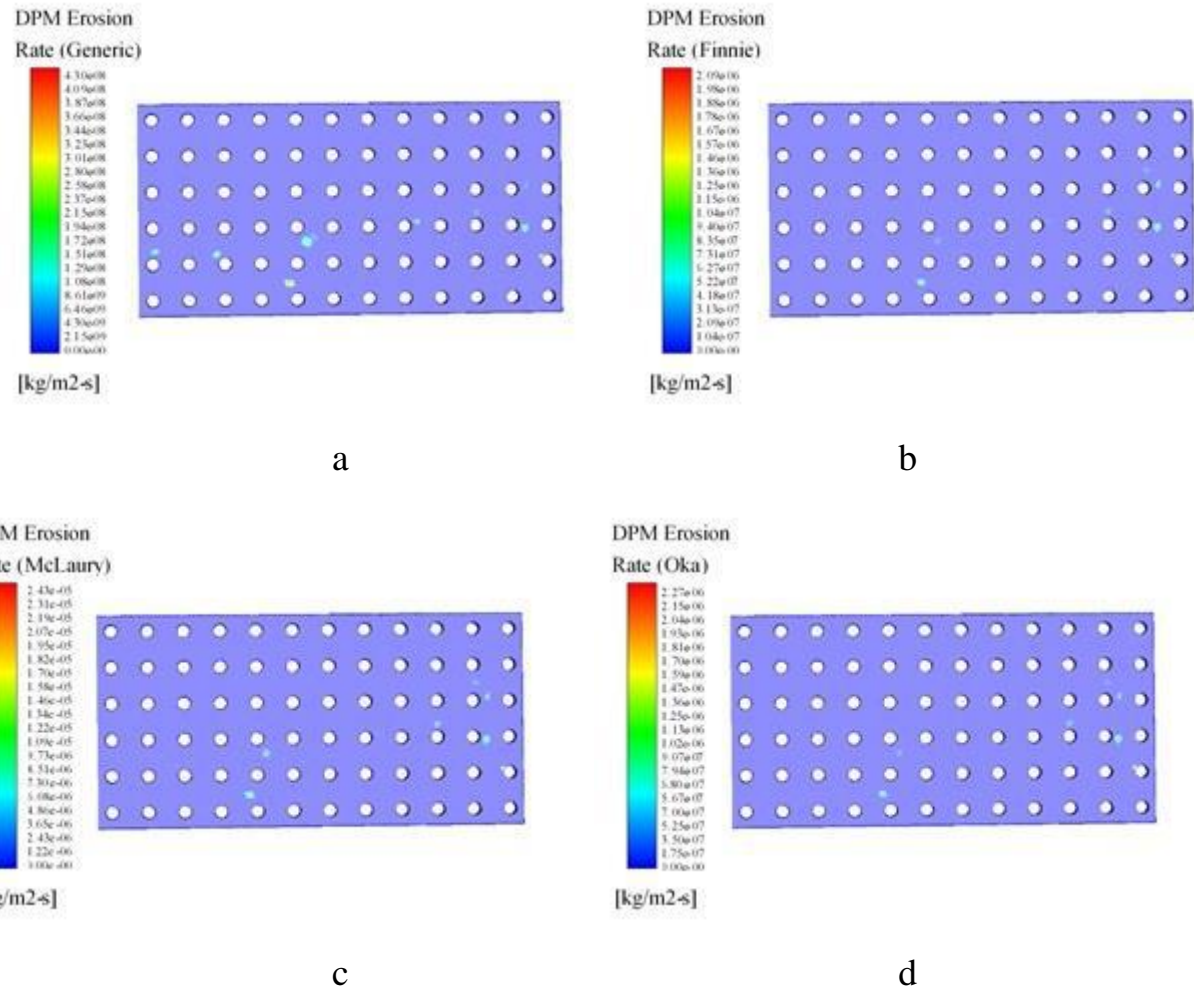


Fig. 57. Contour graphs of DPM erosion rate in Ansys Fluent, shelf material – PTFE, drying material – ammonium nitrate.

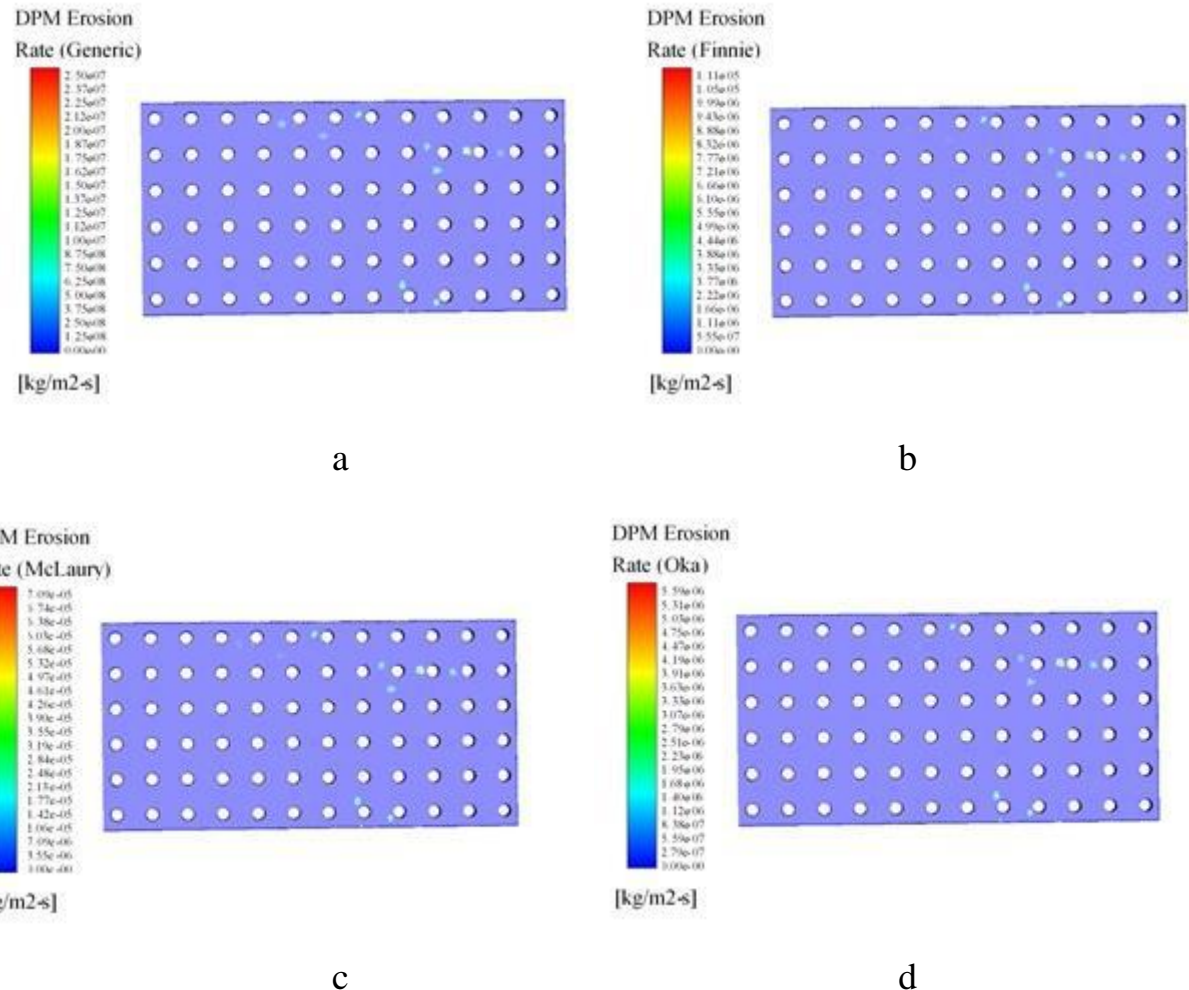


Fig. 58. Contour graphs of DPM erosion rate in Ansys Fluent, shelf material – steel, drying material – wheat.

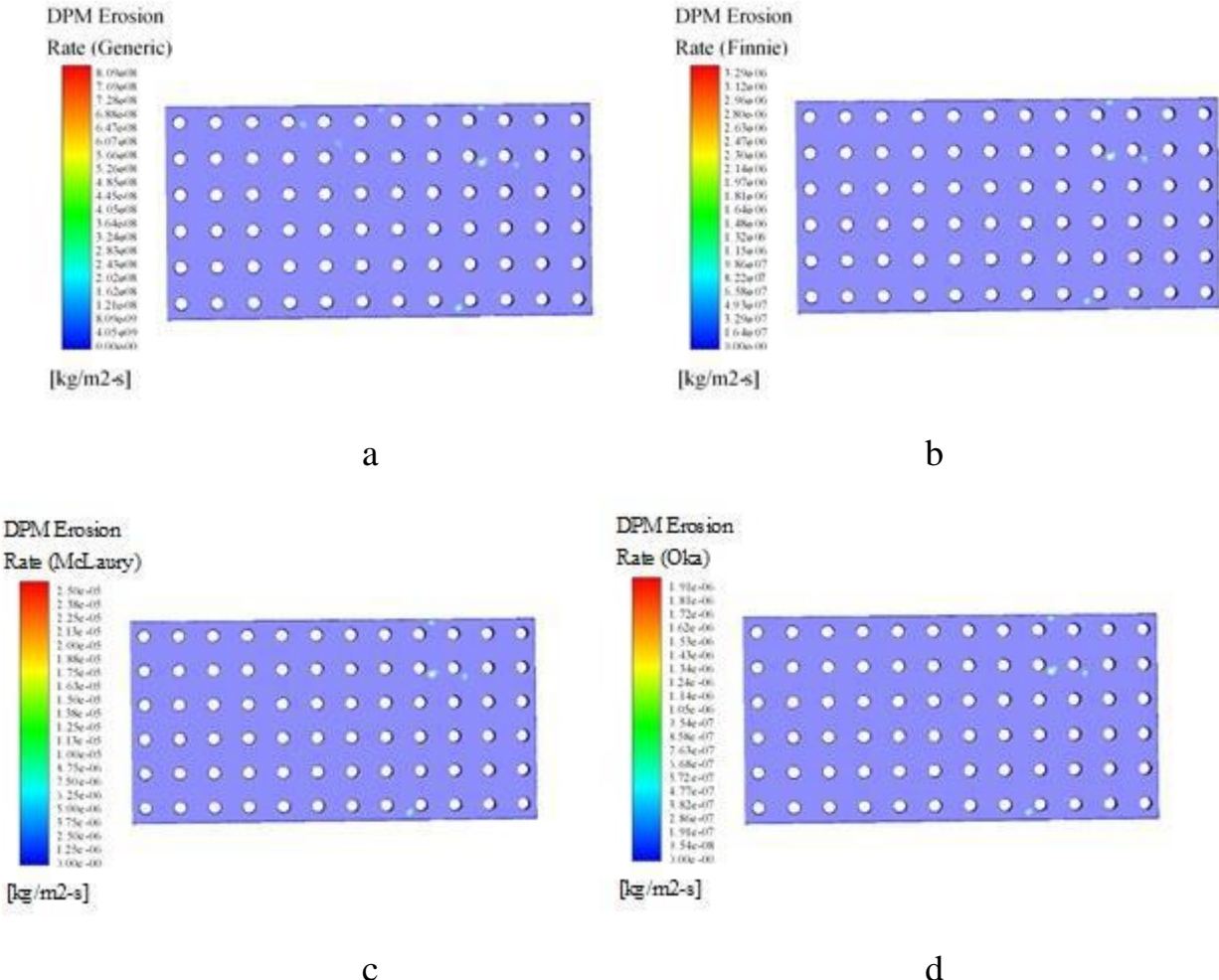


Fig. 59. Contour graphs of DPM erosion rate in Ansys Fluent, shelf material – PTFE, drying material – wheat.

The speed of erosion particles has a very strong effect on the wear process: when the speed is low, the stress on the impact of the particle is insufficient to cause plastic deformation and erosion wear, which is associated with surface fatigue; when the speed increases, the eroded material can be plastically deformed by the impact of the particle. The morphology of eroded surfaces determines the mechanisms of wear and the presence of microcutting, microcracks, and other characteristics of plastic deformation of the polymer.

From the comparative analysis of fig. 58 and 59 it can be concluded that the value of the erosion rate is almost the same for both experimental materials. The temperature

range of the drying process does not allow an objective comparison of the experimental materials. In the case of drying wheat, when the temperature is an order of magnitude lower and the process conditions are different than for ammonium nitrate, the determining factor is the chemical inertness and stability of the shelf material.

1. The analysis of the used construction materials for the manufacture of basic parts of drying units of different types allows to state that companies-manufacturers of dryers traditionally use carbon, construction and stainless steels. While scientists are working on the problem of reducing metal and energy consumption, testing different non-ferrous metals and non-metallic materials.

2. Surface erosion of materials as a result of impact of solid particles is a serious problem for many types of industrial equipment using multiphase flow. Erosion causes point corrosion, which leads to functional failure of the part, although the rest of the equipment may not be damaged. Since the erosion rate is considered as a function of the local particle impact velocity and the impact angle, these parameters are widely studied and vary for different classes of materials.

3. When choosing structural materials for chemical industrial equipment, the following properties should be considered: high corrosion resistance and sufficient mechanical strength in aggressive environments, availability of the material in terms of cost and prevalence, safe and easy disposal or recycling.

4. Computer simulation of the behavior of materials in the conditions of erosion wear in the software package Ansys Fluent 18 makes it possible to predict the results of laboratory tests. The obtained research results predict the prospects for the use of PTFE in the construction of convective dryers as an alternative to construction steels for reducing the metal consumption of equipment. A further area of research is related to the conduct of experimental work based on computer simulation data.

## CONCLUSIONS

*This section is prepared in according to data [1-9].*

The analysis of the computer simulation results proves that the amount of the drying agent, which is repeatedly used as a recirculating flow, has a considerable influence on the moisture of the dried disperse material. Herewith, the quality of the final product is also predetermined by the initial characteristics of the drying agent (temperature and moisture).

The selection of an optimal technological mode of the dryer with the inner space sectioning is a multifactor task, the solution of which considers the peculiarities of the technological process, a constructive design and energy expenditures on heating and transferring the drying agent in the porous medium.

Based on the analysis of the ways to obtain the granulated product in units with implementation of the directed fluidized bed of the dispersed particles, it was defined that today there are no reliable mechanisms which control the residence time of the dispersed particle in the workspace of the device for such methods. It made impossible to obtain the granulated product with given qualitative indices with minimum energy costs for this process.

Cluster Granulation Unit<sup>©</sup> enables to carry out the optimization calculation of the main technological equipment in the granulation unit at the stage of its design without the expensive multifactorial experiment. The software peculiarities also let to carry out the equipment changeover if the raw material features and the productivity of the unit are changed.

The results of the optimization calculation with the software products and cluster implementation let to provide:

- a minimum “hydrodynamic” residence time of the particle in the device, which will not exceed “thermodynamic” time (minimum time of particles dehydration to the normative index is determined by the dehydration kinetics laws, thermodynamic indices of the dehydration process);

- implementation of different temperature and humidity potential of the heat transfer agent in some sections in the devices;

- variety of the device construction;

- possibility to use the recirculation of the heat transfer agent.

The original methods of the equipment engineering calculation with the directed fluidized bed as a part to obtain the granulated products are found.

The main recommendations to improve the technological equipment construction of the granulation unit have been implemented in the new methods of granulation, drying and classification in the directed fluidized bed and in devices for their fulfilment, protected by the patents.

Studies regarding the nanoporous structure morphology of PAN granules demonstrate that the final drying stage can improve product quality indicators. Although the PAN production technology using the final drying stage increases the cost of production (compared with the basic scheme for PAS production in a vortex granulator), the cost for storing granules can be reduced. Besides, due to the compactness of the multi-stage dryer, it seems possible to create mobile eco-friendly installations to obtain PAN.

Samples of PAN granules after final drying are characterized by a developed network of nanopores with various configurations. Nanopores do not only absorb diesel distillate but also successfully retain it in the granules. Thanks to the improved technology, the granules undergo a polymorphic transformation, which does not affect the granule's strength. Moreover, the granule's low moisture content allows it to be stored for a long time without loss of strength and specific (absorptivity and retentivity) properties. Compared with the “porization” process, the proposed technology has several advantages, including:

- minimal destruction of the granules;

- minimal formation of “mechanical” micropores with an emphasis on the “modification” nanopores formation;

- the shape of the nanopores allows increasing the retentivity of the granules.

The objective of further research is to study the dependence of the final drying time

effect on nanopores' structure and the quality indicators of PAN granules.

Due to the creation of an active hydrodynamic mode to weigh solid particles in a layer, a multistage fluidized bed device with inclined perforated shelves provides efficiency to carry out heat-mass transfer processes.

Changes in the constructive parameters of the inclined shelf (the width of the outloading space and the shelf perforation degree) identify the different nature of the gas flow distribution between the holes of the shelf and the outloading space.

Various hydrodynamic modes during operation of the device were revealed: the “gravitationally falling layer” mode and the “weighted layer” mode. The first mode is effective in carrying out pneumatic classification processes, and the second—in cooling and drying of granular materials.

The study of interphase heat transfer showed a higher intensity of heat transfer in the weighted layer on an inclined perforated shelf compared to a traditional fluidized bed on a horizontal gas distribution grid.

The theoretical model enables to present the gas flow velocity profiles depending on the length and perforation degree of the shelf contact, as well as to estimate the residence time of material particles in the workspace of the device.

Further research will point to develop the mathematical model of the weighted layer hydrodynamics on an inclined perforated shelf. The corresponding scientific and methodological approaches based on using artificial neural networks for parameter identification of the proposed mathematical model will be developed.

The necessity of the final drying stage in the PAN production is proved. An improved scheme for obtaining PAN is shown. Based on the literature data, the authors propose to use a new design of the drying device. The proposed design of a multistage shelf dryer allows being carried out the drying process in a differentiated mode (the contact of the material at each stage is carried out with a drying agent with different temperature and humidity potential), which creates conditions for controlling the dehydration process and forming a nanoporous structure.

The heating and drying process of PAN granules are described. Dependencies for determining the temperature and humidity features of PAN granules during the drying stage are obtained. The temperature and humidity feature of the material closes the system of heat and mass transfer equations. For drying process calculation in the concentration zones, in this case, it is necessary to know the thermophysical properties of the dispersed material. Moreover, one can use a similar temperature-humidity approximation to define the mass transfer coefficient and mass transfer properties. The material is heated with different intensities at a constant radius of the particle, depending on its thermophysical properties. The particles with similar thermophysical properties are heated more intensely when their radius decreases.

A comparative study regarding the surface morphology of PAN granules is carried out. The main features of the nanoporous structure of the samples after the final drying stage are presented. On the surface, there are twisted and deep nanopores of different sizes. The surface structure of granules is changed toward decreasing the number of cavities and their replacement by deep pores increases tortuosity nanopores, their number and the relative area of the porous surface.

Comparative analysis of the quality indicators of PAN granules using the final drying stage and without it, demonstrates usefulness to introduce the final drying into the PAN production. Behind the realization of the final drying stage in the gravitational shelf dryer, the strength of the granules does not decrease since a new cycle of heat treatment is absent and the granule continues to dry at the same temperature. The indicator of absorptivity index increases because instead of cavities on the granule; the indicator of retentivity index increases because the number of twisting deep micropores increases. The relative value of mechanical pores decreases because the total number of micropores / mesopores / macropores increases. The ratio between micropores / mesopores / macropores changes increasing micropores.

## REFERENCES

1. A. Artyukhov, J. Krmela, N. Artyukhova, R. Ostroha. Modeling of the Aerodisperse Systems Hydrodynamics in Devices With Directional Motion of the Fluidized Bed // In: Encyclopedia of Organizational Knowledge, Administration, and Technologies, IGI Global, USA, 2020, 1289-1307.
2. J. Krmela, N. Artyukhova, A. Artyukhov Investigation of the Convection Drying Process in a Multistage Apparatus with a Differential Thermal Regime / Manufacturing Technology 2020, 20(4): 468-473.
3. N.O. Artyukhova. Morphological Features of the Nanoporous Structure in the Ammonium Nitrate Granules at the Final Drying Stage in Multistage Devices / J. Nano-Electron. Phys. 2020, 12 (4), 04036.
4. Yukhymenko, M., Artyukhov, A., Ostroha, R., Artyukhova, N., Krmela, J., Bocko, J. Multistage shelf devices with fluidized bed for heat-mass transfer processes: Experimental studies and practical implementation / Applied Sciences (Switzerland), 2021, 11(3), pp. 1-20, 1159.
5. Artyukhova N.O., Krmela J., Krmelova V. Experimental-industrial implementation of the technology for producing nanoporous layers on ammonium nitrate: the final drying stage in multistage devices. Applied Nanoscience (Switzerland), 2022, 12(4), pp. 1235–1244.
6. N. Artyukhova, J. Krmela, V Krmelová, A. Artyukhov. Drying Machines with Combined Hydrodynamic Regimes. 2021 IOP Conf. Ser.: Mater. Sci. Eng. 1199 012093.
7. N. Artyukhova, J. Krmela, V Krmelová, A. Artyukhov, M. Gavendová. Fluidized bed in gravitational shelf dryers: optimization calculation. Bull. Pol. Acad. Sci. Tech. Sci. 69(3) 2021, e137388.
8. Ablieieva I., Artyukhova N., Krmela J., Malovanyy M., Berezhnyi D. Parameters and Operating Modes of Dryers in terms of Minimizing Environmental Impact and Achieving the Sustainable Development Goals. Drying technology. 2022. Vol. 40, Issue 8. P. 1598–1608.

9. Krmela J, Berladir K, Pozovnyi O, Artyukhova N. Erosion Modelling of Structural Materials in the Working Space of Multistage Convective Dryers. *Manufacturing Technology*. 2022;22(3):307-318.
10. Small-scale energy-saving modules with the use of multifunctional devices with intensive hydrodynamics for the production, modification and encapsulation of granules: Development and creation of test equipment for the production of monodisperse droplets from solutions and melts with vibrating influence on the melt stream and the granulation of mineral fertilizers in the vortex gas stream, carrying out of testing: report on research work (intermediate) / manager of research work A. E. Artyukhov. — Sumy : Sumy State University, 2019. — 59 p.